Diplomarbeit

EFFECTS OF ARTIFICIAL GRAVITY ON MOLECULAR MECHANISMS

eingereicht von

Aleksandar Andjelic

geboren am 15.3.1984

zur Erlangung des akademischen Grades

Doktor der gesamten Heilkunde

(Dr. med. univ.)

an der

Medizinischen Universität Graz

ausgeführt auf dem

Institut für Physiologie

unter der Anleitung von

Ass.-Prof. Priv.-Doz. Dr.med. Nandu Goswami

und

Dr. Patrick De Boever

Flemish Institute for Technological Research
(Vlaamse Instelling voor Technologisch Onderzoek VITO), Belgium

Graz, 13. März 2014 **Aleksandar Andjelic**

Eidesstattliche Erklärung

Ich erkläre ehrenwörtlich, dass ich die vorliegende Arbeit selbstständig und ohne fremde Hilfe verfasst habe, andere als die angegebenen Quellen nicht verwendet habe und die den benutzten Quellen wörtlich oder inhaltlich entnommenen Stellen als solche kenntlich gemacht habe.

Graz, 13. März 2014 *Aleksandar Andjelic*

Declaration of Commitment to the Standards of Good Scientific Practice of the Medical University of Graz

As a researcher or co-worker in the area of research, I, Aleksandar Andjelic, at the Institute of Physiology, commit myself to adhering to the Standards of Good Scientific Practice valid at the time of my research related activities at the University.

Graz, March 13, 2014 Aleksandar Andjelic

ACKNOWLEDGEMENT

In the first place, I would like to express my gratitude to Prof. Dr. Nandu Goswami for his mentorship during my scientific work at the Institute of Physiology. Without his selfless dedication to young graduands and without his great amicability, the accomplishment of this thesis would not have taken place. I am also indebted to Dr. Patrick De Boever who helped me with the statistical analysis and the interpretation of the results.

I also want to give thanks to Prof. Dr. Sadjak, who gave me the opportunity to work on the Institute of Pathophysiology and Immunology for so many years, during which I was able to learn different laboratory methods as well as to teach young students by conducting courses. I also would like to thank Prof. Dr. Kresse and Dr. Ghaffari Tabrizi-Wizsy from the same institute for letting me work in their research groups.

I feel deeply obliged to my parents, Dr. Nenad and Ljiljana Andjelic, who supported me not only during the period of this thesis but also in every stage of my life and thanks to whom I had the opportunity to take my studies and to prepare this thesis after all.

I would also like to express my gratitude to my girlfriend Kristina and to all my dear friends, who supported me mentally during the preparation of this thesis.

ZUSAMMENFASSUNG

Einführung: Schwerelosigkeit hat viele, zum Teil gefährliche Einflüsse auf die menschliche Physiologie. In einem System ohne ständigen Einfluss der Schwerkraft muss sich der Körper zunächst an die neue Umgebung gewöhnen. Die Gewöhnung verursacht Veränderungen kardiovaskulärer, renaler, endokriner sowie neurovestibulärer Funktionen. Darüber hinaus führt die Minderbelastung von Knochen und Muskeln im Weltraum zu deren strukturellen Veränderungen. Ein wichtiges Prinzip zur Vorbeugung negativer Folgen der Schwerelosigkeit stellt Training mit künstlicher Schwerkraft durch Zentrifugation dar. Die Effekte künstlicher Schwerkraft wurden in zahlreichen Studien untersucht. Bislang hatte sich jedoch keine solcher Studien mit den Auswirkungen der Anwendung künstlicher Schwerkraft auf molekulare Mechanismen beschäftigt. In dieser Studie untersuchten wir molekulare, durch künstliche Schwerkraft verursachte Veränderungen anhand der Gesamtheit der mRNA (Transkriptom) aus dem peripheren Blut mittels DNA Microarray.

Methodologie: 12 Versuchspersonen unterzogen sich einem gemeinsamen kontinuierlichen Zentrifugationsprotokoll auf einer Kurzarmzentrifuge. Zusätzlich wurde ein zweites, intermittierendes Protokoll bei 6 der 12 Versuchspersonen angewendet. Blut von jeder Person wurde vor und nach jedem Versuch entnommen und die RNA wurde isoliert. Diese RNA wurde verwendet, um floureszenzmarkierte cRNA herzustellen und anschließend auf Microarrays kompetitiv zu hybridisieren. Die Signale wurden unter Anwendung verschiedener *p*-Werte und Fach-Abweichungen (fold change, FC) analysiert und Korrekturen vielfacher Testung wurden durchgeführt. Die Analyse differentiell exprimierter Gene wurde mit Gene Ontology durchgeführt, eine Genclusteranalyse wurde mit PANTHER durchgeführt.

Ergebnisse: 661 Gene waren signifikant verändert bezüglich ihrer Expression bei Anwendung des kontinuierlichen Protokolls (n = 12), 234 Gene bei Anwendung des intermittierenden Protokolls (n = 6; beide mit $p \leq 0.05$ and $FC \geq 1.5$). Mit höherer Signifikanz waren 42 Gene im kontinuierlichen Protokoll und 8 Gene im intermittierenden Protokoll verändert ($p \leq 0.01$, $FC \geq 2$). Die Clusteranalyse mit PANTHER für das kontinuierliche Protokoll ergab signifikant veränderte Gene, die in 3 Pathway-Clustern, 5 Clustern biologischer Prozesse und 2 Proteinclustern organisiert sind. Eine Clusteranalyse des intermittierenden Protokolls ergab keine signifikanten, in Clustern organisierten Gene.

Diskussion: Wir haben beobachtet, dass die Anwendung von Zentrifugation Effekte auf molekulare Mechanismen hat. Da Untersuchungen des Transkriptoms Rückschlüsse auf die Genexpression erlauben, haben wir geschlossen, dass Zentrifugation zu veränderter Genexpression führt. Darüber hinaus zeigten sich Unterschiede hinsichtlich Genexpression zwischen beiden Protokollen. Wir glauben, dass diese Studie die erste ist, die Effekte künstlicher Schwerkraft auf molekularer Ebene untersucht hat.

ABSTRACT

Background: Weightlessness (or microgravity) is known to have multiple effects on human physiology. In absence of gravity, the body has to adapt to the new environment. This adaptation causes changes of cardiovascular, renal, endocrine and neurovestibular function. Furthermore, the disuse of bones and muscles in space leads to structural alterations of these tissues. An important principle to prevent negative effects of microgravity represents artificial gravity training with human centrifuges. The effects of application of artificial gravity have been investigated in numerous studies. Until now, however, no studies have focused on effects of artificial gravity on molecular mechanisms. With this study, we have examined molecular changes caused by application of artificial gravity with regard to the entirety of mRNA (transcriptome) present in the peripheral blood and using the DNA microarray technique.

Methodology: 12 test subjects underwent a mutual 'continuous' centrifugation protocol on a short-arm human centrifuge. A second 'intermittent' protocol was used for 6 of the 12 subjects, additionally. Blood was taken from test subjects before and after each experiment. RNA from each blood sample was isolated and used to generate labeled cRNA, which was competitively hybridized to microarrays. Signals were analyzed using different thresholds of *p*-value and fold change (*FC*) and multiple testing corrections were performed. Analysis of differential gene expression was performed with Gene Ontology, gene cluster analysis was performed with PANTHER.

Results: 661 genes were significantly affected by AG in continuous protocol, 234 genes in intermittent protocol ($p \leq 0.05$ and $FC \geq 1.5$). More significantly, 42 genes were affected in constant protocol and 8 genes in intermittent protocol ($p \leq 0.01$, $FC \geq 2$). PANTHER analysis revealed genes organized in 3 significant pathway clusters, 5 clusters of biological process and 2 of protein classes for continuous protocol and no clusters in intermittent protocol.

Discussion: We have observed that application of centrifugation as the method of generating artificial gravity has effects on molecular mechanisms, using the transcriptomic technique of DNA microarray. Since investigations of the transcriptome allow to draw inferences on the level of gene expression, we have concluded that centrifugation leads to altered gene expression. Furthermore we have observed that application of two different centrifugation protocols has differences on the molecular level. We think that this study is the first to examine effects of application of artificial gravity in terms of molecular mechanisms in humans.

TABLE OF CONTENTS

LIST OF ABBREVIATIONS

ADH	—	antidiuretic hormone (= AVP)
ANP	—	atrial natriuretic peptide
ATP	—	adenosine triphosphate
AVP	—	arginine–vasopressin (= ADH)
BH—FDR	—	Benjamini—Hochberg false discovery rate
cDNA	—	complementary DNA
cGMP	—	cyclic guanosine monophosphate
CO	—	cardiac output, CO = SV × HR
cRNA	—	complementary RNA
CTP	—	cytosine triphosphate
CVP	—	central venous pressure
DLR	—	Deutsches Zentrum für Luft- und Raumfahrt
ECG	—	electrocardiography
EEG	—	electroencephalography
ESTs	—	expressed sequence tags
FC	—	fold change
GLOC	—	*g*–related loss of consciousness
GO	—	Gene Ontology
GTP	—	guanosine triphosphate
HR	—	heart rate
HUGO	—	Human Genome Organisation
IPA	—	Ingenuity Pathway Analysis
ISS	—	International Space Station
LBNP	—	lower body negative pressure
LEO	—	low Earth orbit
LVEDD	—	left ventricular end–diastolic diameter

MMLV–RT	—	Moloney Murine Leukemia Virus reverse transcriptase
NIRS	—	near–infrared spectroscopy
NTP	—	nucleoside triphosphate
p	—	*p*–value
PCR	—	polymerase chain reaction
PKC	—	Proteinkinase C
PKG	—	Proteinkinase G
POMS	—	programs operation manual system
PS	—	processed signal
QCT	—	quantitative computerized tomography
RAAS	—	renin–angiotensin–aldosterone system
RCF	—	relative centrifugal force
RNase	—	ribonuclease
rpm/rps	—	revolutions per minute/second
SAGE	—	serial analysis of gene expression
SAHC	—	short–arm human centrifuge
SV	—	stroke volume
TCVP	—	transmural central venous pressure
TF	—	transcription factor
TPR	—	total peripheral resistance
TTP	—	thymidine triphosphate
ULLS	—	unilateral limb suspension
UTP	—	uridine triphosphate

LIST OF FIGURES

LIST OF TABLES

I. Introduction

I.1. Spaceflight

I.1.1. Historical Perspective

For ages, humankind has been fascinated by the imagination of flight. In mythology, the figures of Icarus and Daedalus appear as evidence for this very human curiosity of lifting off to spheres and moving through the air (figure **I.1**). The craftsman Daedalus and his son Icarus, who had been banished to Crete, nurture ambitions to escape from their involuntary exile and since they cannot flee by sea, they decide to do so by air. A talented craftsman, Daedalus models wings from bird feathers sticking them on his son's as well as his own arms using wax. Then, just before their maiden flight begins, he warns his son not to fly too high nor to low

> Instruit et natum, »Medio« que »ut limite volas,
> Icare«, ait, »moneo, ne, si demissior ibis,
> unda gravet pennas, si celsior, ignis adurat.
> Inter utrumque vola!« […][1]

Icarus, however, neglected his father's warnings and the wax melted more, the higher Icarus flew and thus he lost his wings, plunged into the sea and died. Beside this mythological parable, some attempts of constructing first (unmanned) flying devices can be found in the *Peristera* ('the pigeon'), crafted by the Greek philosopher Archytas, as well as in *sky lanterns* (or *Kongming lanterns*) and *Bamboo–copters* from ancient China. It is said, that the first manned and heavier-than-air flying device has been built by the polymath Abbas Ibn Firnas in the 9th century using the air gliding technique, allowing horizontal flight—the same principle the English Benedictine Eilmer of Malmsbury is said to have used. In the Renaissance, Leonardo da Vinci visioned his famous hang glider in his drawings—an object that was, much later in the 20th century, accurately reconstructed and

[1] Ovid, Met. Liber VIII, Verses 202-206

actually shown to fly. Beginning with the 18th century, hot air balloons as well as aircrafts were sequentially developed and improved.

Figure I.1: *La caduta di Icaro*, Carlo Saraceni (1585—1620), oil on canvas. Reproduced from http://ksbuelach.ch/fach/as/gallerie/myth/daedalus/05.htm

The era of spaceflight starts in the early 20th century. Although the physical principle of an object lifting off the Earth is given as early as in 1687 (first published in *Mathematical Principles of Natural Philosophy*) by Newton's third law (see below), it would take more than two hundred years until the launch of the first object to reach outer space. The Russian scientist Konstantin Tsiolkovsky is regarded as a pioneer in terms of theoretical and technological approaches. With his equation (Tsiolkovsky equation) from the year 1897 and his notable work *The Exploration of Cosmic Space by Means of Reaction Devices,* he contributed the theory of propulsion of heavier-than-air ships, postulating later in his article *Investigation of Outer Space Rocket Devices*, that a launch can be accomplished by a rocket missile using fluid hydrogen and oxygen. The American physicist Robert H. Goddard is considered to be the first to construct and successfully launch a liquid-fuel rocket. With his notable work *A Method of Reaching Extreme Altitudes*, published in 1919, he provided mathematical theory as well as ideas on rocket engineering. The V-2 rocket (Vergeltungswaffe-2) is considered to be the first rocket to reach outer space. The development, which encompassed several years, was led by

German scientist Wernher von Braun, a student of Austro–Hungarian physicist's Hermann Oberth's. During World War II on behalf of Nazi war politics, thousands of V-2 rockets were fired at various cities in the United Kingdom, Belgium, France and as well as the Netherlands, killing thousands of civilians. After the capitulation of the Axis Powers, two 'great powers', the USA and Soviet Union, emerged from the Allies. The following forty years and more, these two great powers competed in terms of military superiority, but also in terms of technological improvement in every thinkable sense. One of the venues of their sedulous competition lied in the field of spaceflight realization, known as the *Space Race*. In the 1950s, Russia sent the first unmanned Sputnik 1 to the orbit, a few months later the US sent their Explorer 1 to space. In 1961, the Russian cosmonaut Yuri Gagarin was the first human to orbit the Earth for about 100 minutes on the spacecraft Vostok 1, a few weeks later the American Alan Shepherd was sent to space on the spacecraft Freedom 7, but did however not orbit the Earth. In the following years, the Americans established their research program Apollo and the Russians their Soyuz, both with similar goals, namely to orbit and to land on the Moon, and both not without sacrifices, for the limping technical improvement could not hold up continuously with the increasing eagerness of the two nations. Finally in July 1969, Neil Armstrong, Michael Collins and Edwin Aldrin launched on the spacecraft Apollo 11 and performed a successful landing on the Moon, where they set foot as the first humans in history, and returned to Earth—an event that marked the peak of the Space Race. Discouraged by this huge achievement of the US, the Soviet Union ceased their ambition for Moon missions and soon, the Space Race ended and cooperation was striven rather than competition.

From the beginning of spaceflight to now, over 300 human missions were performed on which several hundreds of astronauts have been sent to space. During this period, various physiological, partially hazardous conditions due to exposure to weightlessness have been observed in astronauts and cosmonauts. Additionally, several studies have been performed using simulation models of weightlessness. One important aim of research in spaceflight medicine represents the development of effective countermeasures against those physiological conditions in weightlessness. Before we focus on weightlessness, its impacts on humans and possible countermeasures, general physical principles of spaceflight will be discussed first.

I.1.2. What is Gravitation? Physical Principles.

Gravitation is a universal phenomenon between two physical objects. It appears as a force *F* that acts on a body in presence of another body with a certain distance (or displacement) between them. In *Newton's law of universal gravitation* (or simply *law of gravitation*), this connectedness is described as it is sketched below.

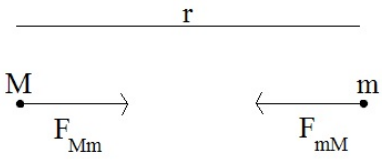

$$F_{Mm} = F_{mM} = \frac{mMG}{r^2}$$

M, m are bodies with different masses, *r* is the displacement and *G* the gravitational constant ($G = 6.67 \times 10^{-11}$ $m^3kg^{-1}s^{-2}$). F_{Mm} and F_{mM} are forces from the body M on m and from m on M, respectively. Their equality is given by *Newton's third law of motion* (action–reaction principle); they are equal in magnitude but show in opposite directions.

For two masses of 1 kg with a displacement of 1 m between them, the force would equal the value of *G* with approximately 6.67×10^{-11} N, an extremely small force. With large masses like the Earth ($M_E = 5.97 \times 10^{24}$ kg), however, the gravitational force becomes large and the effect of gravitation, as we are used to it, becomes apparent.

When *M* is the mass of Earth, the law of gravitation can also be written as

$$F = mg, \text{ where}$$

$$g = \frac{MG}{r^2}$$

g is called *gravitational acceleration*. Its value depends on Earth radius which is determined by the altitude above sea level as well as by the latitude (smallest on the poles, largest on the equator). Approximately, $g = 9.81$ ms^{-2}. It is clear that in order to overcome Earth's gravitation, a force needs to be created, which is greater than the gravitational force of Earth (hypergravity).

Although we consider and experience gravitational acceleration as a constant value on Earth, it is important, however, to emphasize that this is only true because even large heights such as 10,000 m, which can be reached by aircraft, are negligible compared to Earth radius (about 1/60). If an object, for instance, is 6,375 km apart from Earth (which is approximately as large as the Earth radius r_E = 6.375 x 10^6 m), the gravitational acceleration *g*, with which the object is accelerated towards the Earth, is approximately only 2.45 ms^{-2}.

For any given displacement *r* between an object and a gravitating body *M*, there is a corresponding potential energy, which is called *gravitational potential energy U*. The change of potential energy is accomplished by and, hence, proportional to a force *F* and inversely proportional to the displacement *r*,

$$dU = Fdr \Leftrightarrow F = \frac{dU}{dr} \text{ OR } U = \int_C Fdr$$

where the force *F* can be gravitation (attracting objects to each other) or a force in the opposite direction, tearing the object apart from the gravitating body (e.g. rocket propulsion). Through combination with the law of gravitation, the *gravitational potential energy* (or simply *gravitational energy*) can be expressed as

$$\frac{dU}{dr} = F_g$$

$$U = \int_\infty^r F_g dr = \int_\infty^r \frac{mGM}{r^2} = -\frac{mGM}{r}|_\infty^r$$

Thus,

$$U = -\frac{mGM}{r}$$

The gravitational energy can also be described as the energy needed to move an object from infinity to a reference point *r* relative to the gravitating body. When this work is done by gravitation, the values are negative. When an object is torn apart from a gravitating body (e.g. a spacecraft from Earth) to a reference point *r*, the values of *U* are positive.

The *gravitational potential V* is defined as gravitational potential energy *U* per unit mass *m*,

$$V = \frac{U}{m} = -\frac{GM}{r}$$

According to *Newton's first law of motion*, an object that is at rest stays at rest, as well as an object that performs a linear movement stays in a linear movement, as long as the sum of all forces acting on the object remains zero. Since all planets of our solar system rotate around the Sun (as satellites rotate around planets), the sum of all forces cannot be zero. The Sun as well as all planets therein exert forces on each other (as it is stated by Newton's law of universal gravitation), which eventually keep them in orbits.

The motion of planets is described with *Kepler's laws of planetary motion*. Basically, the laws state that movements are elliptic around the Sun, which stands in one of the two foci of the ellipse (*Kepler's first law*). An important parameter of the ellipse is the *eccentricity e.* It is defined as $e = c/a$ (figure **I.2**) and can range from 0 (both foci are on the same point; perfect circle) to < 1, $0 < e < 1$. Regarding figure **I.2**, it is obvious that the greater the eccentricity, the more stretched the ellipse becomes. Planetary motions in our solar system generally show ellipses with a small eccentricity from almost 0 (Neptune's Moon Triton) to 0.2 (Mercury). Furthermore, as a planet rotates, equal areas of the ellipse are swept by the planet in equal intervals of time (*Kepler's second law*). This is expressed as

$$\frac{dA}{dt} = const$$

If *r* is the displacement between the Sun and a planet at a certain point of time and θ the angle that has been swept in an interval of time *dt,* then

$$\frac{dA}{dt} = \frac{r^2\theta}{2} \cdot \frac{1}{dt}$$

This has the following consequence: When a planet is at the nearest point to the Sun (*periapsis* generally or perihelion, when speaking of the Sun), the tangential speed of the planet is the largest, similarly when a planet is at the farthest point to the Sun (*apoapsis* or aphelion, respectively), the tangential speed is the lowest. Also, the angular speed is not constant. Of course, this is also true for spacecraft, since their motion is based on the same principles as is the motion of planets around the Sun. The physical reason for variations in

tangential speed lies in the fact that gravitation is inversely proportional to the square of the displacement, as it is stated above in the law of gravitation.

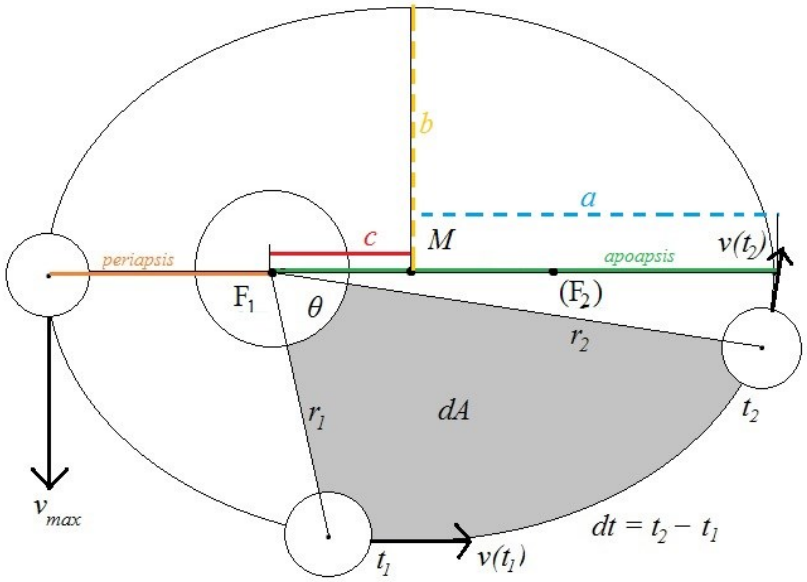

Figure I.2: *Kepler's first and second law of planetary motion*. A planet is rotating around a gravitating center F_1 (i.e. the Sun) in an elliptic orbit. The quotient *dA/dt* is constant (*area velocity*). The orbital speed *v* (*tangential bold arrows*) is inversely proportional to the root of the distance r_x at a certain point of time t_x. It is the largest at periapsis (v_{max}) and the smallest at apoapsis (v_{min}). The same is with angular velocity $d\theta/dt$. *a* is called the semi–major axis (blue dotted line), *b* the semi–minor axis (yellow dotted line). c is the linear eccentricity c, not to be confused with eccentricity (see text).

I.1.3. Overcoming Earth's Gravitation

Rocket launch is based on the following principle: The rocket is provided with a tank that contains a chemical propellant, which can either be solid, liquid or hybrid. By combustion of the propellant, the mass of the content in the tank (and thus of the rocket) becomes smaller or —one can say—mass is being expelled. Combustion can, in this case, be regarded as a measure for how fast expulsion of mass happens. The force with which mass is expelled implicates a reaction force in opposite direction, according to Newton's third law, which is called the *thrust*. The thrust provides a change of velocity (acceleration), which is described by the *Tsiolkovsky rocket equation*

$$\Delta v = v_e \ln \frac{m_0}{m_1}$$

where v is the velocity change, m_0 is the mass of the rocket before firing, m_1 is the mass at a certain point of time and v_e is the effective exhaust velocity. The effective exhaust velocity (not to be confused with escape velocity) is described with the equation

$$v_e = I_{sp} g_0$$

where g_o is the gravitational acceleration at sea level and I_{sp} is the *specific impulse*. The specific impulse is a measure for the force (or thrust) that can be generated with respect to the mass or weight of propellant. When propellant is given as mass, the specific impulse has the unit of speed [m/s]; when given as weight, the impulse has the unit of time [s].

In order to reduce the mass of the propellant required, launching is ideally performed near the Earth's equator and towards east where the *tangential speed* with approximately 463 m/s (or 1,667 km/h) is the largest. This tangential speed can be 'added' to the generated Δv in order to create at least orbital speed.

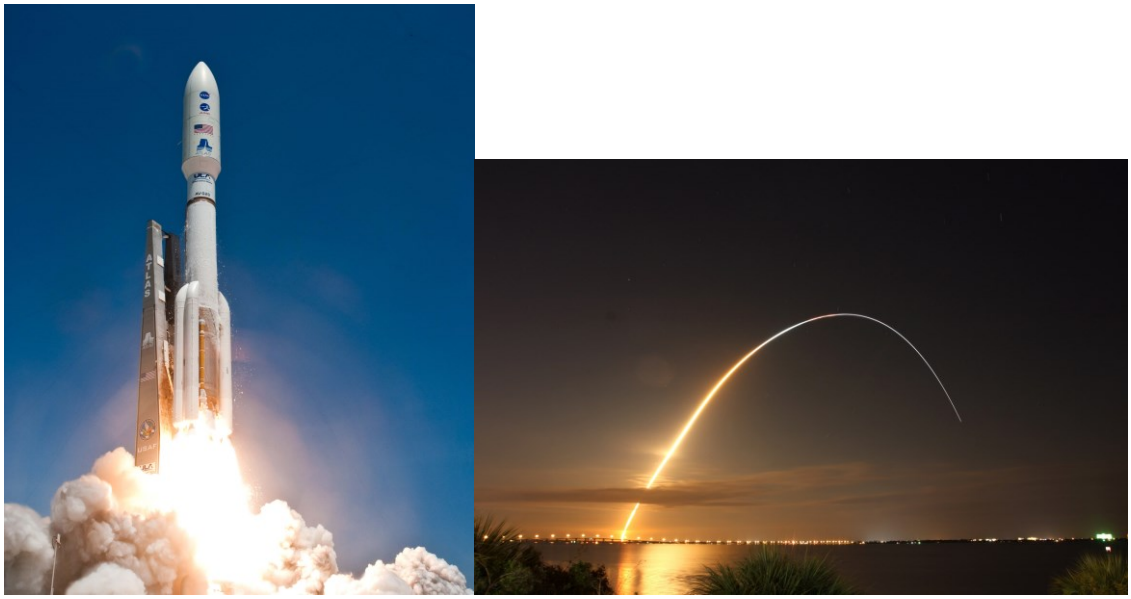

Figure I.3: *Rocket launch close-up (left side) and viewed from a certain distance (right side)*. Reproduced from http://www.nasa.gov/mission_pages/juno/launch/#.UwyqtbQ4nHQ (left) and http://roxannestclaire.com/blog/?p=1307 (right)

After launching, a spacecraft performs a nearly vertical flight that eventually becomes orbital (figure **I.3**, right side). It has to reach at least 150 km of height (thermosphere) for at this height, the atmosphere is rather thin causing only little drag and negligible decelerations. Depending on the planned route, the spacecraft is placed into an orbit where its further motion is provided by gravitation of planets and the Sun, respectively, as the abovementioned physical principles obtain (figure **I.4**). When a spacecraft has reached the desired orbit, it rotates with *orbital speed* v_O. The orbital speed is the speed required for an object m to stay in orbit of another object M, where m and M are masses of the objects and m is negligible compared to M. In other words, the centrifugal force $|-F_Z|$ acting on the rotating object must equal the gravitational force F_g acting on the object (or, equally, the centrifugal acceleration $|-a_Z|$ must equal the gravitational acceleration g)

$$F_Z = Fg \Rightarrow \frac{mv^2}{r} = \frac{mGM}{r^2} \Rightarrow \frac{v^2}{r} = \frac{GM}{r^2} \Rightarrow a_Z = g$$

hence,

$$v_O = \sqrt{\frac{GM}{r}}$$

It is clear that the orbital speed is inversely proportional to the distance r between a launched object and the planet, as it arises from Kepler's second law (see above). As a spacecraft performs an orbital motion with its orbital speed, it actually 'falls freely' around the planet (the Sun, respectively) without ever hitting it. As during a *free fall* is to expect, both the spacecraft and the astronauts are falling with the same speed around the Earth when orbiting it. This leads to weightlessness, as it will be discussed below in the next chapter (*m'* and *m''* in figure **I.4**)

The speed required to leave an orbit without ever getting dragged back by the gravitating body is called *escape velocity* v_E. Escape velocity arises from *conservation of energy* and can be expressed as the speed required to move an object m from a certain point to infinity so that in infinity, the kinetic energy E_{kin} of the object as well as the gravitational potential energy U (see above) of the gravitating body M become zero, where m is negligible compared to M.

$$E_{kin} + U = \frac{1}{2}mv^2 + \left(-\frac{mMG}{r}\right) = 0$$

hence,

$$v_E = \sqrt{\frac{2GM}{r}}$$

Both orbital speed and escape velocity are valid, if m is very small compared to M and therefore negligible. The equations can be applied when, for instance, the Earth m (~10^{24} kg) is orbiting the Sun M (~10^{30} kg), as well as when a spacecraft m is orbiting the Earth (or any other planet or the Sun) M.

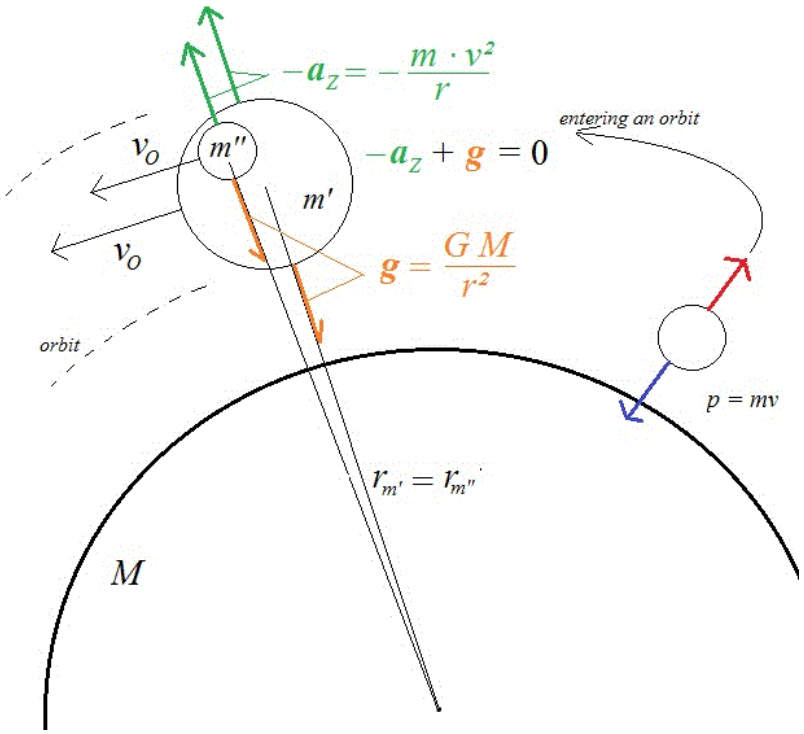

Figure I.4: In order to launch (right side) from the Earth M, a momentum has to be created (blue arrow). Its reaction (red arrow) pushes the spacecraft up. After a horizontal flight, the spacecraft enters an orbit and moves along with orbital speed v_O. Therefore, centrifugal acceleration $-a_Z$ must equal the gravitational force g. Since the spaceship m' and the astronaut m'' are negligible compared to the mass of Earth M, they 'fall' with the same orbital speed v_O around the Earth. In order to leave the current orbit towards one with a greater distance r, m' and m'' would need to accelerate to *escape velocity* (v_E; not shown).

I.1.4. Weightlessness and its Impact on the Human Body. Spaceflight Deconditioning.

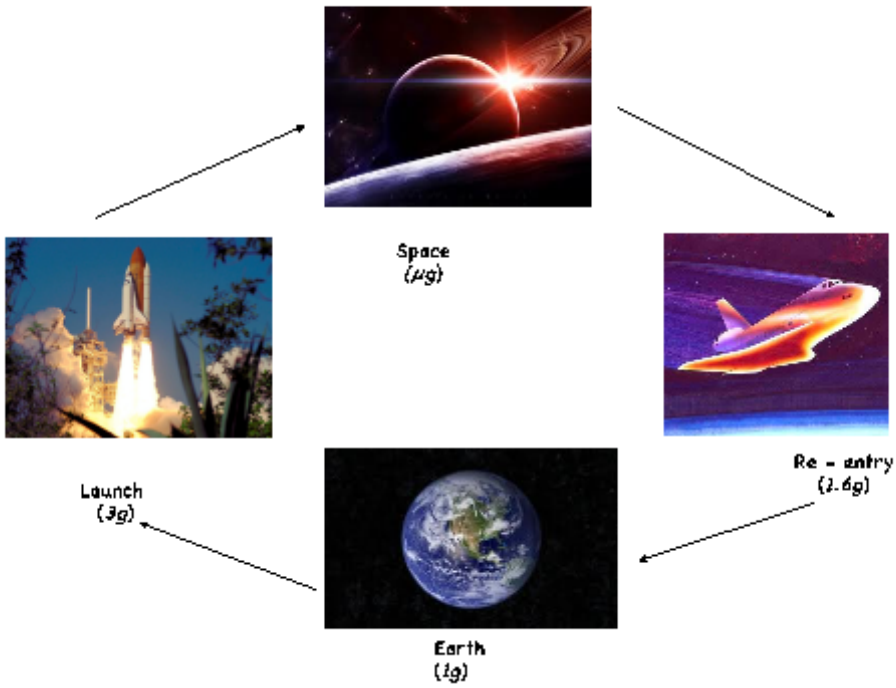

Figure I.5: During launch (left), accelerations have to be generated that are beyond gravitational acceleration *g* (hypergravity). As soon as a spacecraft enters an orbit, it performs a free fall around a center of mass, leading to weightlessness on the craft (microgravity). The reentry leads again to at least gravitational acceleration *g* or more.

Weightlessness is a state, where the gravitation of an orb (e.g. the Earth) on an object with a mass like the human body is abolished. Since gravitation is inversely proportional to the square of the displacement, it approaches to zero as the displacement approaches infinity and is therefore never completely abolished. We also speak of *microgravity*; thus, the terms 'weightlessness' and 'microgravity' will be used synonymously.

On Earth, weightlessness can occur during a free fall or a parabolic flight with an aircraft for short periods of time. In space, spacecraft and so to speak astronauts mostly orbit and operate in the Low Earth orbit (LEO) at a height of approximately 370 km, a height that is not sufficient to overcome the Earth's gravitation. At this height, the gravitational acceleration averages about 90% of the gravitational acceleration on sea level. Nevertheless, weightlessness occurs in this case due to equality of centrifugal force (forcing the object to vanquish Earth's gravity) and gravitation, which represents the centripetal force (forcing the object towards the Earth), as it was shown in the previous

chapter. Due to the equality of gravitation (centripetal force) and centrifugal force, there is a balance of forces in both directions equally to free fall (figure **I.4**)

To all creatures on Earth, gravitation is essential and—so to speak—inherent. All life has developed under influence and perpetuous impact of gravitation. Thus, weightlessness, although not directly threatening, is an abnormal condition to humans as it is to other species and is followed by physiological adaptational and counteregulatory mechanisms (figure **I.6**)

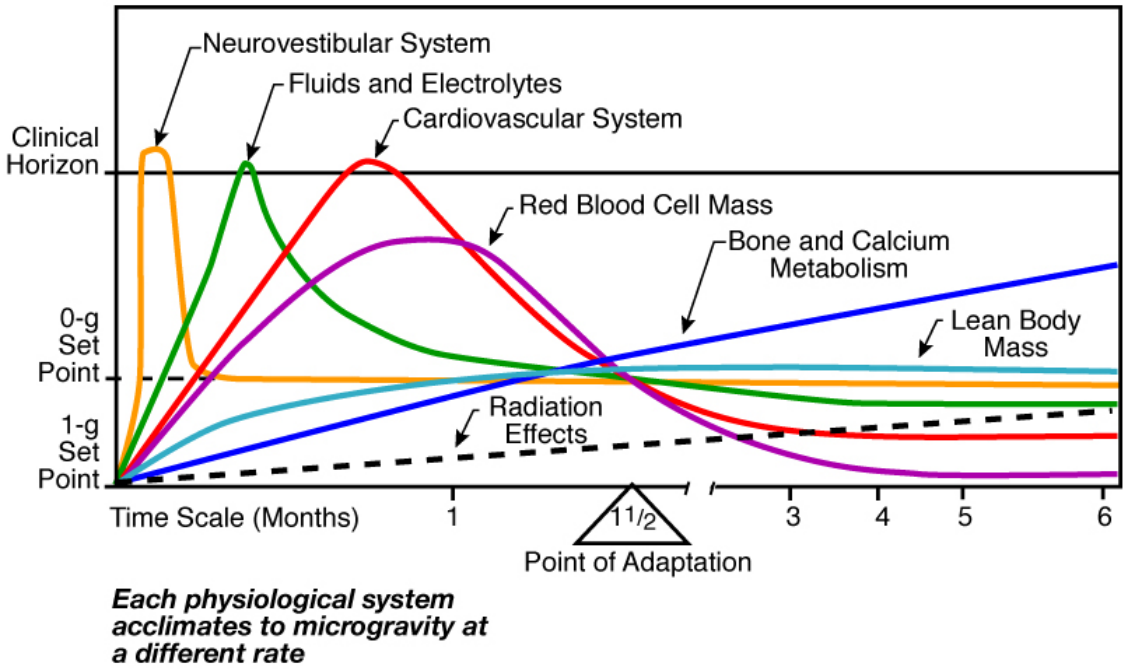

Figure I.6: *Physiological effects of microgravity and associated adaptations*

Due to microgravity, all anti–gravitational **muscles** mainly in legs and back, i.e. muscles required for standing or maintaining an upright posture, are not required to the extent compared with their usage on Earth, which induces their atrophy (1,2). Studies performed with astronauts or persons who have been exposed to actual microgravity ordinarily show a low number of test subjects (3), but do however reveal a decrease of muscle mass (4-6). An established model for simulating the effects of microgravity on the muscles represents prolonged bed rest over days to months, often combined with head–down tilt (7) as well as unilateral limb suspension (ULLS). In astronauts as well as in test subjects of both models, a descrease of whole muscle mass has been shown (8-10). It has been suggested that it is not only the absence of gravity, which causes muscle atrophy and muscle weakness, but

also an alternated neuro–muscular interplay (11) as well nutritive factors with a lower food intake during space missions (12).

Similarly, as long as **bones** are not required for static and postural purposes, bone substance tends to diminish (13). Investigations on bone density were already performed during American Gemini and Apollo missions using X–Ray photodensitometry (14), single–photon densitometry as well as determining Ca^{2+} balance (14,15), that showed altogether a decrease in bone density, especially in the calcaneus, combined with an increase of Ca^{2+} excretion. Similar results were gained from Skylab missions (16,17) as well as during Russian investigations from Soyuz and Mir missions (18-20), which also included analyses of alternations of secretion of n–telopeptide and osteocalcin, the former being a bone resorption marker, the latter a bone formation marker (21). Later, from the period of the International Space Station (ISS) on, quantitative comupterized tomography (QCT) was added as a more sophisticated method for examination of bone density, which confirmed the loss of bone stubstance and contributed further information on its morphological and structural nature (22,23). Similar to studies concerning microgravity–induced muscle atrophy, bed rest studies play an important role as a model mechanism for bone demineralization (24,25). Such studies have provided similar results, namely a decrease in bone density and alterations of bone markers (26-29). As to expect, there is also a connection between muscle atrophy and decrease of bone density due to unloading (30).

Concerning the **cardiovascular system**, various and partially severe changes can be observed during exposure to weightlessness. In absence of grativy, an instant upward shift of blood towards higher body compartments such as abdomen, thorax and head is to expect, leading to an increase of preload and afterload (figure **I.7**). First, it was assumed that—due to increase of blood volume in the thorax—the central venous pressure (CVP) would increase. In fact, it was shown that the CVP drops in microgravity to lower levels compared with reference values on Earth (31)—contrary to prior postulations as well as to intuitive understanding of basic physiological principles. At the same time, it was observed that stroke volume (SV) and cardiac output (CO) increased in weightlessness in the initial phase of hours after exposure (32). The exact mechanism of these two coexisting, physiologically contradictory phenomena (decreased CVP and increased SV and CO) are not fully explained yet; however, besides a decreased CVP, a decreased interpleural (or

intrathoracical) pressure—measured indirectly by esophageal pressure—, as well as an increased transmuric CVP (TCVP) were registered during parabolic flights, furhter suggesting that an increased diameter of the left atrium and, thus, increased cardiac filling (referred to as left ventricular end–diastolic diameter, LVEDD) as well as an increased stroke volume accrue from the fact that interpleural pressure decreases to a greater extent than the CVP does (33). Increased atrial diameter leads further to an enhanced excretion of atrial natriuretic peptide (ANP). On one hand, ANP affects resistance vessels (arterioles) such that through binding on its receptors NPR1 and NPR2, it activates a membrane–bound guanylyl cyclase leading to an increase of cGMP, which activates protein kinase G (PKG) and which eventually phosphorylates Ca^{2+} channels of vascular smooth muscle cells, leading to a decrease of cytosolic Ca^{2+} and thus relaxation of the smooth muscle (vasodilatation). On the other hand, ANP also affects the kidneys, leading to vasodilatation of vasa afferentia and, in further consequence, to diuresis, as well as to cGMP dependent phosphorylation of epithelial sodium channels (ENaC) in collecting tubes and thus to decreased sudium reabsorption (decreased natriuresis) and inhibiting secretion of renin and aldosterone. Vasodilatation of resistance vessels leads to a diminished total peripheral resistance (TPR) and, hence, to a decreased diastolic blood pressure, which is also documented to occur during spaceflight (34). However, the role of ANP in cardiovascular deconditioning is still not well understood (figure **I.8**).

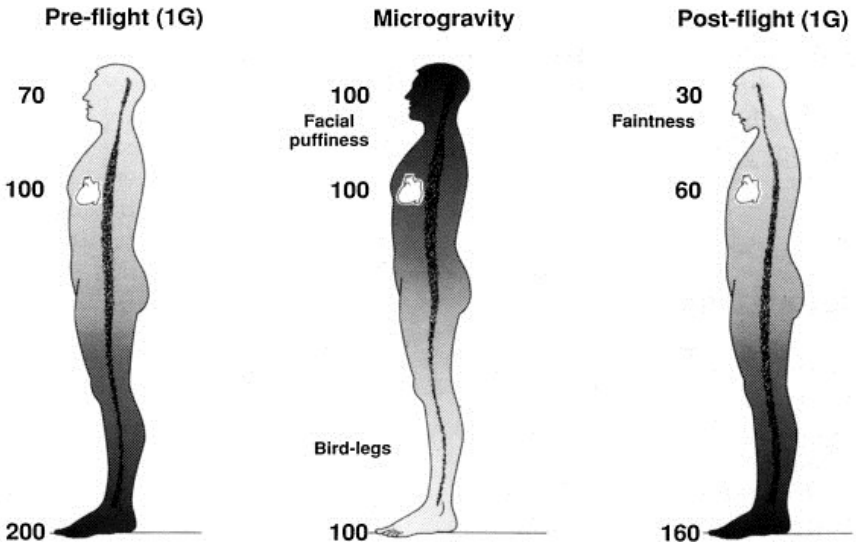

Figure I.7: Effects of entry into weightlessness and of return to Earth with respect to the cardio-vascular system, reproduced from Watenpaugh and Hargens, 1996

Numerous model mechanisms are used for simulation of microgravity and studies of cardiovascular deconditioning, such as ground–based bedrest studies with head–down tilt (see below) and immersion, which can be both used for studies of long–term effects, but also parabolic flight for studies of short–term effects of weightlessness. It is crucial, however, to emphasize that ground–based investigations cannot reproduce alterations of hydrostatic pressure that occurs in real weightlessness. Effects of these alterations are therefore not well understood yet, especially when it comes to fluid shifts and regulation of the vessel tonus (35). Concerning, plasma volume, bedrest studies have shown similar results to those of spaceflight, however (36).

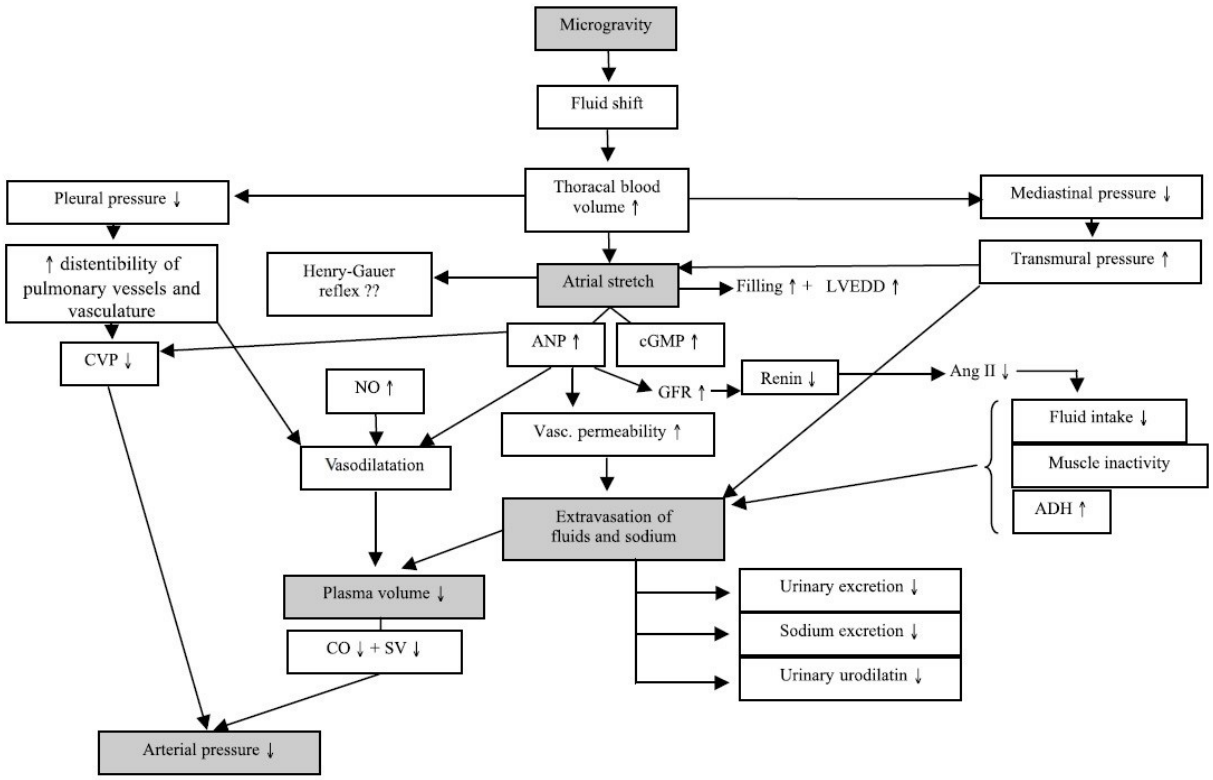

Figure I.8: *Physiological effects of weightlessness at the initial state*, reproduced from Aubert, Beckers and Verheyden, 2005

After prolonged stay in microgravity, **adaptational mechanisms** (figure **I.9**) can be observed that are contrarious to initial cardiovascular changes, mainly a decrease of stroke volume as well as persisting low ANP levels and a decreased atrial diameter (37,38), most likely resulting from a decreased plasma volume. Also, a reduction of left ventricular mass was shown (39), being of major importance for cardiac atrophy (40). An established model

for cardiovascular changes—similar to investigations on bone density and muscle mass—represents prolonged bedrest with head–down tilt of 6° (41). The tilt induces an upward shift of blood towards thorax and head just like in actual microgravity. Mean heart rate and heart rate variability were shown to remain unchanged in prolonged weightlessness (42). Likewise, in bedrest studies an initial increase of LVEDV after one hour of bedrest was shown, followed by a decrease of LVEDV after weeks of experiment—a circumstance that was observed earlier, as it is mentioned above. Furthermore, the very same study provided insights in how countermeasures can affect and modulate physiological adaptations to microgravity (43). Similarly, alterations of left atrial and ventricular volumes were also reported during parabolic flights (44). Also, altered sympathetic activity in astronauts during spaceflight was observed, in the first place elevated levels of norepinephrine in plasma but also increased sympathetic activity, expressed as sympathetic bursts in peroneal nerves explored with microelectrodes. (45), a finding that is consensual with increased levels of norepinephrine as depicted above. Moreover, the vagal limb of the baroreflex was reported to be degraded during spaceflight (46,47).

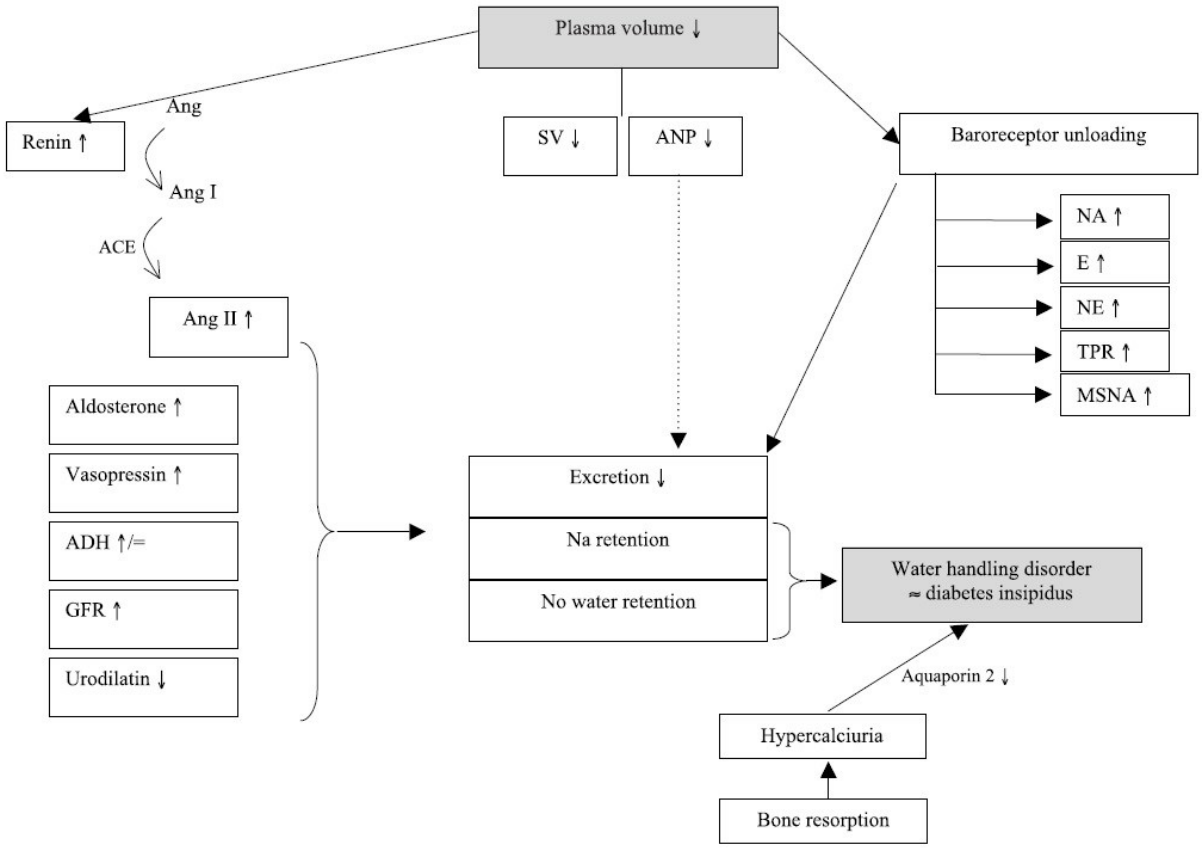

Figure I.9: *Physiological effects after prolonged microgravity*, reproduced from Aubert, Beckers and Verheyden, 2005

The most prominent changes in **renal funtion** as a concequence of microgravity concern hypercalciuria—elevated calcium concentration in urine that is caused by bone demineralization—leading to an increased risk of developing renal stones, most of them consisting of calcium phosphate and calcium oxalate (48,49). In the beginning, an increase of circulating blood volume was suggested due to the upward shift of blood in absence of gravity and, in further consequence, stronger natriuresis and diuresis due to weightlessness (50). It was widely assumed that this centralization of blood would lead to an increased *Henry–Gauer response* (51): An increase of circulating blood volume is registered by baroceptors located in the right atrium and transduced to the pituitary gland, where secretion of arginin–vasopressin (AVP, also called antidiuretic hormone ADH) is inhibited, thus that AVP–induced resorption of sodium and water (by AVP–mediated expression of *aquaporin*–2 in colleting tubules) is decreased. In fact, urinary excretion remains normal or even becomes lower in weightlessness (52-54). Interestingly, increased urinary concentration of calcium also modulates aquaporin–2 (55). An important impact on water homeostasis and diuresis is also represented by diminished fluid intake during a space mission as well as by diminished dermal evaporation (54). A net sodium and water retention has been observed during spaceflights and simulation analogues, leading to increased body weight, and the extent of sodium retention has been reported to be greater than the one of water retention (56). Changes of ANP have been a controversial but very little studied topic, however. Although it has been proposed that ANP does not contribute to natriuresis during spaceflight to a great extent (53), a recent Chinese investigation has reported an increased expression of ANP in rats after simulated microgravity (57). Even after infusion of isotonic saline solutions, urinary excretion seems to be lower compared to reference levels on Earth. (58). Also, an enhanced activation of the renin–angiotensin–aldosterone system (RAAS) has been reported (54). Even though prolonged bed rest represents a good model for studying effects of weightlessness on muscles and bones (see above), it does only partially apply for the renal (and the cardiovascular) system, however (38). This is due to the fact that in spaceflight, sodium retention and activation of the sympathetic system seem to be stronger than in model mechanisms such as bedrest (59).

Effects of microgravity on **blood cells** comprise a decreased number of erythrocytes but also of reticulocytes, as well as decreased levels of erythropoietin (60,61).

I.1.5. Spaceflight–induced Orthostatic Intolerance

Spaceflight deconditioning refers to physiological changes that rose within weightlessness and that appear after returning to Earth with its environment of 1*g*, chiefly cardiovascular changes (62). The most common problem amongst astronauts outlines orthostatic intolerance that is defined as demeanor of sypmtoms such as palpitations, dizziness, nausea and impaired vision and signs such as tachycardia, paleness or even syncopy in upright posture and that can affect between 9 and 64% of astronauts (37). Causes for orthostatic intolerance are multifactorial: deficiency of plasma volume (hypovolemia), alterations of vascular compliance and of regulation of total peripheral resistance (TPR), reduction of heart mass (cardiac atrophy) as well as altered capillary filtration (63). All of these issues are determining factors of a sufficient SV; while plasma volume and the heart's size determine the preload, the afterload is concordantly changed with TPR. A decreased SV leads to cerebral hypoperfusion and thus to neurological symptoms and is counterregulated with an increase of heart rate (HR), provided by the sympathetic nervous system, in order to maintain the currently needed CO, according to CO = SV × HR. Also, alterations of the baroreflex are regarded as a potential cause for orthostatic intolerance (64). In a study performed with 27 astronauts, the cerebral blood flow was explored before and after flight and during a stand test. The study reported significant differences between finishers (subjects who could perform the stand test over 10 minutes) and non–finishers in blood pressure and mean blood flow velocity of the middle cerebral artery (65). Another study reported an alteration of arterial and aortic compliance in astronauts, which can also contribute to orthostatic intolerance after return (66).

Figure I.10: The effect of *spaceflight–induced orthostatic intolerance* can be seen upon return to earth: The Russian cosmonaut is unable to walk.[2]

[2] reproduced from http://www.thetimes.co.uk/tto/science/space/article3462376.ece

I.2. Artificial Gravity

Artificial gravity, as the name suggests, means artificially created acceleration (or force, respectively) that can be applied to an organism. Physically, artificial gravity can be generatad employing either rotation or linear acceleration.

In the principle using **rotation** (figure **I.11**), centrifugal acceleration is the substitute for gravitational acceleration and equals the centripetal acceleration but in opposite direction (not towards the center of rotation). *Centripetal acceleration* a_Z is directly proportional to the radius r and to the square of *angular* velocity ω, expressed in the equation

$$a_Z = \omega^2 r,$$

where the *angular velocity* ω—the swept angle $d\theta$ in an interval of time dt—is the product of 2π (angle of a whole cirlce in radiant) times rotational frequency f (revolutions per second),

$$\omega = \frac{d\theta}{dt} = 2\pi f$$

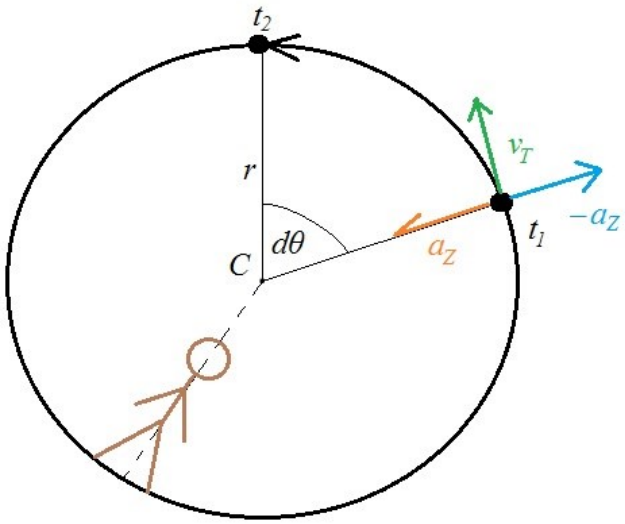

Figure I.11: *Creation of artificial gravity using the principle of rotation* (centrifuge). $-a_Z$ is the centrifugal acceleration and the substitute for gravitation. $-a_Z$ is equal to centripetal acceleration a_Z but antiparallel. The angular velocity ω is a pseudovector and shows from C towards the reader (right–hand rule)

The *centrifugal force* is a fictious force that appears for an observer located in a rotating reference frame due to *inertia* (e.g. in a rotating device in which a human is placed; also the Earth represents a rotating reference frame). A rotating body needs a continous force (F_Z, centripetal force) in order to perform an orbital movement, otherwise the body would go along v_T (figure **I.11**, green arrow) as soon as the centripetal force disappears (see also *Newton's third law of motion*, chapter I.1.2). v_T is the *tangential speed* of the rotating object. It is proportional to the angular velocity ω and to the radius r,

$$v_T = \omega \times r.$$

In three dimensions, v_T is the cross product of ω and r. In two dimensions, however, it simplifies to the dot product $v_T = \omega \cdot r$.

Similarly, the *Coriolis force* is another fictious force, which can also only be experienced whithin a rotating reference frame and which is likewise due to inertia. If e.g two persons were seated opposite and face to face on a rotating centrifuge and one threw a ball to the other one, both persons would observe a curved path of the ball. In a counter–clockwise rotating centrifuge the thrower would obsrerve a right–curved path and the catcher a left–curved one. If the path of the ball, however, is observed from an inertial reference frame (i.e. from outside), the path of the ball appears as a straight line. The Coriolis force is proprtional to the angular velocity,

$$F_C = -2m\omega \times v$$

where m is the mass of the rotating body, ω the vector of angular velocity and v the tangential velocity.

The 'force' exerted on a person who is placed in a centrifuge (as it is depicted in figure **I.11**) is called *relative centrifugal force* (RCF) and is definded as the ratio of the generated acceleration a_Z and the gravitational acceleration g,

$$\mathrm{RCF} = \frac{r\omega^2}{g}.$$

RCF is without dimension but very often—incorrectly—referred to in g (ms^{-2}).

While creation of linear acceleration plays a role during the launch of a spacecraft leading to multiple *g*s (hypergravity) and is abolished as soon as a spacecraft enters its desired orbit and runs out of fuel, the technical implementation of centrifugal force generating devices can be realized through *centrifugation* or—theoretically—through a rotating spacecraft. In both cases—according to the equation above—, either larger radii or higher rotational frequencies have to be implemented in order to achieve higher centrifugal accelerations and thus levels of *g*. However, both parameters are limited in increase in different ways. Firstly, as a centrifuge represents a rotating reference frame, fictious forces appear within, such as the centrifugal force and the Coriolis force. While the centrifugal force can be felt as the sensation of being pulled down towards the feet (figure **I.11**), the Coriolis force acts on the endolymph in the semicircle canals of the inner ear, which are responsible for registration of rotations and which are integrated in perception of the position of the head relative to the surrounding. Head movements during centifugation increase the Coriolis forces on the endolymph. The conflict between the sensation of the position and the actual position can cause motion sickness with symptoms like disorientation, vertigo and nausea. The Coriolis effect and thus symptoms of space sickness depend on the rotational frequency (as it is stated above in the equation) and are stronger, the higher the frequency is. Secondly, larger radii of a centrifuge demand more space and more powerful machines and are thereby limited in terms of constructional realizability. In order to create a centrifugal acceleration of 1*g* at 2 rpm (revolutions per minute) or, equally, 1/30 rps (revolutions per second)—a rotational frequency that mildly affects the vestibular system—the required radius would amount to 223.6 m, which would demand a centrifuge or a spacecraft of nearly half a kilometer in diameter, not to speak of disproportionally more powerful machines that would be required in order to propel such a centrifuge. Thus, as the construction of such large centrifuges has not succeeded yet, higher rotational frequencies must be accepted. Theoretically, gravity could also be generated with mass or magnetism, in first case even natural gravity. The mass, however, that would be required to create 1*g* would have to be so large that a launching procedure would become impossible; similarly with the weight of magnets, besides the high current in the region of some megawatts that would be required.

Effects of microgravity, espcially those of fluid redistribution as well as those on the cardiovascular system and on bones can be reduced by applying artificial gravity to human body. Artificial gravity created by short–arm human centrifuges (SAHC) represents a practicable method for this purpose.

I.2.1. Historical Perspectives

Practically, centrifugation is the only realizable method to create artificial gravity. As early as in the late 18th century, Erasmus Darwin was the first to describe medical impacts of a centrifuge on human body. Later, under Ernst Horn who became the first professor of psychiatry in Germany in the early 19th century, a rotating bed (*Drehbett*; figure **I.12**) was constructed in order to treat mental ilnesses; a patient was placed into the bed in supine position with his/her feet towards the center—the opposite direction than the one that is used in a modern short–arm human centrifuge. Although the Drehbett was operated by human power, levels of 4—5 g could still be reached in the region of the patient's head for about 1—2 minutes of treatment period. Symptoms that were documented, included nausea and vomiting, dyspnea, slight tachycardia and hyperthermia and vertigo after the procedure (67).

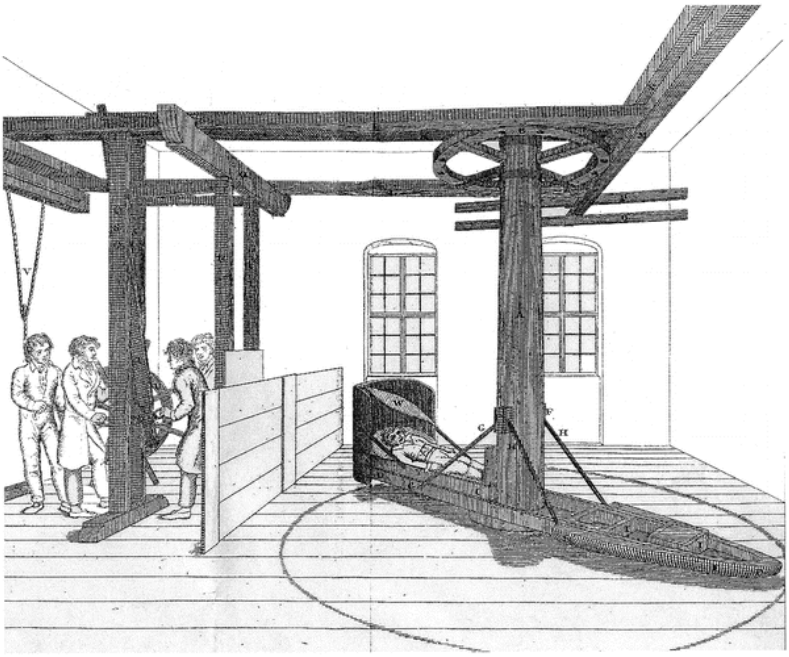

Figure I.12: *A centrifuge in the early days*. Reproduced from Harsch et al., 2006.

During World War I and II and with progressing airflight, impacts of *g*–related loss of conciousness (GLOC) became apparent in combat manoeuvres, leading to multiple accidents due to 'human failure'. In the 1950s, Oberth, von Braun and Clarke proposed centrifugation as a countermeasure for adversed effects of microgravity. Since a rotating spacecraft is technically challenging and aims of developing have not been successful yet, main devices remain human ground–based centrifuges as well as human powered on–board centrifuges.

I.2.2. Human Centrifuges

Mainly, two types of human centrifuges can be differentiated, one being short–arm human centrifuges (SAHC), the other large radius human centrifuges.

An **SAHC** (figure **I.13**) is a centrifuge with an armwidth of about 2—3 m, in which a person is positioned directly on a rotating arm that represents the radius of the rotating device, with his/her head towards the center (axis of rotation) and his/her feet towards the circumcircle of rotation (brown stickman in figure **I.11**), either supine or seated. Since the centrifugal force—as it was mentioned above—is directly proportional to the radius, different forces and thus levels of *g* arise throughout the body. Parts that are located near the center (like the head) underlie to lower levels of *g* or even near to zero gravity, whereas parts near the circumcircle can be affected by multiple g levels ('*gravity gradient*'). Since the armwidth (radius) is constant, different levels of g can only be created by varying rotational angular velocity ω by increasing or decreasing the amount of rpm, ranging from 5 to 40 rpm and thus creating g levels from 0.1 to 4 *g*—depending on the location of the particular body part.

Figure I.13: *Short–arm human centrifuge* (SAHC) in the *Deutsches Zentrum für Luft- und Raumfahrt* (DLR), Cologne. Reproduced from http://www.dlr.de

The principle of **a large radius human centrifuge** is the same but with few differences. Firstly, in contrast to the SAHC, the armwidth is much longer, about 7 m in average, but can also reach up to 15 m like in the Naval Air Warfare Center Warminster (NADC) centrifuge. The advantage of a longer arm is that lower rotational angular velocities (and thus rpm) are required in order to generate the same level of *g* compared with an SAHC. Secondly, in a large radius centrifuge a person is seated in a so called gondola—a closed facility that is equipped with communication features such as closed circuit television (CCTV), a gadget for monitoring the person during testing runs, as well with air and water support. A gondola can be rotated in different directions, adjusting a test person to different forces relatively to the rotational movement of the centrifuge. If the test person, for instance, is seated with his/her left body side towards the circumcircle and his/her right side towards the center of rotation, the gravity gradient increases from the right to the left side of the body, which means that his/her right body parts underlie to lower *g* levels than those on the left. This is expressed as $+G_y$. Alternatively, if the test person is seated with his/her back towards the circumcircle of movement of the gondola and the front towards the center of rotation, the gravitational gradient increases from the front to the back (colloquially called 'eyeballs in' by astronauts), which is expressed as $+G_x$. Finally, if the

test person is positioned horizontally (like in supine position in an SAHC, as it was mentioned above), the gravitational gradient increases from the head to the feet, expressed as $+G_z$ (figure **I.14**).

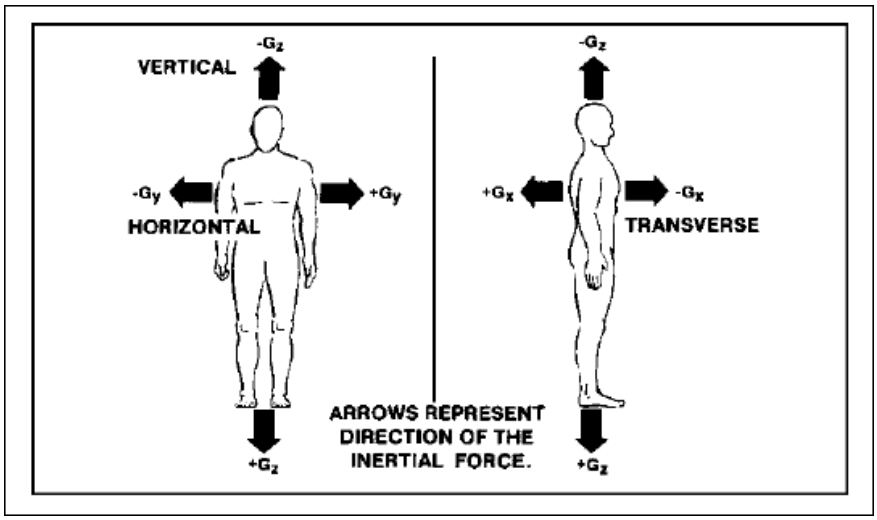

Figure I.14: *Forces obtaining during centrifugation and their directions*, reproduced from http://www.cavalrypilot.com/fm1-301/ch4.htm

x, *y* and *z* refer to directions given in a Cartesian coordinate system with three dimensions, where + and – mark the directions of the force vectors and where the minus sign refers to opposite directions than the ones depicted above. It is obvious that, in order to simulate gravitation, it is important to operate in the direction of $+G_z$, resulting in a pull–down of blood towards the feet, which normally shifts up in weightlessness. Simultaneously, $+G_z$ is also of prior interest to high–g training for any pilots or astronauts, for in this situation and especially under multiple *g*s, blood is continously hindered from reaching the brain, since the heart cannot sufficiently compensate the ongoing pull–down, a circumstance that can culminate in visual impairments and GLOC and that can be fatal to a maneuvring pilot or a launching astronaut when he/she has to sustain multiple *g*s.

I.2.3. Artificial Gravity Training in Medical Research

Numerous papers have investigated the effect and benefit of application of artificial gravity, especially of SAHC, on the human body in terms of—especially—skeleto–muscular and cardiovascular changes induced by weightlessness. A study, which compared a group of test subjects after 21 days of bedrest with a second group of those with bedrest, to whom centrifugation was applied daily for a duration of one hour and *g* levels of 2.5 at the feet, showed that the cross–sectional area of the soleus muscle was reduced in the bedrest group but not in the artificial gravity group. Similarly, the strenght of the musle (torque–velocity) was significantly reduced in the bedrest group compared to the artificial gravity group (68). Another head–down tilt bedrest study for 14 days, which contained a group of test subjects to whom artificial gravity (centrifugation) was applied on 10 of 14 days and a control group with bedrest alone, showed a significantly lower loss of plasma volume in the centrifugation group (–5.0 ± 2.4%) compared to the control group (–16.4 ± 1.9%). Also, the increase of mean heart rate (gained from continous recordings during the study) was significantly greater in the centrifugation group than the one in the control group. Furthermore, the study showed significantly elevated angiotensin levels in the control group as well as decreased sympathetic activity in the centrifugation group but increased in the control group (69).

A lately published head–down bedrest study with 14 test subjects, who were similarly assigned to either an artificial gravity group (centrifugation for one hour a day) or a control group over a period of 21 days, showed a significantly better orthostatic tolerance in the centrifugation group than in the control group. The orthostatic tolerance was indirectly evaluated as the maximum time a test subject can withstand in 80° head–up tilt until the demeanor of presyncopal symptoms and signs. Consensually, norepinephrine elevations were significantly greater after 80° tilt in the centrifugation group than in the control group (70).

Application of artificial gravity on the human body, however, also entails undesired side effects. Among those, the most prominent one represents the Coriolis effect (see above). Effects of Coriolis forces on the canals of the labyrinth comprise symptoms of disorientation, vertigo, nausea and emesis (*motion sickness*) and are stronger, the greater the angular velocity is. Despite the fact that disorientation can be problematic in

maneuvres, which might be more important for aircraft pilots than for astronauts (71), motion sickness is a crucial psychological factor and can lead to decreased motivation for astronauts in order to maintain their required on–board training schedule. It has been shown, however, that one can adapt to Coriolis–induced misperceptions with time (72). Furthermore, it has been shown that arterial pressure drops as a consequence of motion sickness; a fact, that also limits the application of artificial gravity in terms of intensity (73).

It has been pointed out that it is unclear whether artificial gravity (centrifugation) alone is powerful enough to prevent loss of bone substance. Moreover, bedrest studies are rather partly convincing, as they are very often performed with untrained test subjects, in whom application of high levels of *g* is limited by earlier demeanor of symptoms of orthostatic intolerance during centrifugation as well as by symptoms of motion sickness. Although effectiveness of an SAHC as countermeasure has been shown in regard to cardiovascular function and muscle atrophy, little is known about duration and intensity of artificial gravity required. It has been suggested that intensity of artificial gravity on an organism has its optimal range resulting in the fact that too high or too low intensities have little or no effect (74).

I.3. Molecular Mechanisms and Transcriptomics

I.3.1. Transcriptomics: Definition and Historical Background

Transcriptomics (literally: the research on the transcriptome) represents a relatively young discipline in the fields of medical research. The suffix ―*omics* is built upon the suffix ―*ome*. Generally, ―*ome* is referred to the meaning 'whole', 'universal' or 'entire', although there is no known word in Ancient Greek, from which its derivation seems likely. The first term to appear with that suffix was *genome* and goes back to Hans Winkler and his work *Verbreitung und Ursache der Parthenogenesis im Pflanzen- und Tierreiche* from 1920. Winkler is said to have built the term *genome* in analogy to the term *chomosome*, which refered to the haploid chromosome set. *Chromosome*, however, is formed from the words *χρῶμα* (chroma; color) and *σῶμα* (soma; body). Therefore, it is very unlikely that the suffixes ―*ome* and ―*omics* do reflect a specific meaning. The term *genomics* was used in 1986 for the first time, when the geneticist Thomas Roderick discussed with his colleagues about the naming of the then–edited and now well known journal *Genomics*. The terms proteomics and transcriptomics as well as metabolomics, lipidomics, spliceomics and other, seem to have been built later in analogy to the term genomics (75).

The term transcriptome refers to the entirety of the transcripts of DNA, a double–stranded molecule, that is present in each nucleus of every eukaryotic cell, from unicellular to multicellular organisms, from yeast to humans. The transcripts, i.e. the entirety of RNA, serve as a connector between genes and proteins by representing the guidance towards the phenotype (often referred to as *intermediate phenotype*), as it will be discussed below.

I.3.2. Chemical Structure of RNA

RNA is composed of chain–forming molecules consisting of single *pentose* (or, more precisely: aldopentose) molecules that are attached to eachother by *phosphate* molecules. Pentoses are monosaccharides that consist of five carbon atoms; they can either be provided with an aldehyde group on the first carbon atom (aldopentoses) or with a ketone group on the third or fourth carbon atom (ketopentoses). There are eight possible stereoisomeric forms of aldopentoses (ribose, arabinose, xylose and lyxose in two enatiomeric forms each, D– and L–), of which only D–*ribose* represents the biogenic material for RNA as well as for DNA in its slightly modified form (see below). D–ribose exists in distinct forms: as a chain molecule (depicted by means of Fischer projection in figure **I.15**) or in two cyclic forms (D–ribopyranose and D–ribofuranose), of which D–ribofuranose is the structural element for RNA (depicted by means of Haworth projection in figure **I.15**). Phosphate (PO_4^{3-}) is the third conjugate base of phosphoric acid (H_3PO_4). Phosphate provides the linkage between one ribose molecule from its carbon atom on position 5' and another ribose molecule with its carbon atom on position 3'. Furthermore, each ribose molecule has one specific *nucleobase* attached to its carbon atome on position 1'. Nucleobases are heterocyclic (as they contain nitrogen) and aromatic compounds belonging either to purines (one 5–membered imidazol ring and one 6–membered pyrimidine ring) or pyrimidines (solely one 6–membered pyrimidine ring). There are four *primary nucleobases*, two in each group: adenine and guanine (purines) as well as cytosine and uracil (pyrimidines). Besides, there are also *modified nucleobases*. In DNA, the most common modified nucleobase is 5–methylcytosine. It is the product of RNA–directed DNA methylation, an epigenetic mechanism of gene silencing by siRNAs (76). Dihydrouridine is found in tRNA (D–loop see) and in rRNA (77), smilarly with pseudouridine (78). Hypoxanthine is found in tRNA. Its property is the ability to form Wobble base pairs (see below) between tRNA and mRNA within translation, as hypoxanthine can form hydrogen bonds with adenine, cytosine and uracil (79). For siRNA, rRNA and tRNA as well as for further information see chapter I.3.5.

The unit of ribose and a nucleobase is called a *nucleoside* (i.e. adenosine, guanosine, cytidine, uridine), the unit of a nucleoside (ribose and nucleobase) together with a phosphate molecule on position 5'–C is called a *nucleotide* or *nucleoside phosphate* (e.g. adenosine triphosphate, ATP). The chain formed of nucleotides is RNA sensu stricto (figure **I.15**).

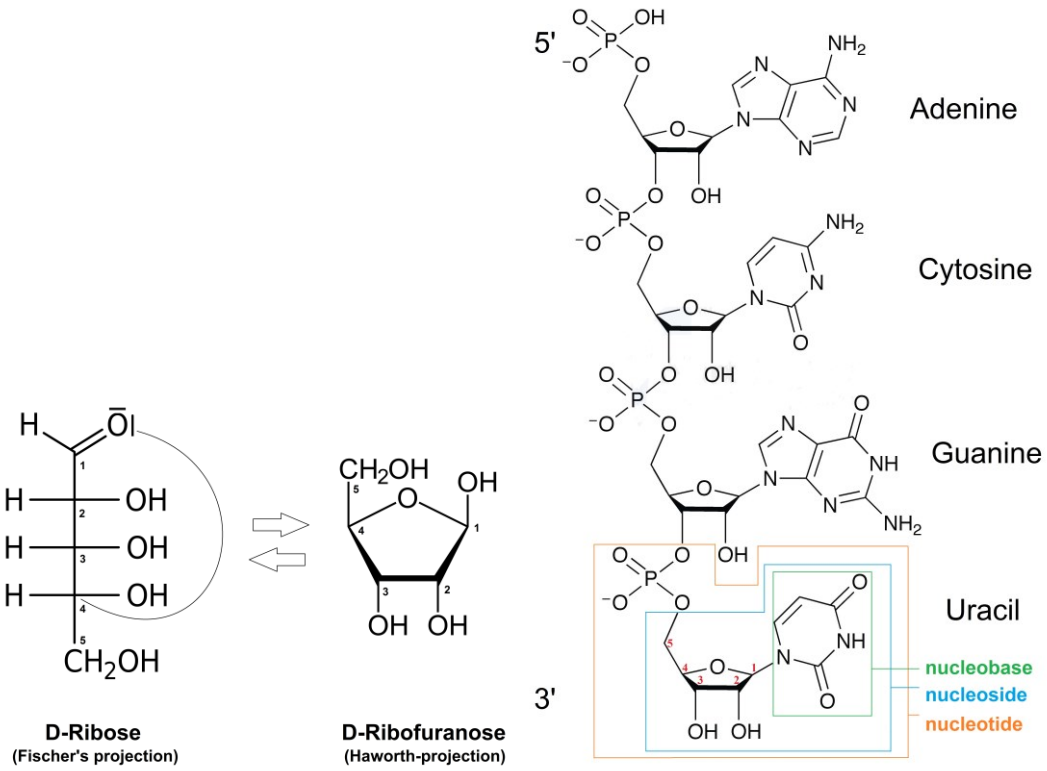

Figure I.15: *Linear and cyclic form of ribose* (left) and the *chemical structure of RNA* (right).

The DNA, however, is a chain of nucleotides with the following differences to RNA:

- Instead of ribose, DNA contains deoxyribose (the functional hydroxyl group on the 2' carbon atom is deoxygenated and is therefore missing);

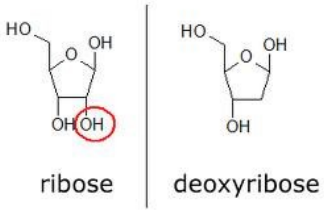

- Instead of uracil, DNA contains the pyrimidine–base thymine, which is methylated on the carbon atom on position 5';

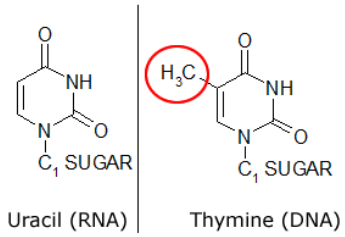

Source: http://biochem.co/2008/08/transcription-dna-rna/

- DNA is double–stranded: two DNA chains form a double–stranded helix by building hydrogen bonds between complementary nucleobases. Adenine builds double bonds with thymine, whereas guanine builds triple bonds with cytosine. This is also known as *Watson—Crick base pairing*.

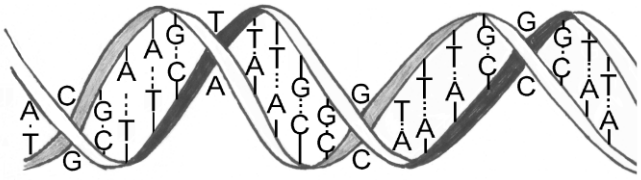

Source: http://daddystractor.com/2013/06/17/my_meeting_with_monsanto_president/

I.3.3. Synthesis of RNA

The sequence of different reactions, which lead to formation of RNA, is called ***transcription*** and takes place in the nucleus of a cell. During transcription, a chain of RNA is built from nucleotide triphosphates such as ATP, CTP, GTP and UTP, during which pyrophosphate is hydrolysed and a new nucleotide monophosphate is attached with its phosphate on position 5' to the oxygen on position 3' of the previous nucleotide. This reaction is catalysed by *DNA–dependent RNA polymerases*, core enzymes consisting of multiple subunits for different tasks, i.e. loosening the DNA double helix, reading nucleobases of the *template strand* of the DNA and catalysing the formation of a chain of complementary nucleobases. Regarding the sequence of nucleobases, the newly

synthesized RNA strand is identical to the DNA strand that has not been read during transcription (*coding strand*) except the fact that uracil apears in the RNA where thymine appears in the coding strand of the DNA or where adenine appears in the template strand, respectively.

In eukaryotic cells, the initiation of transcription requires *transcription factors* (TFs) as well as different proteinaceous *activators* and *repressors*. Together with a specific RNA polymerase, they form a complex that is able to bind on specific promoter sequences on the DNA like the TATA-box and start the transcription there.

Depending on the type of RNA synthesized, different processes can follow such as poly-adenylation, alternative splicing and translation. On these issues, however, it will not be dwelt further here.

I.3.4. The Traditional Biological Role of RNA

When Crick published his article *The Biological Replication of Macromolecules* in 1958, he could only vaguely hypothesize about RNA and protein synthesis. Some works on viruses (especially on the tobacco mosaic virus) from this time indirectly pointed out that protein synthesis must somehow be linked to RNA. Furthermore, it was known that RNA was spread throughout the cell (nucleus, cytoplasm and 'microsomal particles', which were later named ribosomes), whereas DNA seemed to be concentrated in the nucleus; Crick also was aware of the fact that protein folding could result solely from the sequence of amino acids given by the sequence of nucleotides in RNA and DNA, respectively, as it had been shown that a substitution of a single amino acid of the β–chain of haemoglobin could change the entire structure of the haemoglobin molecule leading to sickle–cell anemia (80).

In 1970, Crick published another important article in which he phrased what is now known as the *Central Dogma of Molecular Biology*: DNA is transcribed to RNA and RNA is translated to proteins. More precisely, Crick differentiates two groups of transfer of genetic information: general transfers and special tranfers, listed in table **I.1**; the name of the process, in which a particular transfer occurs, is put in brakes (figure **I.16** and table **I.1**)

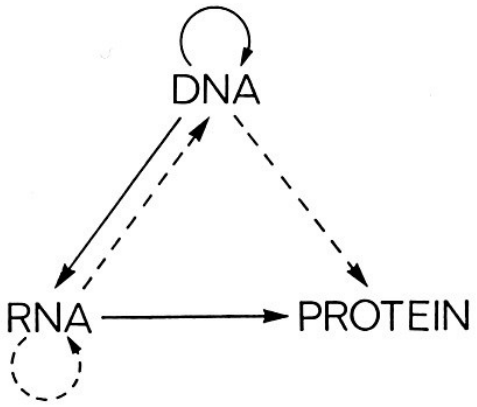

Fig. 3. A tentative classification for the present day. Solid arrows show general transfers; dotted arrows show special transfers. Again, the absent arrows are the undetected transfers specified by the central dogma.

Figure I.16: *Central Dogma of Molecular Biology*. DNA is transcribed to RNA, RNA is translated to proteins. When cells are dividing, DNA must be replicated (circular arrow). Dotted arrows show 'special transfers'. Reproduced from Crick, 1970.

Table I.1: General and special transfers

General transfers	*Special transfers*
DNA → DNA (DNA replication)	RNA → DNA (reverse transcription)
DNA → RNA (transcription)	RNA → RNA (RNA replication)
RNA → Protein (translation)	DNA → Protein *

Reverse transcription occurs in Retroviruses (e.g. in HIV) whereas RNA replication occurs in negative–sense single stranded (–)ssRNA viruses, in which the RNA is replicated by an *RNA–dependent RNA polymerase,* creating a positive–sense RNA that represents mRNA and which can eventually be translated to protein (e.g. in Influenca virus, Hantavirus, Rabies virus). However, Crick negated the possibility of transfers from proteins to nucleotides, which also dissents with the Wobble hypothesis and the degeneracy of the genetic code. Since more than one triplet of nucleobases can stand for a particular amino acid, the results of a 'reverse translation' are naturally ambiguos (figure **I.17**). Transfers such as protein → DNA, protein → RNA or protein → protein are still unknown to occur in Nature.

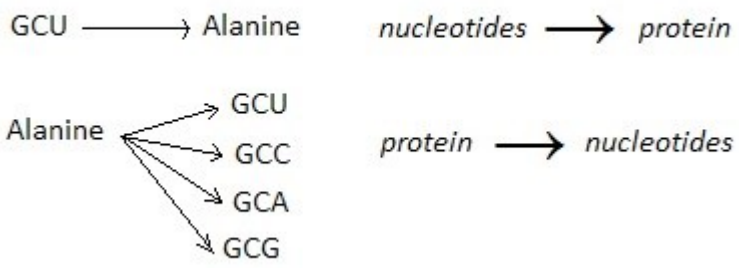

Figure I.17: The translation from a base triplet into an amino acid is plain whereas a 'reverse translation' is ambiguous; example on alanine and the corresponding codons.

I.3.5. Types of RNA

It is recognized that in humans (but also in other species), only a small part of the transcriptome consists of RNA that corresponds to a certain gene and encodes a certain protein (**protein–coding RNA** or **mRNA**, see below) and that this part is encoded by about 2% of the whole genome. The majority of the human transcriptome comprises various species of RNA that can be subsumed to **non–coding RNA** (or ncRNA, see below). Furthermore, it is estimated that the percentage of DNA transcribed to ncRNA averages 43%. For approximately 55% of the DNA no corresponding RNA can be found and thus it is assumed that 55% of the entire DNA remains untranscribed (81). Interestingly, it seems that the more complex a species is, the greater the percentage of ncRNA within the transcriptome (82). In prokaryotes, for example, the contrary seems to obtain, as it is found that mRNA represents the greater part of their transcriptome (83). E. coli has 88% of its genome transcribed into mRNA, only 1% accounts to ncRNA, whereas 11% of the genome are not transcribed (81).

Similarly when regarded from genomic point of view, in human DNA, which contains 3×10^9 base pairs, only 1.5% (or approximately 3×10^6 base pairs) make up coding DNA, which are organized in about 21,000 genes and which can be transcribed into mRNA and translated into proteins then. More than 98% of the DNA, however, does not encode a protein (non–coding DNA or sometimes even 'junk DNA') and is either transcribed to ncRNA (43%) or apparently not transcribed at all (55%; see above) (84).

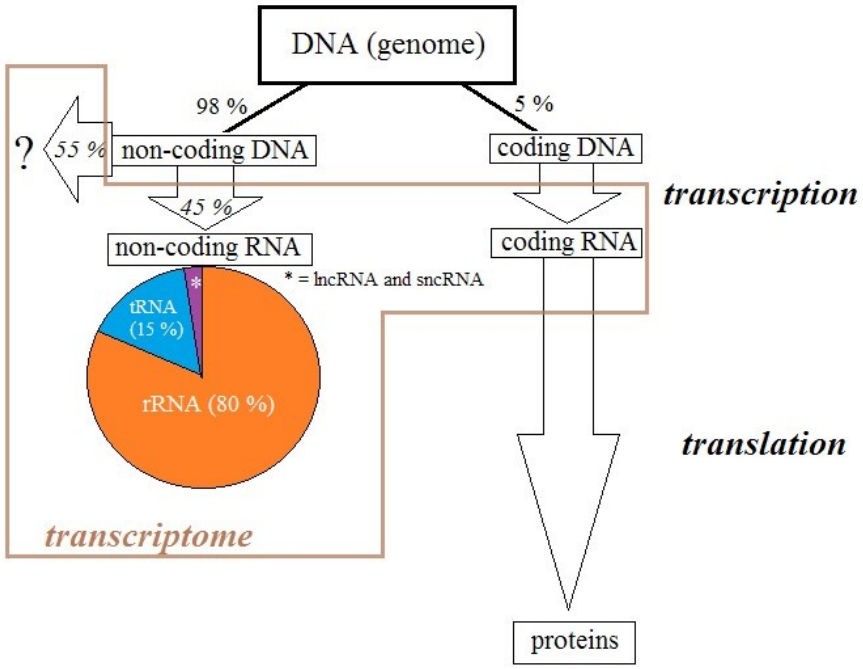

Figure I.18: *Types of RNA*

The fact that even non–coding DNA is transcribed may not seem trivial, but has been documented to obtain to a far greater extent than it is the case in coding DNA (85).

Non–coding RNAs can be subdivided arbitrarily in two groups, of which the first comprises RNAs that are *involved in transcription and translation* and the second comprises RNAs that are further specified by their *number of nucleotides*. This classification is insofar arbitrary as it seems obvious that RNAs from the second group can also be involved in transcription and translation, as it will be discussed below. The first group, however, contains 'traditional', well–known RNAs in contrast to relatively 'new' non–coding RNAs from the second group. RNAs that are directly involved in transcription and translation make up the vast majority of total RNA.

Transfer RNA (tRNA, approximately 15% of total RNA) consists of approximately 80 nucleotides forming a molecule with distinct secondary and tertiary structure. tRNA is transcribed by RNA–polymerase III. The characteristic cloverleaf–like shape is the result of folds of the molecule and formation of four local intramolecular double–stranded RNA parts (*stems*) on the one hand (mostly through Watson—Crick base pairing; see chapter I.3.2), and of three *loops* on the other hand (*D–loop*, *TψC–loop* and *anticodon–loop*) (86).

Each loop also contains modified nucleobases such as dihydrouridine in the D–loop, pseudouridine (Ψ) in the TψC–loop and hypoxanthine in the anticodon–loop. The *anticodon–loop* is provided with an anticodon, a base triplet that is complementary to a certain triplet (codon) on an mRNA strand. The *acceptor stem* is the double–stranded part of the 5' and 3' ends of the RNA molecule and is therefore the only stem that does not form a loop. Between both strands of the acceptor stem, also non–Watson—Crick base pairings can occur. The 3' tail is provided with the nucleobase sequence CCA; it is the 'transition point' from DNA to amino acids and, hence, the crux to protein synthesis. On its 3'–CCA, each tRNA molecule is *aminoacetylated* according to its anticodon, a task which is performed by specific *aminoacyl–tRNA synthetases*. A protein is formed during elongation by sequential binding of tRNA to mRNA (anticodon to codon) and linking its aminoacid with the previously released one.

Ribosomal RNA (rRNA, approximately 80% of total RNA) is, together with riboproteins, the forming component of ribosomes. rRNA is synthesized in the nucleolus. Eukaryotes have four types or rRNA (excluding mitochondrial rRNA, which appears in two types) classified by their sedimentational coefficient (Svedberg), which is proportional to the number of nucleotides: 28 S, 18 S, 5.8 S and 5 S. The former three types are synthesized from one single transcriptional unit and transcribed by RNA–polymerase I. The latter type (5 S) is transcribed by RNA–polymerase III. Each type of rRNA is encoded in multiple regions, which are spread throughout the genome in order to provide sufficient amount of transcripts. These four types form two subunits, one of them being the *large subunit 60 S* (formed by 28 S, 5.8 S and 5 S), the other the *small subunit 40 S* (18 S). Similarly to tRNA, rRNA is organized in an (even more) distinct secondary and tertiary structure by formation of intramolecular Watson—Crick as well as non–Watson—Crick base pairings. Ribosomes are organelles on which the *translation* takes place. They possess three binding sites for tRNA molecules: an aminoacyl (A), a peptidyl (P) and an exit (E) site. During elongation, the translated mRNA fits between the two subunits, beginning at the *start–codon* (AUG triplet). The corresponding aminoacyl–tRNA with methionine recognizes the start–codon and binds there. After the binding, the ribosome moves along the mRNA in 5'→3' direction and the tRNA is moved from the A–site to the P–site. As the following aminoacyl–tRNA binds the next codon on the mRNA as well as the liberated A–site on the ribosome, the next amino acid is linked to methionine (figure **I.19**). This process is then

repeated hundreds and thousands of times, depending on the size of the protein being sythesized. Thus, the protein is sequentially formed as a growing polypeptide chain on the peptidyl–tRNA (87). rRNAs have catalytic activity (ribozymes), providing peptide bonds between aminoacids during elongation (88).

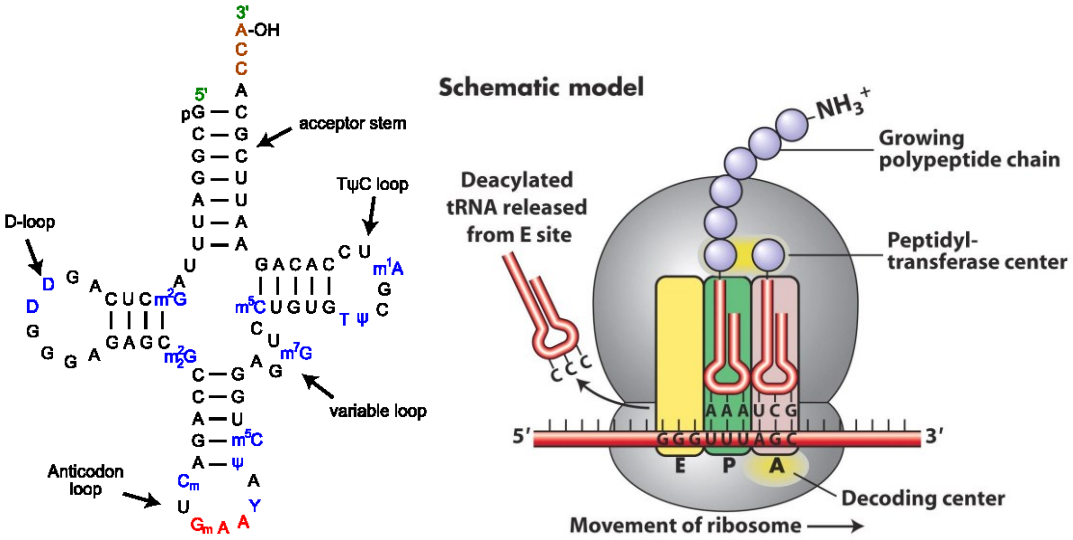

Figure I.19: Structure of *tRNA* with loops and stems (left). Simplified scheme of the *translational apparatus* (right): ribosome (gray), mRNA (dark red) and tRNA (bright red). Reproduced from http://guardianlv.com/2013/10/naked-mole-rat-longevity-explained-by-higher-translational-fidelity/

RNAs classified by their number of nucleotides are further subdivided in **small non–coding RNAs** (sncRNAs) and **long non–coding** RNAs (lncRNAs).

The group of sncRNAs contains short interfering RNAs (siRNAs), micro–RNAs (miRNAs) and PIWI–interacting RNA (piRNAs) that consist of 20—30 nucleotides each. Both **siRNAs** and **miRNAs** are synthesized from double–stranded RNA (dsRNA), which is transcribed from both strands of DNA by Dicer (RNaseIII) and RNA polymerase II Drosha, respectively. Through attachment to Argonaute proteins, they form RNA–induced silencing complexes (RISCs) that interact with mRNAs and cause their degradation or inhibition of translation into proteins. Contrarily to siRNAs and miRNAs that are

expressed ubiquitously, **piRNAs** are found in germ line cells; they are probably synthesized from siRNAs and miRNAs, and seem to be involved in silencing of transposons and the maintenance of integrity of the genome (89).

LncRNAs are RNAs with a length of at least 200 nucleotides. They are very similar to mRNAs in morphology, they can be polyadenylated, processed and altenatively spliced (90). Although relatively little is known about specific functions of lncRNAs and although some works have suggested that transcription of non–coding DNA might be useless for the most part, several papers have outlined regulatory roles in gene expression on a, mainly, epigenetic level. These roles contain transcriptional interference (transcription from upstream 'junk' regions can stimulate or inhibit downstream gene transcription); modifications of histones and chromatin; interaction with RNA–polymerases; modulation of splicing; interaction with proteins, which can lead to conformational changes of and, hence, to modulation of their activity; serving as matrix for small non–coding RNAs (sncRNAs, see above) (91).

I.3.6. Research Techniques in the Field of Transcriptomics

I.3.6.1. Chronological Review: ESTs and SAGE

An important impetus for transcriptomic research comes with the emergence of different biotechnological methods of—mainly—DNA sequencing, which were developed in the 1990s within the scope of deciphering the genome (*The Human Genome Project*, http://www.genome.gov). Expressed sequence tags (**ESTs**) represent, among genomic sequencing, the first steps towards this aim. ESTs are nuclotide fragments from cDNAs (complementary DNAs), which are gained from isolated mRNAs using reverse transcription (92). Depending on whether the sequence of nucleotides of the genome is unknown or known, ESTs can be mapped to chromosomes using different gene mapping techniques or they can be 'mapped' bioinformatically by computerized comparison of the sequence, respectively. Although ESTs are good tools for gene discovery, much redundant analysis has to be done when ESTs are sequenced, since highly expressed genes yield numerous copies of the same mRNA and thus ESTs, which elongates the procedure. On

the other hand, rarely expressed genes require larger amounts of ESTs sequenced in order to be detected.

A similar but less time–consuming method represents serial analysis of gene expression (**SAGE**). Unlike in ESTs, a high number of transcripts (hundreds to thousands) can be analysed simultaneously using the SAGE technique. In SAGE, RNA of interest is isolated and magnetic poly(T) beads are used to trap and isolate RNA molecules with poly(A) tails, which are mainly—but not exclusively—mRNAs. Selected mRNAs are then transcribed to cDNA using reverse transcription with biotinylated oligo(dT) primers, bound to streptavidin and cleaved on restriction sites using type II (Mg^{2+}–dependent) restriction enzymes (anchoring enzyme), producing cDNAs approximately equal in length that are provided with nucleotide overhangs (sticky ends). The cleaved cDNA is then divided in half and two types of linkers A and B are attached to the sticky ends of cDNA molecules. Linkers are provided with a promoter and docking sites for tagging enzyme and anchoring enzyme. cDNAs are then cleaved with tagging enzyme on positions determined by distance from its docking sites (mostly 15 nt), so that SAGE tags are released from the streptavidin-bound complex. The tags from divided cDNA are put together and form ditags with linkers on each end. These ditags are then amplified by PCR using linker–specific primers. Ditags are cut again by anchoring enzyme on specific restriction sites and put together in long chains (concatemers), which are vectored into bacteria, replicated and later on sequenced nucleotide-by-nucleotide (93). Similar to microarrays, SAGE yields large amounts of data and requires mapping and statistical analyses (see next chapter).

Both ESTs and SAGE have in common that the abundance of transcripts and thus the level of gene expression is determined by the abundance of derivatives of cDNA (tags). The abundance of sequenced tags (the number of times a tag is sequenced) allows to draw inferences on the level of gene expression.

I.3.6.2. DNA Microarray—a Powerful Transcriptomic Tool

In contrast to ESTs and SAGE, **DNA microarray**, which evolved from Southern blotting, is based on the principle of *hybridization*. Nucleotide chains (called *probes*) are attached to a solid surface such as a slice (chip). The attachment is accomplished either in the laboratory or by manufacturing companies by means of biotechnological engineering methods providing that tens of thousands of single probes are arranged on a small surface of a slice in high density and the probes form stable (covalent) bonds with the surface. Samples to be hybridized are called *targets*.

DNA microarrays vary in terms of probes that are used and depending on how they are generated as well as in terms of how many different targets can be hybridized to an array simultaneously. There are various forms of nuleotides that can be used as probes such as ESTs, cDNA, PCR–amplified DNA and oligonucleotides. Probes from ESTs, cDNA and other PCR–amplified DNA consist of longer nucleotide chains (600—2000 nt) and provide a more specific binding during the process of hybridization; they can be designed in the laboratory using techniques that were previously described or they can be gained from preexisting libraries. Oligonucleotides consist usually of less nucleotides (short oligonucleotides 12—25 nt, long oligonucleotides 50—120 nt) and provide therefore less specific bindings during hybridization than PCR–based probes. On the other hand, oligonucleotide probes are cheaper. They are generally synthesized in silico according to known genes. The probes can either be attached to chips in the laboratory or, alternatively, ready-to-use chips with attached probes can be purchased manufactured by diverse companies such as Affymetrix or Agilent.

DNA microarrays comprise multiple steps in the procedure, which will be shown using predesigned and ready-to-use Agilent Whole Genome arrays as an example, since those were used as method for evaluation of differentially expressed genes in the present thesis.

I.3.6.2.1. Sample Collection and General Considerations

RNA is obtained from samples of interest using different methods of cell lysis and RNase blocking. These samples can be cells in any form, i.e. tissues, blood or cells from a cell

culture. Thus, RNA is very often obtained from distinct cell types, as tissues are composed of heterogeneous cells. In this case, the extent of gene expression is an information which is related to all present cell types and dependent on the percentage of single types within the sample. Of course, there are methods for isolating certain cell types (e.g. flourescent–activated cell sorting or laser capture microdissection), on which, however, it will not be dwelt further here.

I.3.6.2.2. RNA Isolation and Target Obtainment

Total RNA is isolated from samples using standard operating protocols and kits that are designed for specific tasks and tissues. For the present study, which grounds on blood as the tissue of interest, the Tempus Spin Blood RNA Isolation kit was used. Blood is composed of different cell types (erythrocytes, leukocytes and thrombocytes) with distinct gene expression profiles in a cell type, where erythrocytes make up almost the total amount of cells. Although mature erythrocytes have no nucleus and therefore restricted transcription and translation possibilities, the vast majority (about 70%) of total RNA from peripheral blood is globin–mRNA (required for synthesis of hemoglobin), which originates from erythrocyte precursor cells such as reticulocytes and proerythroblasts. Globin–mRNA is extracted from total RNA in order to eliminate high abundance.

I.3.6.2.3 Target Amplification

Target amplification serves two purposes: (1) Before targets are hybridized to probes, they have to be amplified in order to guarantee a sufficient amount of targets, especially for genes that are rarely expressed and could thus be overlooked. (2) By target amplification, mRNA from the samples of interest is transcribed to antisense or complementary DNA or RNA (cDNA or cRNA/aRNA), respectively.This is important for hybridization, since sequence and direction of nucleotides of the probes is equal to sampled mRNA. First, the RNA of interest is copied to cDNA (complementary DNA) using the principle of reverse transcription. An oligo(dT) primer is a sequence of 15—25 deoxythymidines (dTs) with an upstream (towards 5’ located) promoter and serves as the starting site of transcription. The

advantage of dTs is that only RNAs with a poly(A) tail are copied, which are mainly—but not exclusively—mRNAs. For reverse transcription, the enzyme MMLV-(Moloney Murine Leukemia Virus)-reverse transcriptase was used in the study.

After a first strand of cDNA has been created, it is then amplified using PCR with random primers. For microarrays using PCR products as probes (e.g. ESTs, cDNA), cDNA must be labeled in the first instance.

I.3.6.2.4. Target Labeling

Some microarrays using oligonucleotides as probes, however, require cRNA/aRNA for hybridization, which is gained in a so called Eberwine procedure. Amplified cDNA is transcribed in cRNA (complementary to sampled mRNA) using T7 (bacteriophage) RNA polymerase and nucleotide triphosphate molecules (NTPs). In order to enable detection of cRNA, usually one of the NTPs is marked. There are several techniques for marking biomolecules using the principles of either radioactivity, chemiluminescence or flourescence. The most common principle of labeling in gene expression microarrays represents flourescence using flourophores such as phycoerythrin, cyanines or Alexa dyes. In the present study, two types of cytidin triphosphates (CTPs) were used, marked either with cyanine 3 (Cy3) or cyanine 5 (Cy5), which were incorporated in the cRNA/aRNA during transcription.

1.3.6.2.5. Target Purification

Once cRNA/aRNA is transcribed and labeled, it must be separated from the cDNA. In the present study, this was accomplished with Qiagen's RNeasy mini spin columns, small tubes in which the content is treated with ethanole and buffer and RNA is absorbed to a membrane.

Figure **I.20**, reproduced from the protocol for one-color microarray–based gene expression analysis—quick amp labeling, summarizes the steps described above

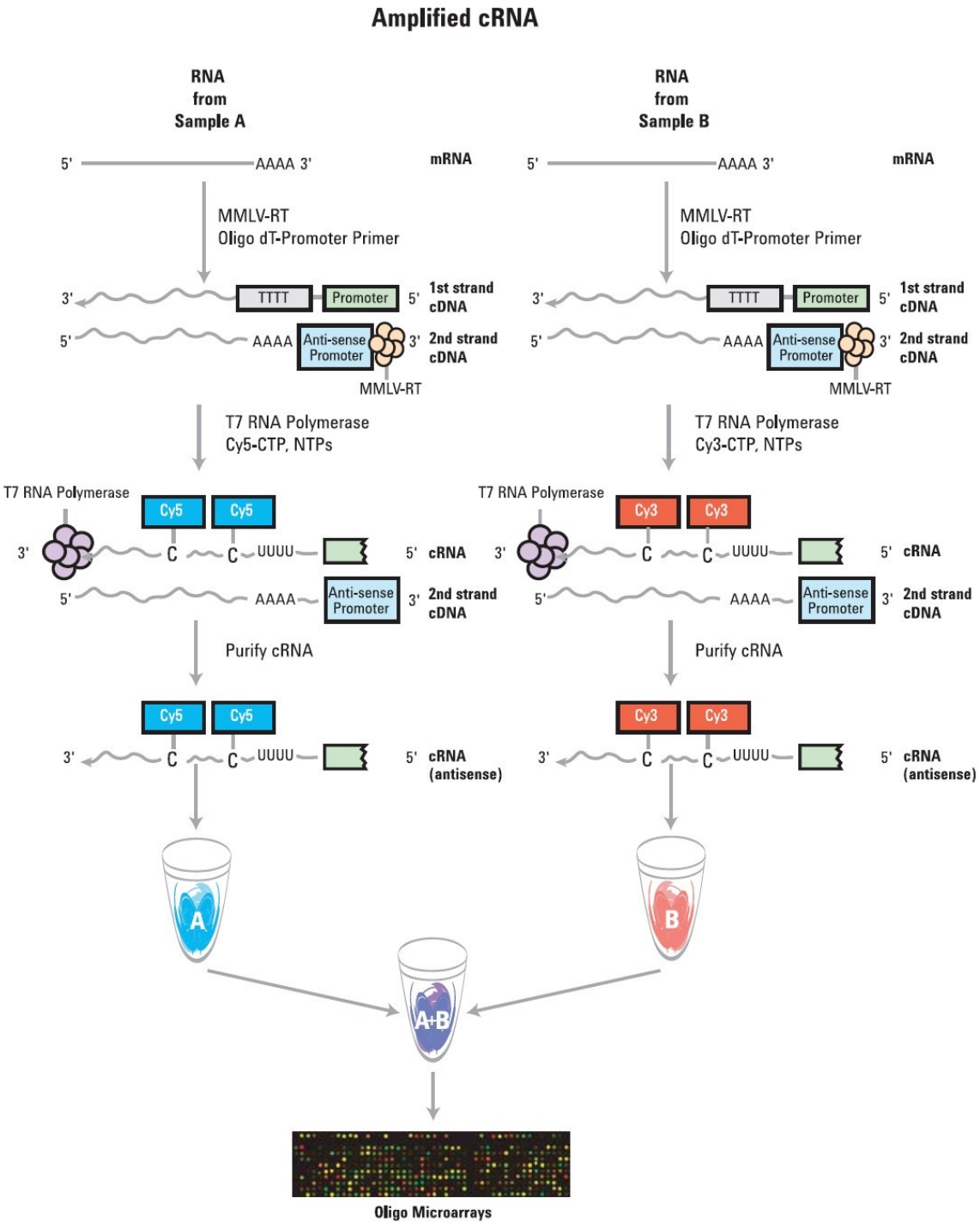

Figure I.20: *From sampled total RNA to labeled targets*. Reproduced from one-color microarray–based gene expression analysis—quick amp labeling protocol.

I.3.6.2.6. Hybridization

Hybridization of purified and labeled cRNA/aRNA targets to probes on a microarray chip is accomplished in so called hybridization chambers, which provide a constant temperature during the period of time required. The added buffers (e.g. formamide, salt) also determine the temperature of the hybridization, where a higher temperature and a longer duration increase the stringency and therefore the specificity of binding. The principle of the process is based on the circumstance that nucleotides from targets form Watson—Crick base pairs with nucleotides from probes, which are, ideally, stable to the following washing steps. After hybridization, chips are dryed and ready for scanning.

A chip can also be *hybridized competitively* with two samples, of which both have to be labeled with distinct fluorophores before hybridization (as shown in figure **I.20**). This strategy is called the *two-color mode*. The advantage of a two-color mode is that samples of interest can be directly compared in terms of their status prior and posterior to an intervention. Hence, each sample serves as its own control.

I.3.6.2.7. Scanning and Principles of Flourescence

Scanning of flourescent-labeled hybridized targets is performed with a device, which eventually transfers gathered signals to a computer. Such scanner is provided with lasers, which emit light of a defined wavelength and corresponding energy, according to

$$E = h\nu = h\frac{c}{\lambda}$$

where v is the frequency of light—equal to the quotient of speed of light c and wavelength λ—and where h is the Planck's constant. When fluorophores are hit by photons (*absorption*), the energy is transformed into internal energy where molecules from a ground state are excited to a state of higher energy (*excitation*). Different fluorophores have distinct spectral characteristics and absorb therefore light of different wavelenghts to their maximum (or, equally spoken, are excited at different wavelengths to their maximum); Cy3 has its absorption maximum at 532 nm (green-yellow), whereas Cy5 has

its absorption maximum at 633 nm (orange). From the excited state, the molecules transition back to ground state by emitting light of a certain, generally longer wavelength (and lower energy, respectively) compared to the one of absorbed light (*emission*; 590 nm for Cy3 and 670 nm Cy5). The difference between excitation and emission energy $h\nu_{EX} - h\nu_{EM}$ is called *Stokes shift* and represents the energy that is lost (e.g. as thermic energy). The emitted light is detected by photomultiplier tubes as a fluorescent signal (signal intensity of emitted light), converted to a voltage signal and processed to a tiff-image with scanned slots appearing as a picture of red and green slots, respectively.

I.3.6.2.8. Image Analysis

The analysis of tiff-images comprises three main steps: (1) *Gridding* refers to the process in which the localisation of relevant spots is scanned and identified by the software according to preset values. These spots mark locations that have been defined by probe attachment.
(2) *Segmentation*. When a spot has been identified, the fluorescent signal has to be demarcated from the background. This is accomplished e.g. by circles (fixed circle and adapted circle segmetation), by more accurate shapes (adapted shape segmentation) according to the spot image or by a histogram, where only pixels with defined intensities out of the whole pixel-intensity distribution are included into further analysis. (3) *Intensity extraction*. Once spots have been segmentated, the intensities of single pixels whithin the spot are summed, meaned and extracted from background signal intensities, which are due to unspecific binding or local deposit of flourescent-labeled targets. By application of various algorithms, the signal of each feature is processed whithin a precedure comprising multiple steps and the intensities are transferred to a *processed signal* (PS).

When two groups are compared and the two-color mode has been used (e.g. Cy5–labled targets from samples prior to intervention and Cy3–labeled targets from samples subsequent to intervention), features are expressed as logarithmic ratio of red (Cy5) and green (Cy3) processed signals,

$$\log \frac{r\mathrm{PS}}{g\mathrm{PS}}$$

Using two colors implies the requirement of correction of dye biases by means of statistical testings. For detailed algorithms, please refer to the Feature Extraction Protocol.

1.3.6.2.9. Analysis of Differential Gene Expression

The analysis of differentially expressed genes is based on hypothesis testing in statistics. For each gene the assumption (null hypothesis) is made that the gene is expressed equally in two groups to be compared (prior vs. subsequent to intervention). According to Fisher, a null hypothesis is "[…] never proven or established, but is possibly disproved, in the course of experimentation." (Design of experiments, Fischer). The disproof of the null hypothesis leads to its contrary, namely that two genes are *not equally* (= differentially) expressed. If a gene is expressed equally, the ratio of expression with and without intervention equals one (*fold change*). Usually, the logarithmic ratio is used, like log (rPS/gPS) from above; then the ratio for equally expressed genes equals zero. When fold change and logarithmic ratio are regarded alone, a gene is considered differenitally expressed in the case that its fold change is equal or above an arbitrary cut–off, with generally FC ≥ 1.5 or more. Since through such an arbitrary cut–off, important genes could be missed, statistical testing must be performed additionally.

Statistical analysis with *t*–test provides a *p*–value for each gene. The *p*–value expresses the probability for a gene to be considered as differenitally expressed, while it is equally expressed, actually (*false positive* or *error of the first kind*). A result is considered significant in the case that the *p*–value is equal or smaller than the probability of error α (p ≤ α), in medical research usually being α = 0.05 (or 0.01). A *t*–test provides a *t*-statistic for each gene which is described by

$$t_g = \frac{m_1 - m_2}{s_{m_1 - m_2}}$$

where *m* is the mean expression value for each group of two (treated vs. untreated) and $s(m_1–m_2)$ is the estimated variance for the two groups based on consideration of the number of tests *n* and the standard deviations *s*

$$s_{m_1-m_2} = \sqrt{\frac{(n_1-1)s_1^2+(n_2-1)s_2^2}{n_1+n_2-2}\left(\frac{1}{n_1}+\frac{1}{n_2}\right)}$$

Modified *t*–tests use small constants which are added to the estimated variance. This is important as for some genes, the estimated variance can be small coincidentally, providing a large *t*-statistic where the fold change might in fact be small. For a two-color mode microarray, a *paired* t–*test* for two groups should be considered. In such paired *t*–test, corresponding mean expression values from two samples x_i and y_i are paired and their difference is calculated

$$(x_i, y_i) \text{ with } m_i = x_i - y_i \; \forall i$$

then, a *t*–test against zero is performed on each pair, which is defined as

$$t_g = \frac{m_i}{\sqrt{\frac{s_i^2}{n_i}}}$$

Finally, the *t*-statistic is converted into a *p*–value by *Asymptotic analysis* (i.e. according to the distribution) or by a *Permutation test*.

1.3.6.2.10. Multiple testing corrections

In a conventional gene expression microarray, *t*-statistics for thousands and tens of thousands of genes are calculated (the number of tests in the present thesis, for instance, is > 40,000). If the probability of error is set to α = 0.05 (or 5%), then 5 of 100 genes are likely to be reported as differentially expressed while being equally expressed instead (see above). For 40,000 test, however, one can expect that, statistically, 2000 false positive reports are made. In order to correct such a large number of false positive reports, the gained *p*-values have to be adjusted. This can be accomplished by different methods. In the present thesis the method of Benjamini—Hochberg was used. This method is based on the following principle: Genes are ordered according to their *p*-value, ascending from small to

large $p_1 < \ldots < p_n$, and to each gene, a corresponding ordering number $i = 1, \ldots, n$ is designated. Then, each p is compared to the term $q(i/n)$, where q is an arbitrary false discovery rate (FDR)—usually set to 0.1 or lower—, i is the ordering number and n is the number of the tests (or genes). The null hypothesis for a gene is rejected in the case that

$$p_i \leqslant q \cdot \frac{i}{n}$$

II. Aims and Objectives

The application of artificial gravity on the human body, especially in the +Gz direction, is known to have effects on the cardiovascular system as it counteracts to upward fluid shift that occurs in weightlessness. The exact molecular mechanisms, however, that are responsible for these effects have not been studied yet. The focus of this thesis will be the examination of the abovementioned molecular mechanisms of physiological changes caused by application of artificial gravity.

Recently, 12 subjects were exposed to different conditions of altered gravity, using a short–arm human centrifuge (SAHC). At the start and at the end of the experiment, blood samples were collected for analysing the molecular response to these interventions. The analysis and the biological interpretation of these data will be subject of the thesis. Therefore, existing literature has been researched and current state of knowledge has been provided regarding what are the known proteins that are affected by stress application. The database, consisting of < 500 proteins affected by artificial gravity application, was examined that had been provided and systematically checked, which known proteins are affected. In addition, any new proteins that might be affected by artificial gravity application were also examined and described, which might be seen from the database.

The knowledge gained from this work would be particularly relevant to those future medical practitioners who have an interest in working in the area of cardiology, falls, orthopedics or syncope research.

III. Methodology

III.1. Study Design

The study was performed ambulantly in the physiological laboratory of the Institut für Luft- und Raumfahrtmedizin of the *Deutsches Zentrum für Luft- und Raumfahrt* (DLR) in Cologne on a short–arm human centrifuge (SAHC) that has been loaned to the instutute by the European Space agency.

The staff comprised a centrifuge operator, a medical monitor (physician), an experiment operator entrusted with the performance of the test and a test director observing all functional units. Apart from the test director, all team members were present at the laboratory throughout the entire experiment.

III.1.1. Study Participants

12 volunteers were included in the study having fulfilled strict inclusion criteria.

III.1.2. Inclusion Criteria

- Female and male, healthy test subjects aged between 18 and 55 years, with body weight between 55 and 95 kg and a height between 160 and 190 cm;
- Non–smokers;
- Willingness to participate in the entire experiment;
- Signed declaration of consent before the initiation of the study;
- Negative pregnancy test in female test subjects.

In order to be included in this study, additional inclusional examinations had to be performed, which comprised blood draws, urine specimens, ECG at rest as well as exercise ECG with cycling ergometry, which started at a stress level of 50 W for female and 75 W for male test subjects and during which the stress was increased gradually every 3 minutes by 25 W. This was continued to the point where the test subject felt exhausted, as shown by the exhaustion level on the Borg–scale—a scale for subjective estimation of stress and exhaustion—ranging from 6 to 20 as well as by observing the test subject's heart rate.

III.1.3. Exclusion Criteria

Test subjects that were not taken into the study had either not met all inclusion criteria or they had met at least one exclusion criterion and were therefore considered ineligible for the study. Among exclusion criteria were:

- drug abuse or alcoholism with a consumption of more than 30 g ethanol per diem;
- any ongoing medication;
- smoking;
- obesity with a BMI of 30 or above;
- renal diseases with deviations of plasma creatinine to values greater than 1.2 mg/dL;
- thyroid dysfunction with deviations of plasma TSH out of the range of 0.27—4.20 mU/L;
- fractures in the last 12 months before the study;
- migraine;
- psychiatric disorders in the past;
- claustrophobia;
- hiatic hernia;
- gastro–esophageal reflux disease (GERD);
- diseases of muscles or joints and rheumatic diseases;
- prolapse of intervertebral disc, degenerations of the spine or chronic back complaint;
- orthostatic intolerance;

- vestibular disorders (kinetosis);
- coronary heart disease and other cardiovascular diseases;
- abnormalities in the ECG in the manner of
    - more than 2 monomorphic ventricular extrasystoles (VES) within 1 minute;
    - polymorphic VES;
    - pronounced supraventricular extrasystoles (SVES);
    - disturbances of conduction or repolarization;
- bradycardia with heart rates HR < 50/min;
- tachycardia with HR > 120/min;
- hypertension with blood pressure > 139/89 mmHg;
- hypotension with systolic pressure < 100 mmHg;
- anemia;
- diabetes mellitus;
- a positive HIV–test;
- a positive test on viral hepatitis;
- pregnancy in female test subjects;
- unsigned informed consent;
- any other circumstance or condition that made a test subject ineligible for the study in the estimation of an examiner.

III.1.4. Study Protocols

The study was led as part of a major study, which comprised four different study groups with distinct study protocols: a continuous centrifugation group (SAHC1), an intermittent centrifugation group (SAHC2), a training group and a control group. For the present thesis, only the continuous centrifugation group (SAHC1) and the intermittent centrifugation group (SAHC2) were of interest and results from the other two groups are reported elsewhere. All 12 test subjects were assigned to the continuous protocol (SAHC1) and 6 of the 12 test subjects were assigned to the intermittent protocol (SAHC2).

The continuous centrifugation protocol (SAHC1, figure **III.1**) was subdivided into three phases, whereby the first and the third phase consisted of application of different g–levels for identical periods of time, beginning with 1 *g*, then increasing to 2 *g* and finally to 3 *g*, each of them for 2 minutes.

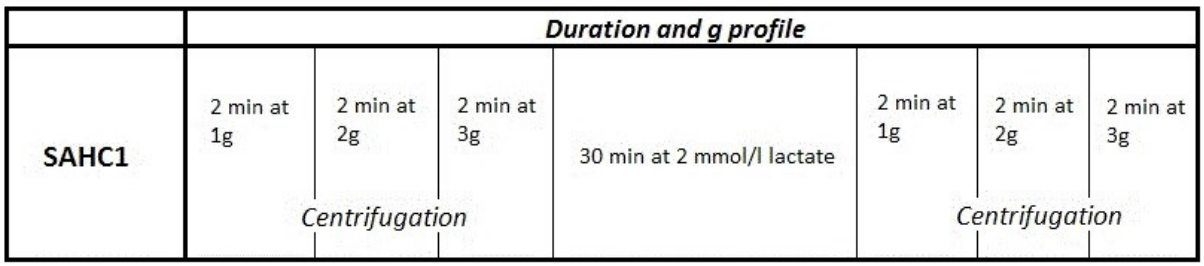

Figure III.1: Continuous centrifugation protocol (SAHC1)

Between those phases, namely during the second phase, a test subject was stressed with muscle work continuously and according to his/her heart rate for 30 minutes and with a lactate level of 2 mmol/L.

Likewise, the intermittent centrifugation protocol (SAHC2, figure **III.2**) was subdivided into three phases, whereby the first and the third phase were the same and identical to those of SAHC1. Unlike in the first protocol, stress was applied to test subjects intermittently over 30 minutes by alternating centrifugation and resting every 3 minutes, resulting in a total of 5 cycles. During the centrifugation, exercises were performed by the test subject according to his/her heart rate with a lactate level of 2 mmol/L. During the resting phases, the rotational rate of the SAHC was throttled to minimal, hardly perceptible values.

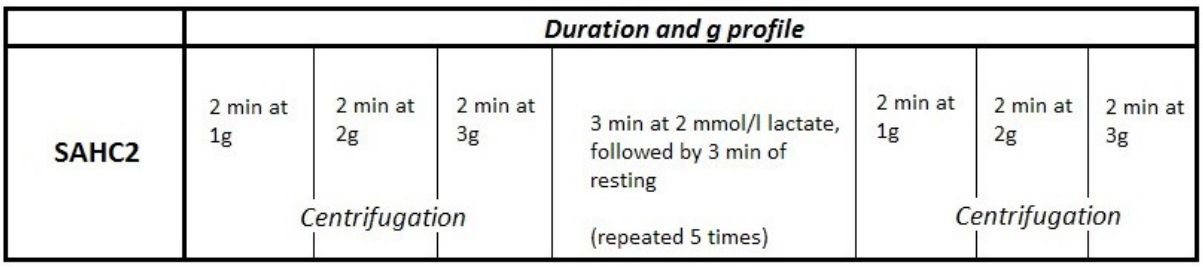

Figure III.2: Intermittent centrifugation protocol (SAHC2)

The other two comparative groups comprised a training group and a control group. In the training group, each test subject performed physical training for 42 minutes and with a subjective stress of 2 mmol/L lactate, whereas subjects in the control group remained inactive for 42 minutes. Results of these two groups, however, did not contribute to the present study and are reported elsewhere.

The *g*–intensities that were applied during the experiment refer to values that obtain in the center of mass (CoM).

A particular study protocol (SAHC1 and 2) as well as training group and control group was embedded into the experimental procedure as follows (figure **III.3**): After a preparation time of about 20 minutes, the program operation manual system (POMS) was pursued and blood samples were collected. Afterwards, electroencephalography (EEG) and near-infrared spectroscopy (NIRS) were performed on the test subjects (reported elsewhere). Then, pending on the group, a particular protocol (SAHC1 or SAHC2) was implemented, followed by EEG and NIRS and afterwards POMS and collection of blood samples once again. After that, cognitive tests were performed on the test subjects (reported elsewhere), followed by EEG and NIRS and then POMS and collection of blood samples for a third time.

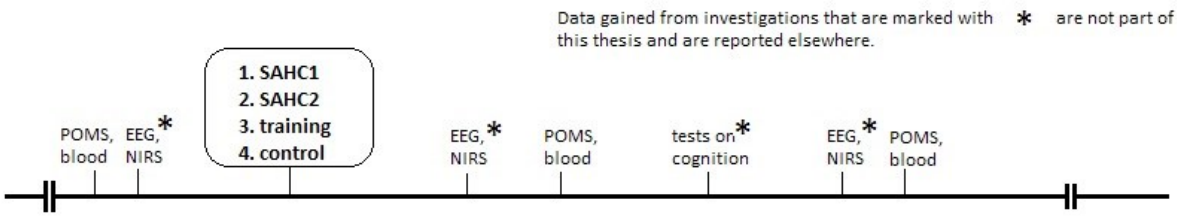

Figure III.3: Implementation of protocols into the experimentational phase

In order to ensure an optimum recovery for a test subject after an experiment, study protocols were performed on different days and the minimal time lag between SAHC1 and SAHC2 did not deceed 48 hours. Furthermore, each test subject passed both study protocols in an identical manner.

Test subjects were allowed to eat 2 hours before an experiment and to drink just before the experiment. The mental state of each test subject was evaluated with a questionnaire before, during and after each centrifugation.

III.1.5 Measurements

During the experiments, different additional testing methods were used, such as continuous ECG, sphygmomanometry for blood pressure and photoplethysmography for oxygen saturation as well as for blood presure (reported elsewhere). Also, measurement of the thoracic impendance (bioimpedance) were performed (reported elsewhere).

Blood samples were collected during the inclusianal examination as well as before and after the experiment using convantional tubes and Tempus blood RNA tubes, respectively. During the inclusional examination, 37.6 ml of blood were collected from each test subject. Before and after each single experiment, three samples of 10 ml each were collected. Since each test subject went through all four groups, a total of 157.6 ml of blood was collected within the whole experiment. During centrifugation, vital parameters of test subjects were monitored continuously by the staff according to standards of an intense care unit by means of ECG, sphygmomanometry, measurements of respiratory rate as well as of bioimpedance. Furthermore, there was permament audio–visual contact between a test subject and the staff via intercom system and monitors, respectively.

III.1.6. Ethical Approvement

An ethical approval was obtained for this study. This was particularly important, as during centrifugation many undesirable effects can occur. These include Coriolis–associated disorientation, vertigo, vestibular irritations or nausea and emesis, cardiovascular stress through downward blood shift, the consequent drop of blood pressure and symptoms of raised sympathetic tone like sweating, ‘grey out’ and ‘black out’, potentially culminating in *g*–related loss of conciousness (GLOC; see chapter I.2). Test subjects were instructed by staff to look out for these symptoms. Development of any of these symptoms and signs led

to an instant termination of the protocol. Both verbal and written informed consents from the volunteers were obtained and are stored at the DLR.

III.1.7. Termination of Protocol Criteria

At any point of time, it was possible for a test subject to quit (or discontinue) the study. Discontinuation criteria comprised:

- Emerging disease during the study;
- Any indication that did not justify the continuation of the study;
- Anytime at will of a test subject, expressed in any form.

If a test subject expressed his/her will to discontinuate a single centrifugation, this circumstance did not lead necessarily to discontinuation of the study.

III.1.8. Data Privacy and Confidentiality

All data and results, which were acquired during the study, were dealt according to policies of data privacy and confidentiality. These data were documented using pseudonymisation. A test subject's name was not used for attribution of data to a person, thus, he/she could not be identified by outside persons. Since the study procedure involved analysis of data and results, such as statistical analyis, it was scheduled that those informations be customized to a third party. After the analysis, all data and results were archived according to legal requirements. Since the study did not respresent a clinical investigation within the meaning of §40 AMG (Arzneimittelgesetz) or §20 MPG (Medizinproduktegesetz), which relate to legal aspects in terms of application of pharmaceuticals and of medical devices within a study in Germany, minor requirements on insurance of test subjects had to be satisfied.

Each test subject was paid EUR 15.— per hour as financial adjustment for the duration of the study.

III.2. Molecular Measurements in the Blood

Molecular measurements were performed with blood samples that were drafted into Tempus blood RNA tubes (Applied Biosystems, Halle, Belgium) before and after each experiment. The content of the tubes was mixed and frozen at –20 °C within one hour after collection and stored until further processing.

III.2.1. RNA Processing and Quantification

For extraction of the entire RNA out of the blood samples, the Tempus Spin Isolation RNA kit was used according to the manufacturer's instructions. After the RNA was extracted, yields were checked in terms of quality using the NanoDrop Spectrophotometer (Isogen Life Science, PW De Meern, the Netherlands). Since globin RNA makes up the majority of RNA of the peripheral blood transcriptome and therefore contributes much redundant information in arrays, it had to be eliminated from the yields as far as possible. Extraction of globin–RNA (purification) was performed using the Ambion Globinclear kit (Applied Biosystems) according to the manufacturer's protocol. After the purification, the remaining RNA was checked in terms of its integrity using Agilent 2100 Bioanalyzer and RNA 6000 chips (Agilent Technologies, Diegem, Belgium). The globin RNA–depleted RNA yields were stored at –80 °C until further analysis.

III.2.2. RNA Amplification and Labeling

In order to generate complementary RNA (cRNA), the globin–depleted RNA was amplified and labeled using the Low Input Quick Amp Labeling one–color kit (Agilent Technologies). Aliquot amounts of 100—200 ng of RNA were reversely transcribed to complementary DNA (cDNA) using T7–promoter primer and MMLV reverse transcriptase. The cDNA was then transcribed to cRNA, whereby a synthetical fluorescent nucleotide was added and thus incorporated into the cRNA during the transcription. For samples taken before the experiment (prior to intervention), cyanine Cy3–Cytidine was

used, whereas for samples taken after the experiment (subsequent to intervention), cyanine Cy5–Cytidine was used. The product—a single–stranded, flourescent-labeled cRNA (Cy3–RNA and Cy5–cRNA, respectively)—was purified with Qiagen's RNeasy mini spin columns (Qiagen, KJ Venlo, Netherlands). Determination of yield quality and its specific activity was performed using the NanoDrop Spectrophotometer.

III.2.3. Microarray Analysis and Data Preprocessing

Aliquots of 1.65 µg cRNA were hybridized on 4x44K Agilent Whole Human Genome microarray slides (design 014850) for 17 hours using the automated HS4800TM pro hybridization station (Tecan, Männedorf, Switzerland) according to the manufacturer's instructions. The arrays were scanned on the Agilent DNA microarray scanner (G2565BA) and processed by means of the Agilent Feature Extraction Software (Version 10.7). The Agilent protocol GE1-10.7-SEP09 was used to convert the scanned tiff-images into text files. The gProcessedSignal per probe was used for analysis. The latter signals were quantile normalized and log2–transformed using GeneSpring 12.1 (Agilent Technologies). Probes that were replicated on the array were reported as median signals. The control probes were removed and data files with the expression signals of 41,093 unique probes were obtained. Probes were further filtered based on an expression intensity filter and a mapping of the probe to a known HUGO gene symbol.

III.3. Statistical Analysis

We considered paired Student's *t*–tests per probe. All *p*–values were adjusted for multiple testings using the Benjamini—Hochberg false discovery rate (BH—FDR). A probe was called significant in the case that its false discovery rate *p*–value was equal or less than 0.05 and the absolute fold change of the probe was equal or larger than 1.5 ($p \leq 0.05$ and $FC \geq 1.5$)

III.4. Biological Interpretation

GeneSpring was used as a primary entry point for biological analysis. The probes were mapped to their corresponding gene symbol. Gene Ontology (GO) analysis was performed with a BH—FDR set at 0.1 . Additional biological interpretation was also performed with Ingenuity Pathway Analysis (IPA version 8.0, Ingenuity® Systems, www.ingenuity.com). Canonical pathway analysis identified the pathways from the IPA library of canonical pathways that were most significant to the data set. The significance of the association between the data set and the canonical pathway was measured with a Fisher's exact test with *p*–values being corrected using BH—FDR, wherefore the threshold was set at 0.1.

Additional biological interpretation was performed using PANTHER. Entrez IDs as well as the corresponding corrected *p*–values were used to create a tab–delimited text file. The text file was submitted and statistical analysis was performed without using an additional Bonferroni correction.

IV. Results

Both cRNAs from the constant centrifugation protocol (SAHC1) and the intermittent centrifugation protocol (SAHC2), which were hybridized on 4x44K Agilent Whole Human Genome microarray slides (design 014850), contributed 41,093 single results for all expressed genes. These results were filtered according to known Entrez ID on the base of Gene Ontology. Thus, 30,953 results were included for further analysis. Assessment of these results was accomplished by different settings of cut–offs for *p*–values and fold changes.

IV.1. Constant Protocol (SAHC1)

IV.1.1. Analysis using the Feature Extraction Software and GeneSpring

Levels of gene expression were evaluated through performance of a paired Student's *t*–test as well as fold change. Criteria and values for these tests can be set arbitrarily, whereby the desired *p*–value did not exceed 0.05 ($p \leq 0.05$) and the fold change did not deceed 1.1 ($FC \geq 1.1$). An overview of the number of included differentially expressed genes according to differently set values for *p*–value and fold change can be seen in table **IV.1**.

661 genes were reported to be differentially expressed at the tresholds $p \leq 0.05$ and $FC \geq 1.5$. For $p \leq 0.05$, 64 genes can be expected to be reported as differentially expressed by chance (false positive). More restrictive criteria with $p \leq 0.01$ and $FC \geq 2$ reported 42 genes as being differentially expressed. With a $p \leq 0.01$, no gene is statistically expected to be false positive.

Table IV.1: Number of differentially expressed genes in the constant protocol (SAHC1), varying with different set of *p*–values and fold changes.

Test Description

Selected Test : T Test Against Zero
p-value computation: Asymptotic
Multiple Testing Correction: Benjamini-Hochberg

Result Summary

	P all	P < 0.05	P < 0.02	P < 0.01	P < 0.0050	P < 0.0010
FC all	30953	1295	292	96	23	0
FC > 1.1	18311	1283	292	96	23	0
FC > 1.5	1565	661	178	61	13	0
FC > 2.0	217	188	101	42	12	0
FC > 3.0	17	15	15	11	6	0
Expected by chance		64	5	0	0	0

For visualisation of the proportion of differentially expressed genes within 30,953 gathered unique results, the Volcano plot (figure **IV.1**) was used. All unique probes were plotted against varying fold changes (x–axis) and varying *p*–values (y–axis). The entirety of 30,953 genes is represented by the entirety of squares within the plot (red and grey squares). Differentially expressed genes, however, are represented by red squares only. Criteria for differential and significant gene expression were set at $p \leq 0.05$ and $FC \geq 1.5$. As it can be seen in table **IV.1**, a total amount of 661 genes met the criteria of differential expression under the abovementioned cut–off values for *p*–value and fold change. These are the ones represented by red squares.

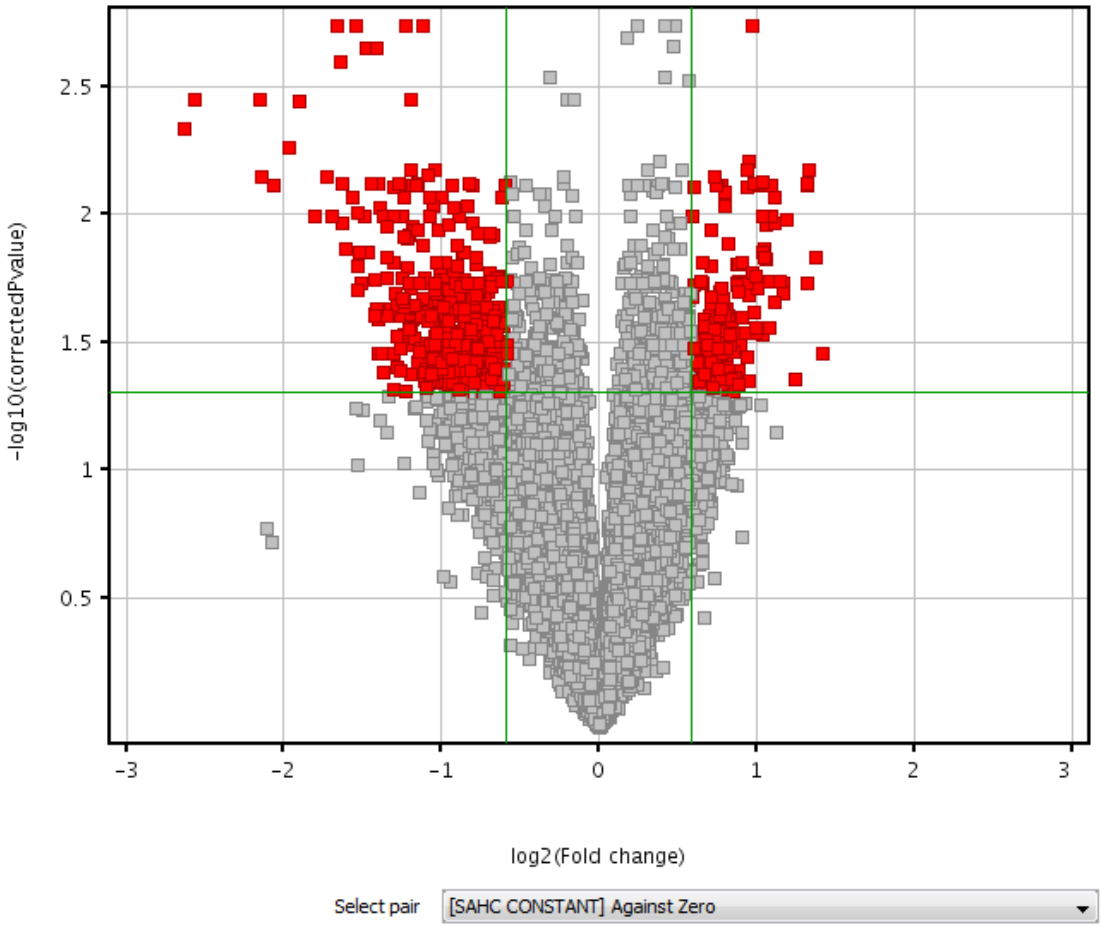

Figure IV.1: Volcano plot for gene expression in the constant protocol (SAHC1). The entirety of all expressed genes is represented by squares. Differentially expressed genes, evaluated according to criteria $p \leq 0.05$ and $FC \geq 1.5$, are shown as red squares. The cut–offs for *p*–value and *FC* are shown as green lines.

For visualisation of differential gene expression within the constant protocol (SAHC1) and the intermittent protocol (SAHC2) together, the Venn diagram was used. The diagram (figure **IV.2**) shows both protocols as circles containing the number of differentially expressed genes each, which were either upregulated or downregulated. The intersection of both protocols represents the number of genes that were differentially expressed in both the constant and the intermittent protocol with total upregulated and downregulated genes, respectively.

List 1 contains 661 differentially expressed genes of the constant protocol (SAHC1) of which 223 (206 + 17) were significantly upregulated and 483 (342 + 96) were significantly downregulated. List 2 contains 243 differentially expressed genes of the intermittent protocol (SAHC2), of which 63 (46 + 17) were significantly upregulated and 180 (84 + 96) were significantly downregulated. There were 17 common genes in both protocols that were significantly upregulated and 96 common genes that were significantly downregulated. The criteria for significance were set at $p \leq 0.05$ and $FC \geq 1.5$.

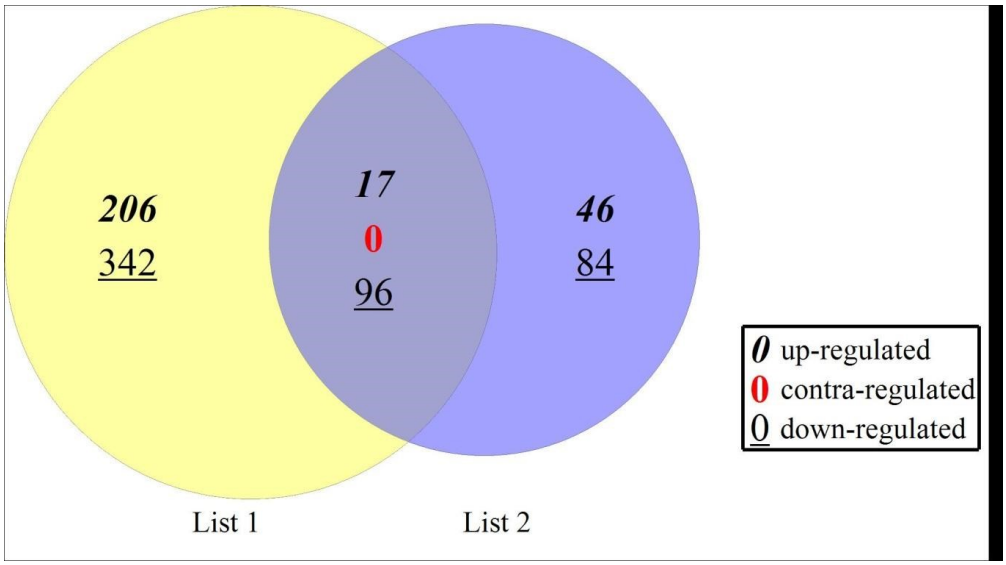

Figure IV.2: Venn diagram for both protocols (SAHC1 and SAHC2).

IV.1.2. Statistical Enrichment Analysis using PANTHER

Pathway analysis

661 unique results from constant protocol, which were significant according to applied statistical tests with $p \leq 0.05$ and $FC \geq 1.5$, were entered into the analysis software PANTHER. The results were converted into a .txt-file with two columnns, one for gene description using Entrez IDs, the other one for adjusted *p*–values. On basis of these two informations about gene description and *p*–values, the software was used to perform a pathway analysis by comparing included genes—with respect to their expression level—with known entries. These entries comprise clusters of known genes, transcripts and proteins, which are involved in a certain pathway. The following two pages show the results for pathways sorted by *p*–value as well as by the number of genes that are common for a pathway, respectively. Column # refers to the number of genes that were reported as significant on the one hand and that are known to be involved in a pathway on the other hand. The column +/– refers to the regulation status of a gene, where plus stands for significant upregulation and minus for likewise downregulation.

Most significantly, 2 genes that are involved in phenylethylamine degradation were upregulated ($p = 0.0381$), namely *retina–specific copper amine oxidase* (AOC2) and *glucose-6-phosphatase* (G6PC). Also, 2 genes that were significantly upregulated ($p = 0.0437$) were found commonly associated with two distinct receptor mediated signaling pathways: *Voltage-dependent L-type calcium channel subunit beta-2* (CACNB2) and *1-phosphatidylinositol 4,5-bisphosphate phosphodiesterase beta-4* (PLCB4), involved both in oxytocin and serotonin $5HT_2$ receptor mediated signaling pathways, shown in figures **IV.5** and **IV.6**. The term *pathway* refers to signal processing of a cell. Numerous molecules are involved in such a process, comprising all classes of biomolecules (nucleic acids, proteins, fatty acids etc.). The process evolves in cascades of chemical reactions, which either stimulate or inhibit following reactions and target different functions, e.g. activation of ion channels, internalisation and degradation of receptors or alternation of gene transcription.

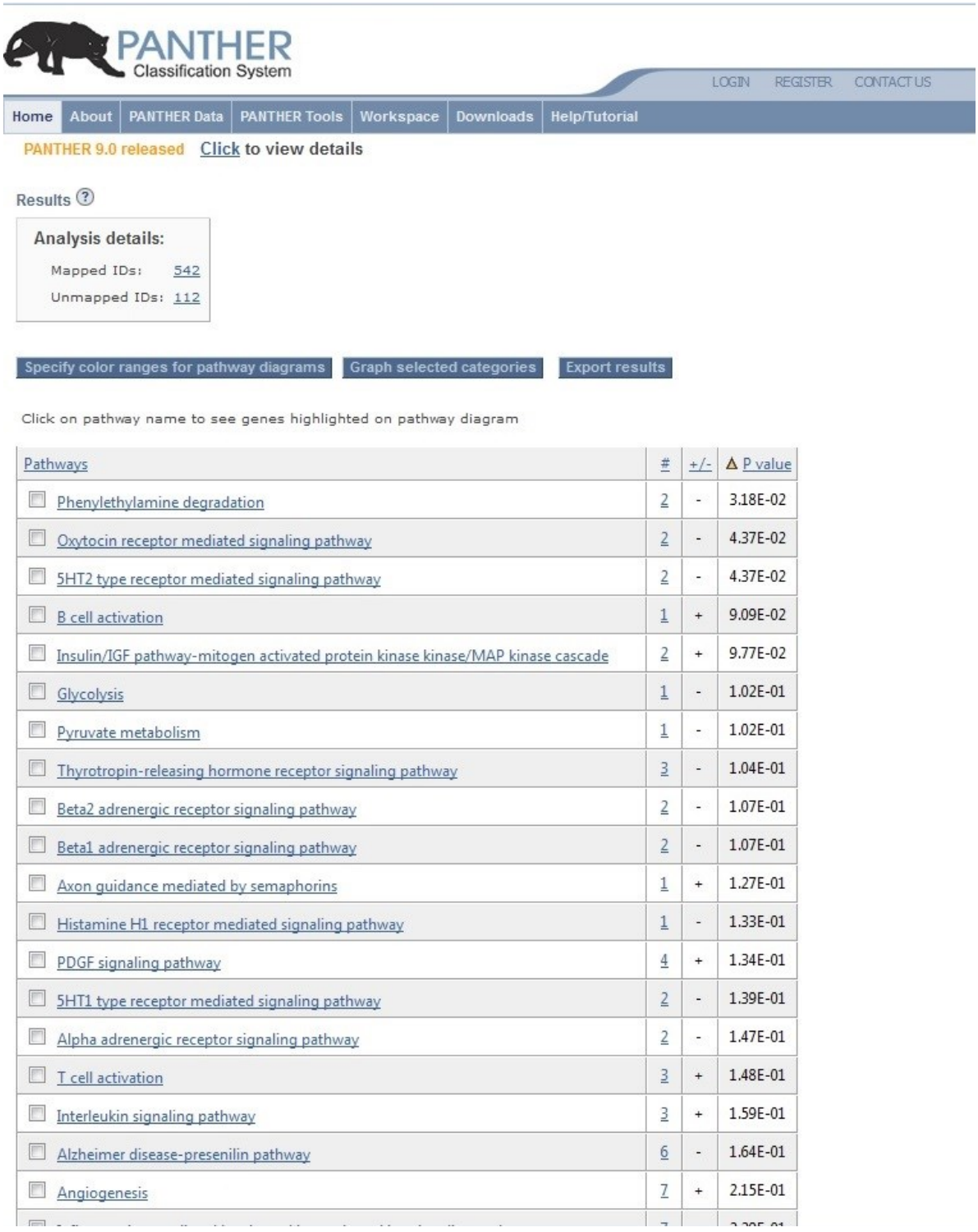

Pathways	#	+/-	Δ P value
Phenylethylamine degradation	2	-	3.18E-02
Oxytocin receptor mediated signaling pathway	2	-	4.37E-02
5HT2 type receptor mediated signaling pathway	2	-	4.37E-02
B cell activation	1	+	9.09E-02
Insulin/IGF pathway-mitogen activated protein kinase kinase/MAP kinase cascade	2	+	9.77E-02
Glycolysis	1	-	1.02E-01
Pyruvate metabolism	1	-	1.02E-01
Thyrotropin-releasing hormone receptor signaling pathway	3	-	1.04E-01
Beta2 adrenergic receptor signaling pathway	2	-	1.07E-01
Beta1 adrenergic receptor signaling pathway	2	-	1.07E-01
Axon guidance mediated by semaphorins	1	+	1.27E-01
Histamine H1 receptor mediated signaling pathway	1	-	1.33E-01
PDGF signaling pathway	4	+	1.34E-01
5HT1 type receptor mediated signaling pathway	2	-	1.39E-01
Alpha adrenergic receptor signaling pathway	2	-	1.47E-01
T cell activation	3	+	1.48E-01
Interleukin signaling pathway	3	+	1.59E-01
Alzheimer disease-presenilin pathway	6	-	1.64E-01
Angiogenesis	7	+	2.15E-01

Figure IV.3: Pathway analysis of the continuous protocol (SAHC1). Explanation in the text.

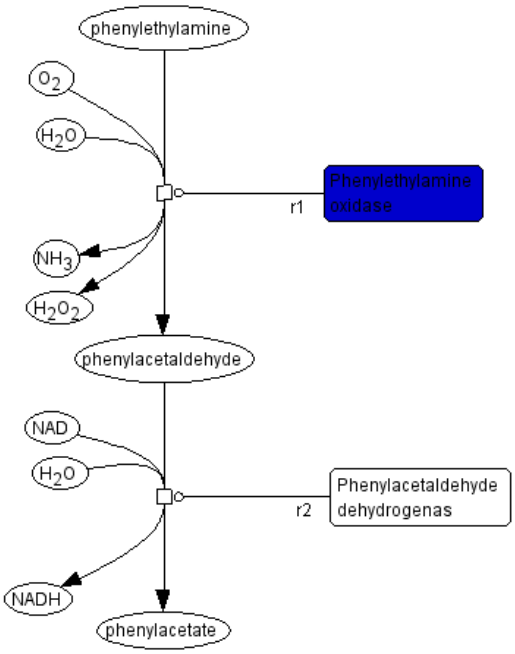

Figure IV.4: *Phenylethylamine degradation*. The enzyme *Phenylethylamine oxidase* is shown in blue.

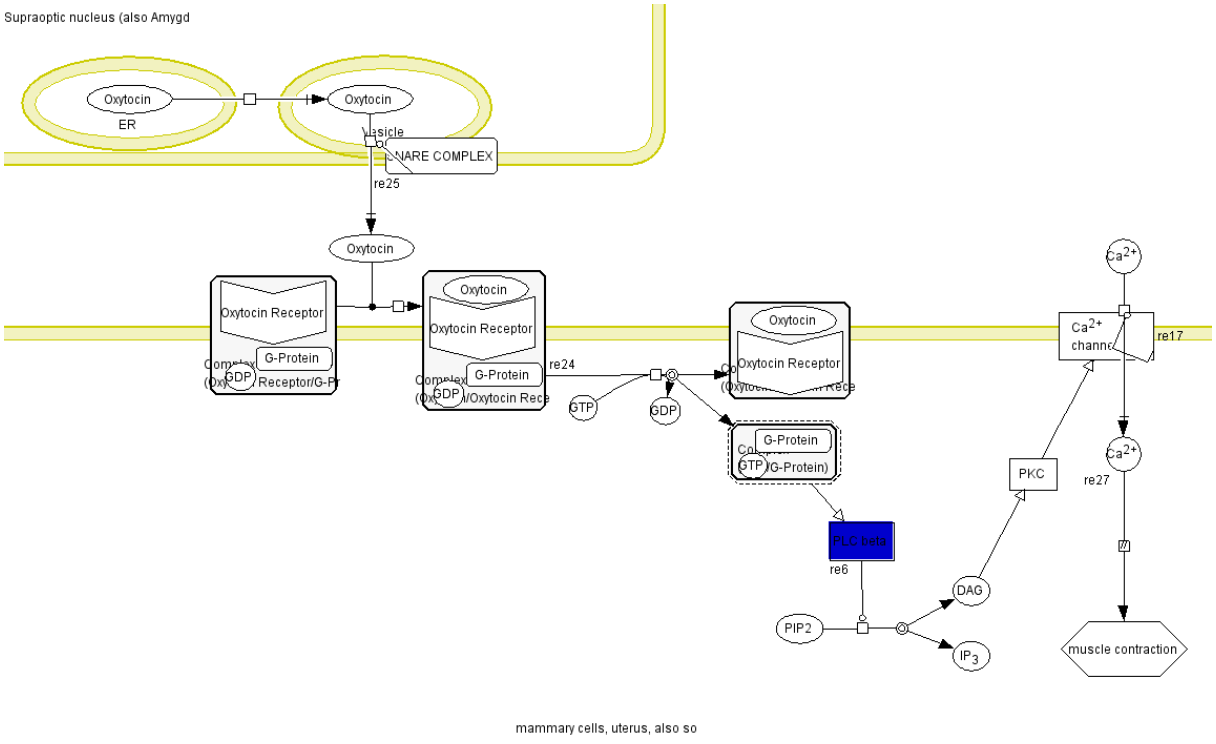

Figure IV.5: *Oxytocin receptor mediated signaling pathway*. The enzyme *Phospholipase C* (PLC) is shown in blue.

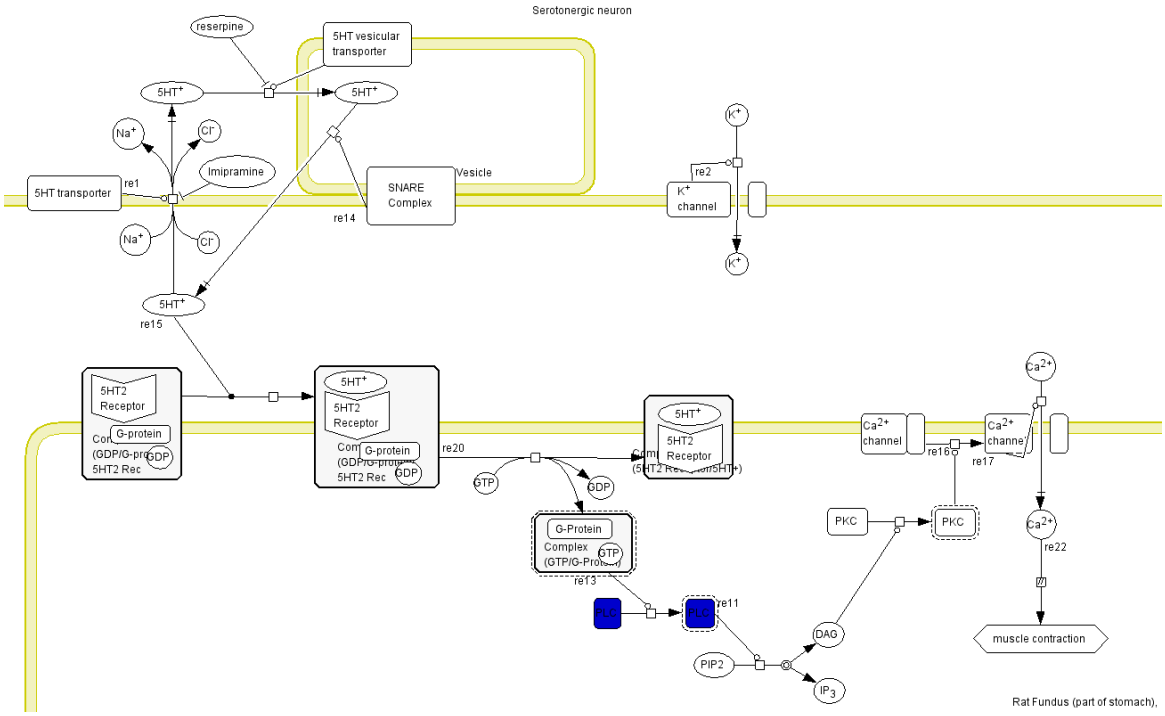

Figure IV.6: *Serotonin 5HT$_2$ receptor mediated signaling pathway*. The enzyme *Phosholipase C* (PLC) is shown in blue.

Analysis of Biological and Molecular Function and of Cellular Component

Similarly as with pathway analysis, the analysis of biological function is an attribution of genes, which were reported as being significantly alternated (either up- or downregulated), to clusters of biological functions. These clusters are made in accordance to databases from Gene Ontology (GO) built upon empiric evidences of certain genes that are associated with a certain biological process. Figure **IV.7** below shows biological processes, where the column # refers to the number of genes, which were found to be significantly altered and which are associated with the specific process, the column +/– refers to the regulation status and the *p*–value refers to the significance of the process.

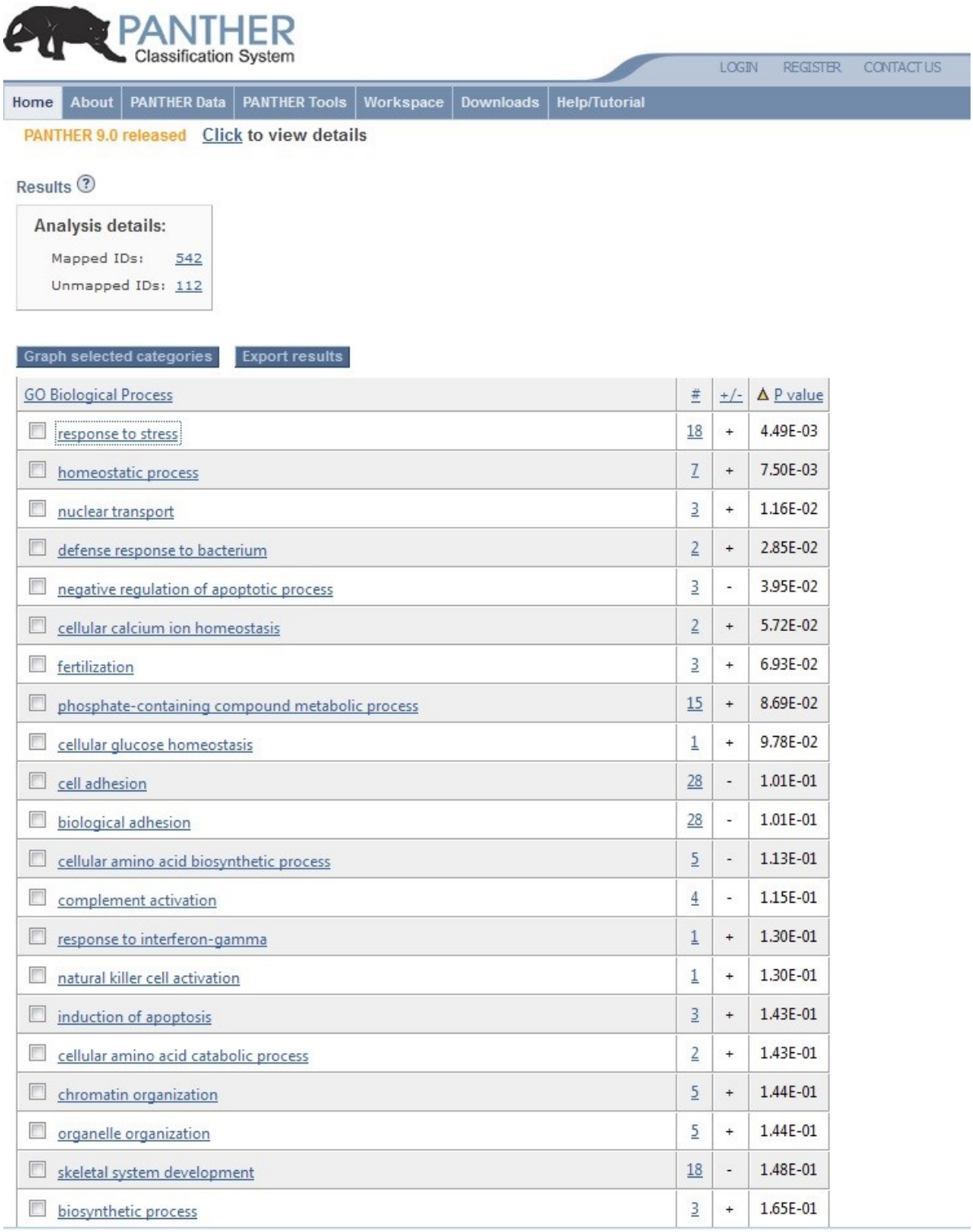

GO Biological Process	#	+/-	Δ P value
response to stress	18	+	4.49E-03
homeostatic process	7	+	7.50E-03
nuclear transport	3	+	1.16E-02
defense response to bacterium	2	+	2.85E-02
negative regulation of apoptotic process	3	-	3.95E-02
cellular calcium ion homeostasis	2	+	5.72E-02
fertilization	3	+	6.93E-02
phosphate-containing compound metabolic process	15	+	8.69E-02
cellular glucose homeostasis	1	+	9.78E-02
cell adhesion	28	-	1.01E-01
biological adhesion	28	-	1.01E-01
cellular amino acid biosynthetic process	5	-	1.13E-01
complement activation	4	-	1.15E-01
response to interferon-gamma	1	+	1.30E-01
natural killer cell activation	1	+	1.30E-01
induction of apoptosis	3	+	1.43E-01
cellular amino acid catabolic process	2	+	1.43E-01
chromatin organization	5	+	1.44E-01
organelle organization	5	+	1.44E-01
skeletal system development	18	-	1.48E-01
biosynthetic process	3	+	1.65E-01

Figure IV.7: Analysis of the continuous protocol (SAHC1) in terms of biological and molecular function and of cellular component.

Most significantly (p = 0.00449), genes involved in *response to stress* were affected by centrifugation, comprising a total of 18 genes and responding with upregulation. 7 genes associated with *homeostatic process* were found to be significantly upregulated (p = 0.0075), 3 genes with *nuclear transport* (p = 0,0116) and 2 genes with *defense response to bacterium* (p = 0,0285). There were 3 genes involved in *negative regulation of apoptotic process* that were significantly downregulated (p = 0.0395).

Figure **IV.8** shows all five significantly affected processes. Colored shapes represent the biological process and the number of each shapes represents the number of genes that were significantly affected. The interpolation of pink triangles stands for the over-all axis of genes that are not affected (just like the grey tapering trunk of a Volcano plot, but compressed and clockwise twisted; see above). Note, that genes below this axis are upregulated and those above the axis are downregulated.

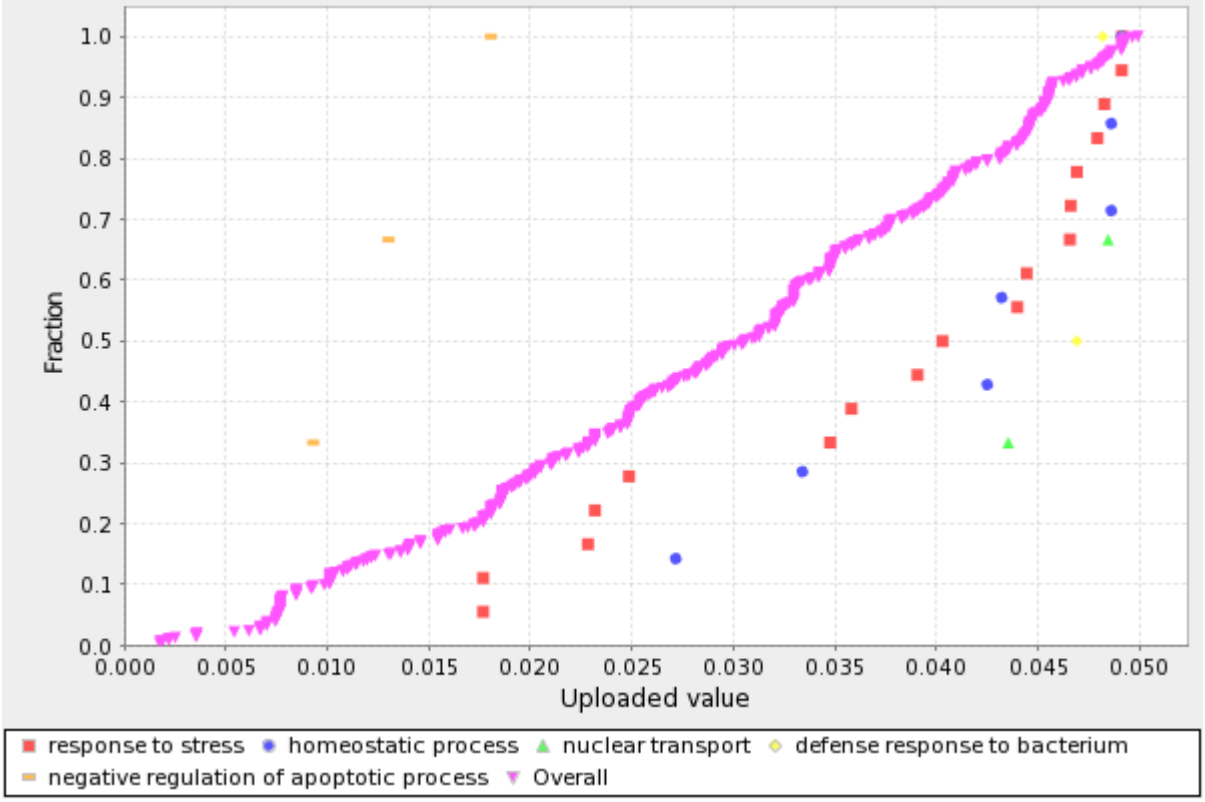

Figure IV.8: Distribution of genes belonging to the five significantly affected GO Biological Processes. Explanation in the text.

Analyses of molecular function and of cellular component according to GO databases, however, did not reveal any significantly affected clusters (p > 0.05)

Analysis of PANTHER Protein Classes

In the following analysis, significantly altered genes from the continuous protocol (SAHC1) were attributed to Protein class entries in PANTHER which consist of 244 terms (http://pantherdb.org/data/, date 02/09/2014). Figure **IV.9** shows protein classes, where column # refers to the number of genes found to be significantly altered and belonging to a certain protein class and where +/– refers to the state of regulation.

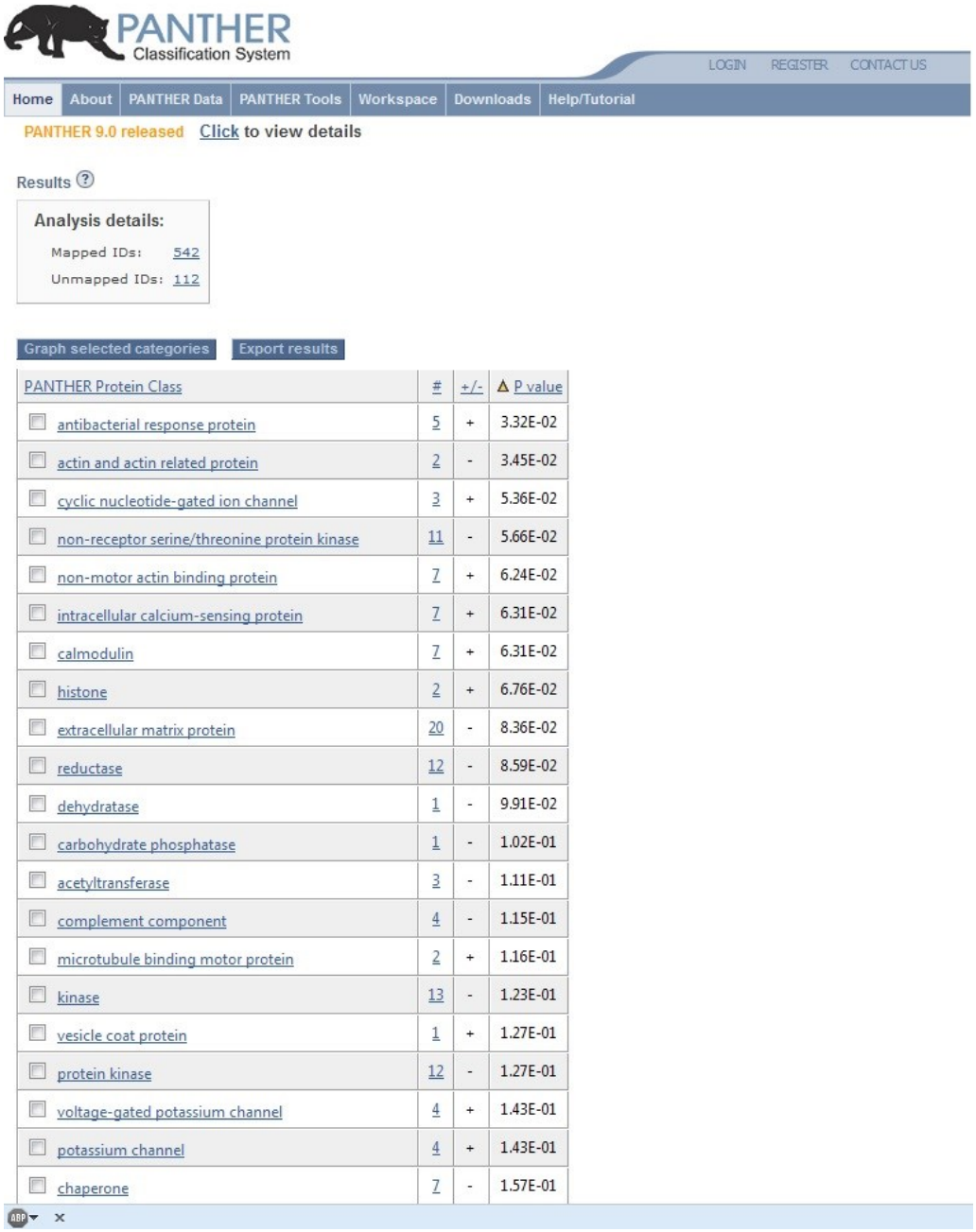

PANTHER Protein Class	#	+/-	Δ P value
antibacterial response protein	5	+	3.32E-02
actin and actin related protein	2	-	3.45E-02
cyclic nucleotide-gated ion channel	3	+	5.36E-02
non-receptor serine/threonine protein kinase	11	-	5.66E-02
non-motor actin binding protein	7	+	6.24E-02
intracellular calcium-sensing protein	7	+	6.31E-02
calmodulin	7	+	6.31E-02
histone	2	+	6.76E-02
extracellular matrix protein	20	-	8.36E-02
reductase	12	-	8.59E-02
dehydratase	1	-	9.91E-02
carbohydrate phosphatase	1	-	1.02E-01
acetyltransferase	3	-	1.11E-01
complement component	4	-	1.15E-01
microtubule binding motor protein	2	+	1.16E-01
kinase	13	-	1.23E-01
vesicle coat protein	1	+	1.27E-01
protein kinase	12	-	1.27E-01
voltage-gated potassium channel	4	+	1.43E-01
potassium channel	4	+	1.43E-01
chaperone	7	-	1.57E-01

Figure IV.9: Analysis of PANTHER protein classes

One significantly upregulated class of proteins (p = 0.0332) was the class of *antibacterial response protein*, to which 5 genes were attributed. A second class (*actin and actin related proteins*) was significantly affected (p = 0.0345) with 2 genes. Figure **IV.10** shows—similar to figure **IV.8** from above—the distribution of genes belonging to one of the two significantly affected PANTHER Protein Classes. The interpolation of green triangles represents the over-all axis of all equally expressed genes. Genes below the axis are upregulated, those above the axis are downregulated.

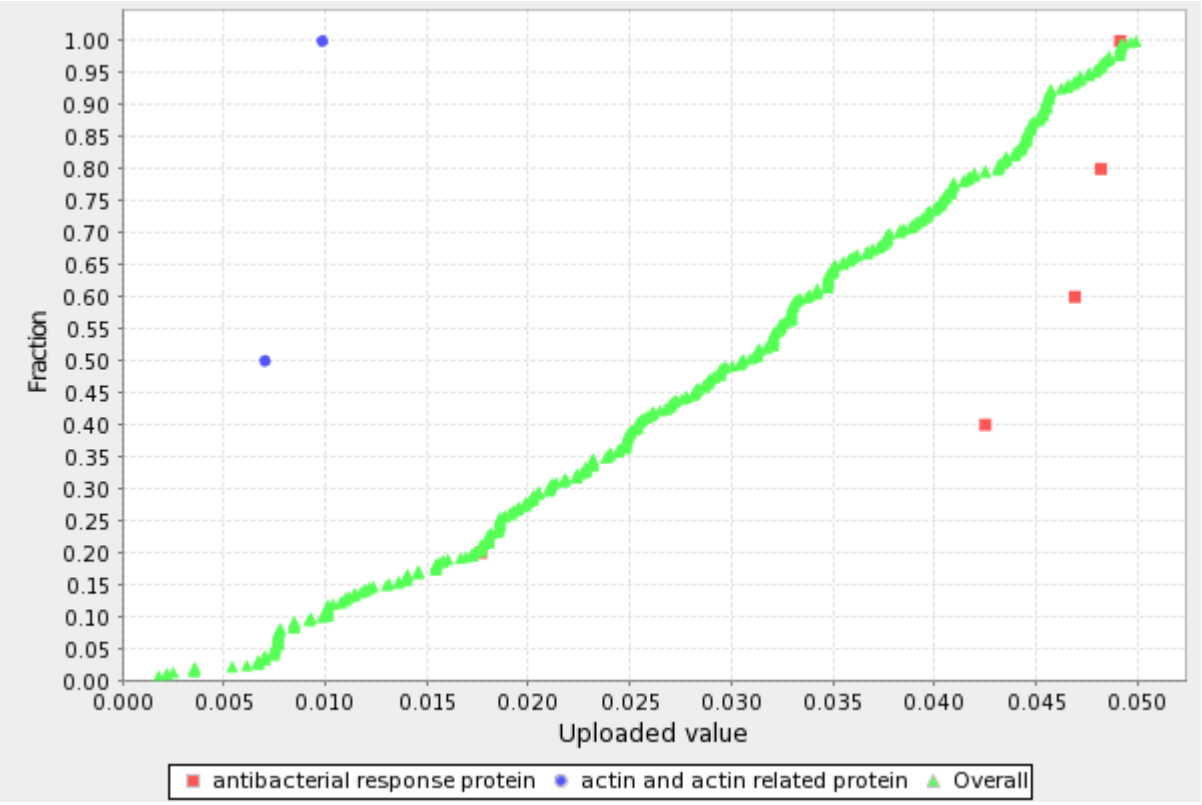

Figure IV.10: Distribution of genes belonging to the two significantly affected PANTHER protein classes. Explanation in the text.

IV.2. Intermittent Protocol (SAHC2)

IV.2.1. Analysis Using Feature Extraction Sofware and GeneSpring

Table **IV.2** shows the number of differentially expressed genes with respect to differently set cut–offs for *p*–value and fold change (*FC*). Just as in the constant protocol, the *p*–value did not exceed 0.05 ($p \leq 0.05$) and the fold change did not deceed 1.1 ($FC \geq 1.1$).

Table IV.2: Number of differentially expressed genes in the intermittent protocol (SAHC2), varying with different set of *p*–values and fold changes

Test Description

Selected Test : T Test Against Zero
p-value computation: Asymptotic
Multiple Testing Correction: Benjamini-Hochberg

Result Summary

	P all	P < 0.05	P < 0.02	P < 0.01	P < 0.0050	P < 0.0010
FC all	30953	3605	1980	1202	5	2
FC > 1.1	15229	3251	1897	1168	5	2
FC > 1.5	1841	243	63	27	0	0
FC > 2.0	339	82	17	8	0	0
FC > 3.0	24	21	8	4	0	0
Expected by chance		180	39	12	0	0

Figure **IV.11** shows the Volcano plot for all expressed genes and differentially expressed genes, respectively. Cut–offs for *p*–values were set at $p \leq 0.05$ and for fold changes at $FC \geq 1.5$. As it can be seen in table **IV.2**, this set included a total number of 243 differentially expressed genes out of all 30,953 unique results. Differentially expressed genes are represented by red squares.

More strict criteria with $p \leq 0.01$ and $FC \geq 2$ show a total amount of 8 differentially expressed genes.

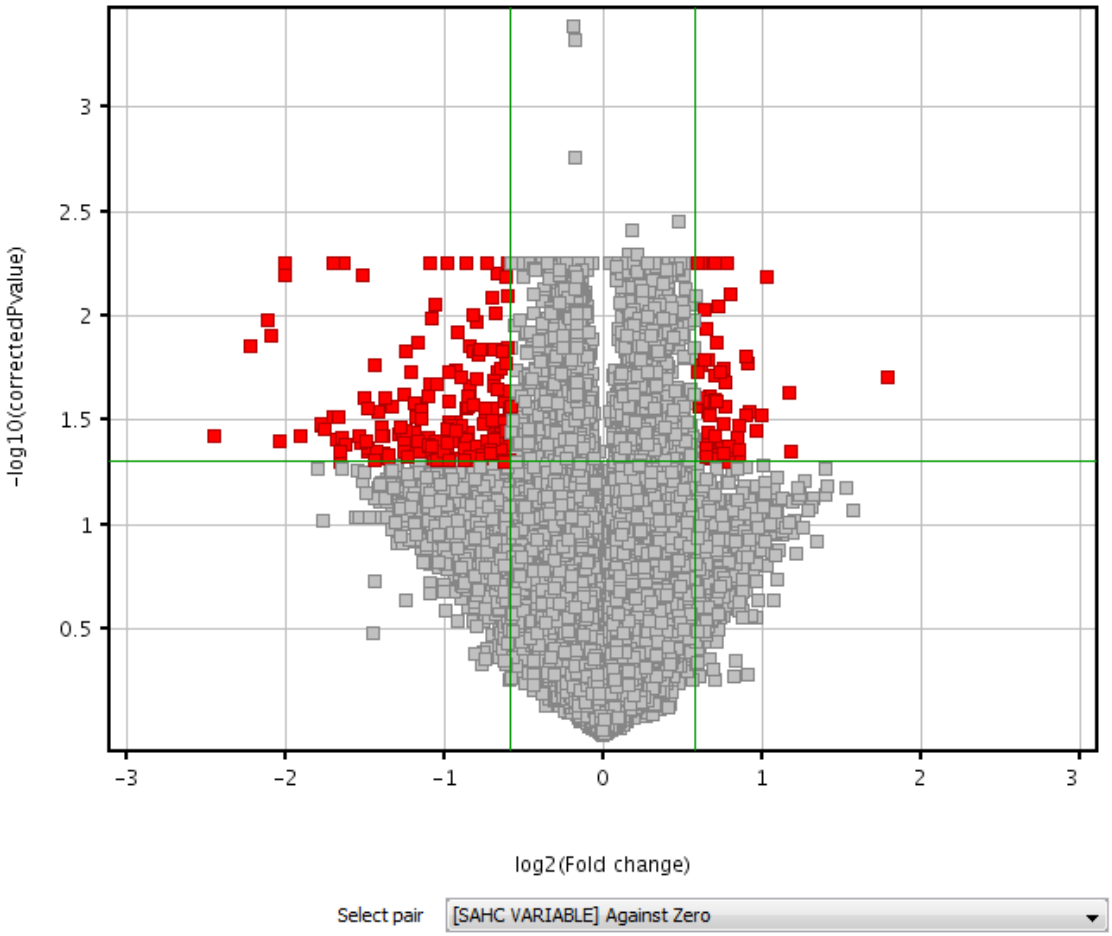

Figure IV.11: Volcano plot for gene expression in the intermittent protocol (SAHC2). The entirety of all expressed genes is represented by squares. Differentially expressed genes, evaluated according to criteria $p \leq 0.05$ and $FC \geq 1.5$, are shown as red squares. The cut–offs for *p*-value and FC are shown as green lines.

IV.2.2. Statistical Enrichment Analysis using PANTHER

The analyses performed were basically the same as for the constant protocol (pathways, GO–based biological and molecular processes and functions and PANTHER Protein Classes). These analyses, however, did not show genes organized in significantly affected clusters ($p > 0.05$). Corresponding figures can be obtained from the Appendix.

V. Discussion

The environment of microgravity (or weightlessness) is known to have several, partially hazardous effects on the human body, such as muscle atrophy, decrease of bone density, alterations of renal, endocrine and neurovestibular function and adaptation of the cardiovascular system, which are responsible for spaceflight deconditioning and orthostatic intolerance upon return to Earth.

Since the beginning of the spaceflight era, which is formally marked by the first human orbital flight with the cosmonaut Yuri Gagarin, until today, strategies of developing effective countermeasures in order to deminish negative effects of microgravity have represented an important goal within spaceflight physiology and spaceflight medicine. The principle of human centrifugation is one of the most important and, probably, most effective countermeasures for this very purpose. In contrast to other principles such as lower–body negative pressure (LBNP), centrifugation is the only practicable method with which a gravity analog by creation of centrifugal forces can be realized. Although centrifugal forces during a centrifugation as the principle of artificial gravity generation show large gravity gradients along their lines of action (e.g. zero gravity in the region of the head and 4 g in the region of the calves, when the subject is positioned in +Gz direction), centrifugation is nevertheless the principle, which comes closest to real gravity, as it is the forces that are crucial for maintenance of natural bone structure and density (94,95). As it was discussed in multiple studies, the integrity of renal function is strongly linked with the integrity of bone substance, thus that the disuse of bones (such as immobilization) leads to altered rates of bone formation and bone resorption with a shift towards bone resorption (29). With bone resorption, a larger amount of calcium and phosphate is deliberated and their plasma levels become increased. Such elevated levels demand an increased renal exrection and the consecutive hypercalciuria bears risks of developing nephroliths and uroliths (96-98). Effects of microgravity on the cardiovascular system can be managed using centrifugation as well as using LBNP, since both principles—although distinct—include the same mode of action by prevention of an upward–shift of blood towards higher located body regions (59). Besides fluid shifts from intravasal to interstitial compartments, the upward-shift of blood is regarded as an

important factor of the complex of symptoms, which is widely known as spaceflight deconditioning and which can lead to orthostatic intolerance postflight (99,100).

Beneficial effects of application of artificial gravity on subjects exposed to real or simulated microgravity have been well documented in several studies. These studies have used various methods. Gene expression profiling by means of transcriptomics has been performed occasionally and mostly in model organisms, which were exposed to simulated microgravity such as roots of Arabidopsis thaliana during parabolic flights (101,102), E. coli during preservation in a Clinostat (103) or Drosophila melanogaster during diamagnetic levitation (104). Analyses of differential gene expression in human tissues have been performed focusing mainly on effects of microgravity on the used tissued. In one study for instance, human endothelial cells were used, which were exposed to microgravity conditions of parabolic flight (105). Another study used human osteoclast progenitor cells, which were exposed to a rotary system as a microgravity analog (106). Up until now, however, no study has investigated the effects of application of artificial gravity on humans in terms of molecular mechanisms such as transcriptomic methods and examination of the transcription rate of mRNA, which allows to draw inferences on the level of gene expression.

In the present thesis, we used the transcriptomic method of DNA microarrays in order to compare a test subject's transcriptome (the entirety of transcribed RNA) prior and subsequent to centrifugation as the method of artificial gravity and a countermeasure to spaceflight deconditioning and orthostatic intolerance. We have observed that the application of centrifugation on test subjects causes changes in the complex 'structure' of the transcriptome. Since a competitive hybridization has been used, each test subject was its own control. We have therefore concluded that centrifugation obviously has effects on gene expression. Furthermore, we have observed that there is a clear difference between the mode of application of centrifugation in terms of molecular mechanisms, as we had compared two different study protocols with distinct procedures in terms of time of centrifugation. This latter circumstance may help elucidate the problem of how large the intensities of centrifugation should be or in which mode centrifugation should be applied in order to prevent negative effects of weightlessness optimally. Finally, such observations might also be helpful for studies of deconditioning which occurs after long-term immobilization, bedrest and geriatrics but also for syncope research.

VI. References

(1) Kozlovskaya IB, Kreidich Y, Oganov VS, Koserenko OP. Pathophysiology of motor functions in prolonged manned space flights. Acta Astronaut 1981 Sep-Oct;8(9-10):1059-1072.

(2) Buchanan P, Convertino VA. A study of the effects of prolonged simulated microgravity on the musculature of the lower extremities in man: an introduction. Aviat Space Environ Med 1989 Jul;60(7):649-652.

(3) Droppert PM. A review of muscle atrophy in microgravity and during prolonged bed rest. J Br Interplanet Soc 1993 Mar;46(3):83-86.

(4) LeBlanc A, Rowe R, Schneider V, Evans H, Hedrick T. Regional muscle loss after short duration spaceflight. Aviat Space Environ Med 1995 Dec;66(12):1151-1154.

(5) LeBlanc A, Lin C, Shackelford L, Sinitsyn V, Evans H, Belichenko O, et al. Muscle volume, MRI relaxation times (T2), and body composition after spaceflight. J Appl Physiol (1985) 2000 Dec;89(6):2158-2164.

(6) Tesch PA, Berg HE, Bring D, Evans HJ, LeBlanc AD. Effects of 17-day spaceflight on knee extensor muscle function and size. Eur J Appl Physiol 2005 Jan;93(4):463-468.

(7) Elmann-Larsen B, Schmitt D. Staying in bed to benefit ESA's astronauts and Europe's citizens. ESA Bull 2003 Feb;113:34-39.

(8) di Prampero PE, Narici MV. Muscles in microgravity: from fibres to human motion. J Biomech 2003 Mar;36(3):403-412.

(9) Narici MV, de Boer MD. Disuse of the musculo-skeletal system in space and on earth. Eur J Appl Physiol 2011 Mar;111(3):403-420.

(10) Miokovic T, Armbrecht G, Felsenberg D, Belavy DL. Heterogeneous atrophy occurs within individual lower limb muscles during 60 days of bed rest. J Appl Physiol (1985) 2012 Nov;113(10):1545-1559.

(11) Desplanches D. Structural and functional adaptations of skeletal muscle to weightlessness. Int J Sports Med 1997 Oct;18 Suppl 4:S259-64.

(12) Stein TP. Nutrition and muscle loss in humans during spaceflight. Adv Space Biol Med 1999;7:49-97.

(13) Ziambaras K, Civitelli R, Papavasiliou SS. Weightlessness and skeleton homeostasis. Hormones (Athens) 2005 Jan-Mar;4(1):18-27.

(14) Mack PB, LaChance PA, Vose GP, Vogt FB. Bone demineralization of foot and hand of gemini-titan IV, V and VII astronauts during orbital flight. Am J Roentgenol Radium Ther Nucl Med 1967 Jul;100(3):503-511.

(15) Brodzinski RL, Rancitelli LA, Haller WA, Dewey LS. Calcium, potassium, and iron loss by Apollo VII, 8, IX, X and XI astronauts. Aerosp Med 1971 Jun;42(6):621-626.

(16) Whedon GD, Lutwak L, Reid J, Rambaut P, Whittle M, Smith M, et al. Mineral and nitrogen metabolic studies on Skylab orbital space flights. Trans Assoc Am Physicians 1974;87:95-110.

(17) Vogel JM. Bone mineral measurement: Skylab experiment M-078. Acta Astronaut 1975 Jan-Feb;2(1-2):129-139.

(18) Caillot-Augusseau A, Lafage-Proust MH, Soler C, Pernod J, Dubois F, Alexandre C. Bone formation and resorption biological markers in cosmonauts during and after a 180-day space flight (Euromir 95). Clin Chem 1998 Mar;44(3):578-585.

(19) Caillot-Augusseau A, Vico L, Heer M, Voroviev D, Souberbielle JC, Zitterman A, et al. Space flight is associated with rapid decreases of undercarboxylated osteocalcin and increases of markers of bone resorption without changes in their circadian variation: observations in two cosmonauts. Clin Chem 2000 Aug;46(8 Pt 1):1136-1143.

(20) Smith SM, Wastney ME, O'Brien KO, Morukov BV, Larina IM, Abrams SA, et al. Bone markers, calcium metabolism, and calcium kinetics during extended-duration space flight on the mir space station. J Bone Miner Res 2005 Feb;20(2):208-218.

(21) LeBlanc AD, Spector ER, Evans HJ, Sibonga JD. Skeletal responses to space flight and the bed rest analog: a review. J Musculoskelet Neuronal Interact 2007 Jan-Mar;7(1):33-47.

(22) Lang T, LeBlanc A, Evans H, Lu Y, Genant H, Yu A. Cortical and trabecular bone mineral loss from the spine and hip in long-duration spaceflight. J Bone Miner Res 2004 Jun;19(6):1006-1012.

(23) Li W, Kezele I, Collins DL, Zijdenbos A, Keyak J, Kornak J, et al. Voxel-based modeling and quantification of the proximal femur using inter-subject registration of quantitative CT images. Bone 2007 Nov;41(5):888-895.

(24) Jost PD. Simulating human space physiology with bed rest. Hippokratia 2008 Aug;12 Suppl 1:37-40.

(25) Spector ER, Smith SM, Sibonga JD. Skeletal effects of long-duration head-down bed rest. Aviat Space Environ Med 2009 May;80(5 Suppl):A23-8.

(26) Zerwekh JE, Ruml LA, Gottschalk F, Pak CY. The effects of twelve weeks of bed rest on bone histology, biochemical markers of bone turnover, and calcium homeostasis in eleven normal subjects. J Bone Miner Res 1998 Oct;13(10):1594-1601.

(27) Rai B, Kaur J, Catalina M. Bone mineral density, bone mineral content, gingival crevicular fluid (matrix metalloproteinases, cathepsin K, osteocalcin), and salivary and serum osteocalcin levels in human mandible and alveolar bone under conditions of simulated microgravity. J Oral Sci 2010 Sep;52(3):385-390.

(28) Belavy DL, Beller G, Ritter Z, Felsenberg D. Bone structure and density via HR-pQCT in 60d bed-rest, 2-years recovery with and without countermeasures. J Musculoskelet Neuronal Interact 2011 Sep;11(3):215-226.

(29) Morgan JL, Zwart SR, Heer M, Ploutz-Snyder R, Ericson K, Smith SM. Bone metabolism and nutritional status during 30-day head-down-tilt bed rest. J Appl Physiol (1985) 2012 Nov;113(10):1519-1529.

(30) Lloyd SA, Lang CH, Zhang Y, Paul EM, Laufenberg LJ, Lewis GS, et al. Interdependence of muscle atrophy and bone loss induced by mechanical unloading. J Bone Miner Res 2013 Oct 11.

(31) Foldager N, Andersen TA, Jessen FB, Ellegaard P, Stadeager C, Videbaek R, et al. Central venous pressure in humans during microgravity. J Appl Physiol (1985) 1996 Jul;81(1):408-412.

(32) Buckey JC,Jr, Gaffney FA, Lane LD, Levine BD, Watenpaugh DE, Wright SJ, et al. Central venous pressure in space. J Appl Physiol (1985) 1996 Jul;81(1):19-25.

(33) Videbaek R, Norsk P. Atrial distension in humans during microgravity induced by parabolic flights. J Appl Physiol (1985) 1997 Dec;83(6):1862-1866.

(34) Norsk P. Blood pressure regulation IV: adaptive responses to weightlessness. Eur J Appl Physiol 2014 Mar;114(3):481-497.

(35) Norsk P. Cardiovascular research in space. Respir Physiol Neurobiol 2009 Oct;169 Suppl 1:S2-3.

(36) Platts SH, Martin DS, Stenger MB, Perez SA, Ribeiro LC, Summers R, et al. Cardiovascular adaptations to long-duration head-down bed rest. Aviat Space Environ Med 2009 May;80(5 Suppl):A29-36.

(37) Aubert AE, Beckers F, Verheyden B. Cardiovascular function and basics of physiology in microgravity. Acta Cardiol 2005 Apr;60(2):129-151.

(38) Drummer C, Heer M, Joosten M, Stormer I, Hesse C, Beck L, et al. Regulation and distribution of body fluid during a 6-day head-down tilt study in a randomized cross-over design. J Gravit Physiol 2000 Jul;7(2):P187-8.

(39) Summers RL, Martin DS, Meck JV, Coleman TG. Mechanism of spaceflight-induced changes in left ventricular mass. Am J Cardiol 2005 May 1;95(9):1128-1130.

(40) Perhonen MA, Franco F, Lane LD, Buckey JC, Blomqvist CG, Zerwekh JE, et al. Cardiac atrophy after bed rest and spaceflight. J Appl Physiol (1985) 2001 Aug;91(2):645-653.

(41) Pavy-Le Traon A, Heer M, Narici MV, Rittweger J, Vernikos J. From space to Earth: advances in human physiology from 20 years of bed rest studies (1986-2006). Eur J Appl Physiol 2007 Sep;101(2):143-194.

(42) Baevsky RM, Baranov VM, Funtova II, Diedrich A, Pashenko AV, Chernikova AG, et al. Autonomic cardiovascular and respiratory control during prolonged spaceflights aboard the International Space Station. J Appl Physiol (1985) 2007 Jul;103(1):156-161.

(43) Arbeille P, Fomina G, Roumy J, Alferova I, Tobal N, Herault S. Adaptation of the left heart, cerebral and femoral arteries, and jugular and femoral veins during short- and long-term head-down tilt and spaceflights. Eur J Appl Physiol 2001 Dec;86(2):157-168.

(44) Caiani EG, Sugeng L, Weinert L, Capderou A, Lang RM, Vaida P. Objective evaluation of changes in left ventricular and atrial volumes during parabolic flight using real-time three-dimensional echocardiography. J Appl Physiol (1985) 2006 Aug;101(2):460-468.

(45) Eckberg DL, Neurolab Autonomic Nervous System Team. Bursting into space: alterations of sympathetic control by space travel. Acta Physiol Scand 2003 Mar;177(3):299-311.

(46) Cox JF, Tahvanainen KU, Kuusela TA, Levine BD, Cooke WH, Mano T, et al. Influence of microgravity on astronauts' sympathetic and vagal responses to Valsalva's manoeuvre. J Physiol 2002 Jan 1;538(Pt 1):309-320.

(47) Eckberg DL, Halliwill JR, Beightol LA, Brown TE, Taylor JA, Goble R. Human vagal baroreflex mechanisms in space. J Physiol 2010 Apr 1;588(Pt 7):1129-1138.

(48) Grigoriev AI. Ion regulatory function of the human kidney in prolonged space flights. Acta Astronaut 1981 Sep-Oct;8(9-10):987-993.

(49) Whitson PA, Pietrzyk RA, Morukov BV, Sams CF. The risk of renal stone formation during and after long duration space flight. Nephron 2001 Nov;89(3):264-270.

(50) Doty SE, Seagrave RC. Human water, sodium, and calcium regulation during space flight and exercise. Acta Astronaut 1999 Nov;45(10):647-654.

(51) Aubert AE, Beckers F, Verheyden B. Cardiovascular function and basics of physiology in microgravity. Acta Cardiol 2005 Apr;60(2):129-151.

(52) Drummer C, Heer M, Dressendorfer RA, Strasburger CJ, Gerzer R. Reduced natriuresis during weightlessness. Clin Investig 1993 Sep;71(9):678-686.

(53) Smith SM, Krauhs JM, Leach CS. Regulation of body fluid volume and electrolyte concentrations in spaceflight. Adv Space Biol Med 1997;6:123-165.

(54) Drummer C, Norsk P, Heer M. Water and sodium balance in space. Am J Kidney Dis 2001 Sep;38(3):684-690.

(55) Gaspare De Santo N, Cirillo M, Valenti G, Perna A, Anastasio P, Drummer C. Renal function in space: the link between osteoporosis, hypercalciuria, and aquaporins. J Ren Nutr 2005 Jan;15(1):183-188.

(56) Titze J, Maillet A, Lang R, Gunga HC, Johannes B, Gauquelin-Koch G, et al. Long-term sodium balance in humans in a terrestrial space station simulation study. Am J Kidney Dis 2002 Sep;40(3):508-516.

(57) Zhang WC, Lu YM, Yang HZ, Xu PT, Chang H, Yu ZB. Four-week simulated weightlessness increases the expression of atrial natriuretic peptide in the myocardium. Sheng Li Xue Bao 2013 Apr 25;65(2):143-148.

(58) Norsk P. Renal adjustments to microgravity. Pflugers Arch 2000;441(2-3 Suppl):R62-5.

(59) Norsk P. Cardiovascular and fluid volume control in humans in space. Curr Pharm Biotechnol 2005 Aug;6(4):325-330.

(60) Alfrey CP, Udden MM, Leach-Huntoon C, Driscoll T, Pickett MH. Control of red blood cell mass in spaceflight. J Appl Physiol (1985) 1996 Jul;81(1):98-104.

(61) Alfrey CP, Udden MM, Huntoon CL, Driscoll T. Destruction of newly released red blood cells in space flight. Med Sci Sports Exerc 1996 Oct;28(10 Suppl):S42-4.

(62) Payne MW, Williams DR, Trudel G. Space flight rehabilitation. Am J Phys Med Rehabil 2007 Jul;86(7):583-591.

(63) Etter KE, Goswami N, Sharp MK. Modelling of cardiovascular response to graded orthostatic stress: role of capillary filtration. Eur J Clin Invest 2011 Aug;41(8):807-819.

(64) Hughson RL. Recent findings in cardiovascular physiology with space travel. Respir Physiol Neurobiol 2009 Oct;169 Suppl 1:S38-41.

(65) Blaber AP, Goswami N, Bondar RL, Kassam MS. Impairment of cerebral blood flow regulation in astronauts with orthostatic intolerance after flight. Stroke 2011 Jul;42(7):1844-1850.

(66) Tuday EC, Meck JV, Nyhan D, Shoukas AA, Berkowitz DE. Microgravity-induced changes in aortic stiffness and their role in orthostatic intolerance. J Appl Physiol (1985) 2007 Mar;102(3):853-858.

(67) Harsch V. Centrifuge "therapy" for psychiatric patients in Germany in the early 1800s. Aviat Space Environ Med 2006 Feb;77(2):157-160.

(68) Caiozzo VJ, Haddad F, Lee S, Baker M, Paloski W, Baldwin KM. Artificial gravity as a countermeasure to microgravity: a pilot study examining the effects on knee extensor and plantar flexor muscle groups. J Appl Physiol (1985) 2009 Jul;107(1):39-46.

(69) Iwase S. Effectiveness of centrifuge-induced artificial gravity with ergometric exercise as a countermeasure during simulated microgravity exposure in humans. Acta Astronaut 2005 Jul-Oct;57(2-8):75-80.

(70) Stenger MB, Evans JM, Knapp CF, Lee SM, Phillips TR, Perez SA, et al. Artificial gravity training reduces bed rest-induced cardiovascular deconditioning. Eur J Appl Physiol 2012 Feb;112(2):605-616.

(71) Gibb R, Ercoline B, Scharff L. Spatial disorientation: decades of pilot fatalities. Aviat Space Environ Med 2011 Jul;82(7):717-724.

(72) Adenot S, Jarchow T, Young LR. Adaptation of VOR to Coriolis stimulation. Ann N Y Acad Sci 2005 Apr;1039:88-96.

(73) Eiken O, Tipton MJ, Kolegard R, Lindborg B, Mekjavic IB. Motion sickness decreases arterial pressure and therefore acceleration tolerance. Aviat Space Environ Med 2005 Jun;76(6):541-546.

(74) Clement G, Pavy-Le Traon A. Centrifugation as a countermeasure during actual and simulated microgravity: a review. Eur J Appl Physiol 2004 Jul;92(3):235-248.

(75) Yadav SP. The wholeness in suffix -omics, -omes, and the word om. J Biomol Tech 2007 Dec;18(5):277.

(76) Zhang H, Zhu JK. RNA-directed DNA methylation. Curr Opin Plant Biol 2011 Apr;14(2):142-147.

(77) Kasprzak JM, Czerwoniec A, Bujnicki JM. Molecular evolution of dihydrouridine synthases. BMC Bioinformatics 2012 Jun 28;13:153-2105-13-153.

(78) Durairaj A, Limbach PA. Mass spectrometry of the fifth nucleoside: a review of the identification of pseudouridine in nucleic acids. Anal Chim Acta 2008 Aug 15;623(2):117-125.

(79) Das G, Lyngdoh RH. Role of wobble base pair geometry for codon degeneracy: purine-type bases at the anticodon wobble position. J Mol Model 2012 Aug;18(8):3805-3820.

(80) PAULING L, ITANO HA. Sickle cell anemia a molecular disease. Science 1949 Nov 25;110(2865):543-548.

(81) Shabalina SA, Spiridonov NA. The mammalian transcriptome and the function of non-coding DNA sequences. Genome Biol 2004;5(4):105.

(82) Frith MC, Pheasant M, Mattick JS. The amazing complexity of the human transcriptome. Eur J Hum Genet 2005 Aug;13(8):894-897.

(83) Mattick JS. Non-coding RNAs: the architects of eukaryotic complexity. EMBO Rep 2001 Nov;2(11):986-991.

(84) Bird CP, Stranger BE, Dermitzakis ET. Functional variation and evolution of non-coding DNA. Curr Opin Genet Dev 2006 Dec;16(6):559-564.

(85) Carninci P, Kasukawa T, Katayama S, Gough J, Frith MC, Maeda N, et al. The transcriptional landscape of the mammalian genome. Science 2005 Sep 2;309(5740):1559-1563.

(86) Kim SH, Quigley GJ, Suddath FL, McPherson A, Sneden D, Kim JJ, et al. Three-dimensional structure of yeast phenylalanine transfer RNA: folding of the polynucleotide chain. Science 1973 Jan 19;179(4070):285-288.

(87) Yusupova GZ, Yusupov MM, Cate JH, Noller HF. The path of messenger RNA through the ribosome. Cell 2001 Jul 27;106(2):233-241.

(88) Rodnina MV, Beringer M, Wintermeyer W. Mechanism of peptide bond formation on the ribosome. Q Rev Biophys 2006 Aug;39(3):203-225.

(89) Gomes AQ, Nolasco S, Soares H. Non-coding RNAs: multi-tasking molecules in the cell. Int J Mol Sci 2013 Jul 31;14(8):16010-16039.

(90) Karapetyan AR, Buiting C, Kuiper RA, Coolen MW. Regulatory Roles for Long ncRNA and mRNA. Cancers (Basel) 2013 Apr 26;5(2):462-490.

(91) Wilusz JE, Sunwoo H, Spector DL. Long noncoding RNAs: functional surprises from the RNA world. Genes Dev 2009 Jul 1;23(13):1494-1504.

(92) Adams MD, Kelley JM, Gocayne JD, Dubnick M, Polymeropoulos MH, Xiao H, et al. Complementary DNA sequencing: expressed sequence tags and human genome project. Science 1991 Jun 21;252(5013):1651-1656.

(93) Velculescu VE, Zhang L, Vogelstein B, Kinzler KW. Serial analysis of gene expression. Science 1995 Oct 20;270(5235):484-487.

(94) van't Veen SJ, Hagen JW, van Ginkel FC, Prahl-Andersen B, Burger EH. Intermittent compression stimulates cartilage mineralization. Bone 1995 Nov;17(5):461-465.

(95) Warden SJ, Fuchs RK, Castillo AB, Nelson IR, Turner CH. Exercise when young provides lifelong benefits to bone structure and strength. J Bone Miner Res 2007 Feb;22(2):251-259.

(96) Pietrzyk RA, Jones JA, Sams CF, Whitson PA. Renal stone formation among astronauts. Aviat Space Environ Med 2007 Apr;78(4 Suppl):A9-13.

(97) Zerwekh JE. Nutrition and renal stone disease in space. Nutrition 2002 Oct;18(10):857-863.

(98) Whitson PA, Pietrzyk RA, Sams CF. Urine volume and its effects on renal stone risk in astronauts. Aviat Space Environ Med 2001 Apr;72(4):368-372.

(99) Coupe M, Fortrat JO, Larina I, Gauquelin-Koch G, Gharib C, Custaud MA. Cardiovascular deconditioning: From autonomic nervous system to microvascular dysfunctions. Respir Physiol Neurobiol 2009 Oct;169 Suppl 1:S10-2.

(100) Hargens AR, Richardson S. Cardiovascular adaptations, fluid shifts, and countermeasures related to space flight. Respir Physiol Neurobiol 2009 Oct;169 Suppl 1:S30-3.

(101) Aubry-Hivet D, Nziengui H, Rapp K, Oliveira O, Paponov IA, Li Y, et al. Analysis of gene expression during parabolic flights reveals distinct early gravity responses in Arabidopsis roots. Plant Biol (Stuttg) 2014 Jan;16 Suppl 1:129-141.

(102) Paul AL, Manak MS, Mayfield JD, Reyes MF, Gurley WB, Ferl RJ. Parabolic flight induces changes in gene expression patterns in Arabidopsis thaliana. Astrobiology 2011 Oct;11(8):743-758.

(103) Arunasri K, Adil M, Venu Charan K, Suvro C, Himabindu Reddy S, Shivaji S. Effect of simulated microgravity on E. coli K12 MG1655 growth and gene expression. PLoS One 2013;8(3):e57860.

(104) Herranz R, Larkin OJ, Dijkstra CE, Hill RJ, Anthony P, Davey MR, et al. Microgravity simulation by diamagnetic levitation: effects of a strong gradient magnetic field on the transcriptional profile of Drosophila melanogaster. BMC Genomics 2012 Feb 1;13:52-2164-13-52.

(105) Grosse J, Wehland M, Pietsch J, Ma X, Ulbrich C, Schulz H, et al. Short-term weightlessness produced by parabolic flight maneuvers altered gene expression patterns in human endothelial cells. FASEB J 2012 Feb;26(2):639-655.

(106) Sambandam Y, Blanchard JJ, Daughtridge G, Kolb RJ, Shanmugarajan S, Pandruvada SN, et al. Microarray profile of gene expression during osteoclast differentiation in modelled microgravity. J Cell Biochem 2010 Dec 1;111(5):1179-1187.

REFERENCES AND FURTHER LITERATURE IN THE WWW

Astrophysics and Principles of Spaceflight

http://www2.jpl.nasa.gov/basics/index.php

http://www.nasa.gov/centers/kennedy/about/history/spacehistory_toc.html

http://www.ifi.unicamp.br/~assis/Annales-Fond-Louis-de-Broglie-V32-p117-120%282007%29.pdf

http://itp1.uni-stuttgart.de/institut/arbeitsgruppen/wunner/AstroRelaSkript.pdf

Centrifuges

http://www.esa.int/Our_Activities/Human_Spaceflight/Human_Spaceflight_Research/DLR_-_Short-Arm_Human_Centrifuge_SAHC

Short arm human centrifuges: Applications for space and earth. Baerwalde S (2011), 1st International :envihab Symposium, 23.-24.05.2011, Cologne, Germany

Transcriptomics and DNA Microarray

http://cage.unl.edu/RNASEQ_Transcriptomics.pdf

http://www.biomedcentral.com/1741-7007/9/34

http://www.genomics.agilent.com/files/Manual/G2505-90021_ScannerC_User.pdf

http://www.genomics.agilent.com/files/Manual/G4460-90025_FE_User.pdf

http://tools.lifetechnologies.com/content/sfs/manuals/fm_1980.pdf

https://www.chem.agilent.com/cag/bsp/products/gsgx/manuals/GeneSpring-manual.pdf

http://www.chem.agilent.com/library/usermanuals/public/g4140-90041_one-color_tecan.pdf

http://media.affymetrix.com/support/technical/datasheets/t7_datasheet.pdf

VII. Appendix

The following lists represent results from PANTHER analysis of Pathway clusters, GO biological processes, GO molecular function, GO cellular component and PANTHER protein classes.

Note: Lists of statistical analyses from primary inputs can be obtained from the Institute of Physiology at the Medical University Graz. For further informations, please refer to the author.

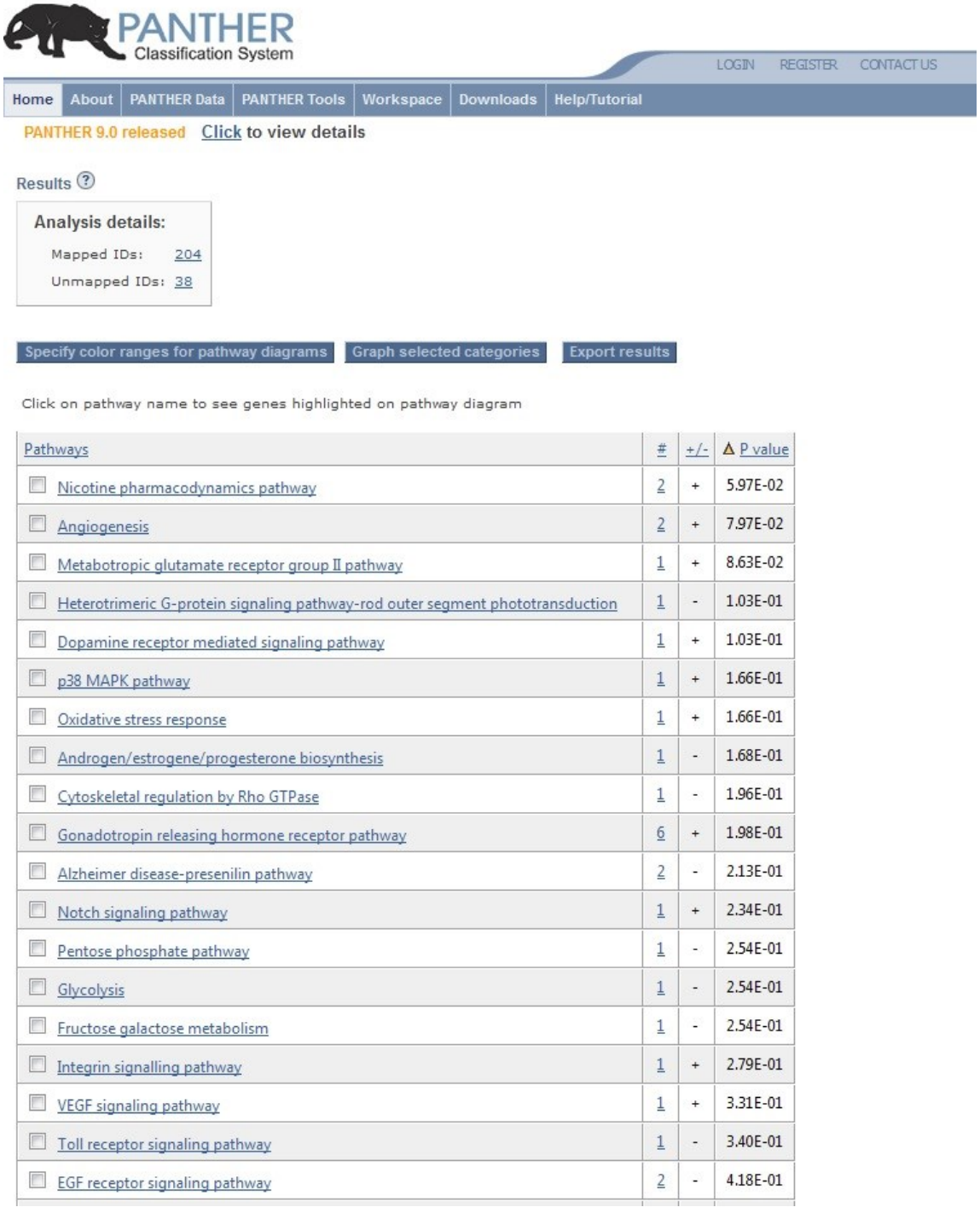

Pathways	#	+/-	Δ P value
Nicotine pharmacodynamics pathway	2	+	5.97E-02
Angiogenesis	2	+	7.97E-02
Metabotropic glutamate receptor group II pathway	1	+	8.63E-02
Heterotrimeric G-protein signaling pathway-rod outer segment phototransduction	1	-	1.03E-01
Dopamine receptor mediated signaling pathway	1	+	1.03E-01
p38 MAPK pathway	1	+	1.66E-01
Oxidative stress response	1	+	1.66E-01
Androgen/estrogene/progesterone biosynthesis	1	-	1.68E-01
Cytoskeletal regulation by Rho GTPase	1	-	1.96E-01
Gonadotropin releasing hormone receptor pathway	6	+	1.98E-01
Alzheimer disease-presenilin pathway	2	-	2.13E-01
Notch signaling pathway	1	+	2.34E-01
Pentose phosphate pathway	1	-	2.54E-01
Glycolysis	1	-	2.54E-01
Fructose galactose metabolism	1	-	2.54E-01
Integrin signalling pathway	1	+	2.79E-01
VEGF signaling pathway	1	+	3.31E-01
Toll receptor signaling pathway	1	-	3.40E-01
EGF receptor signaling pathway	2	-	4.18E-01

LOGIN REGISTER CONTACT US

Home | About | PANTHER Data | PANTHER Tools | Workspace | Downloads | Help/Tutorial

PANTHER 9.0 released Click to view details

Results

Analysis details:

Mapped IDs: 204

Unmapped IDs: 38

Graph selected categories | Export results

GO Biological Process	#	+/-	Δ P value
protein phosphorylation	8	+	9.35E-02
lipid metabolic process	9	+	9.35E-02
endocytosis	7	-	9.97E-02
receptor-mediated endocytosis	2	-	1.02E-01
response to toxic substance	1	+	1.03E-01
cellular component biogenesis	1	+	1.18E-01
phosphate-containing compound metabolic process	7	+	1.20E-01
phospholipid metabolic process	1	+	1.30E-01
mitosis	6	-	1.34E-01
steroid metabolic process	2	+	1.36E-01
RNA localization	1	+	1.66E-01
protein transport	11	-	1.68E-01
intracellular protein transport	11	-	1.68E-01
pattern specification process	3	+	1.73E-01
segment specification	3	+	1.73E-01
nucleobase-containing compound transport	1	-	1.90E-01
organelle organization	2	-	2.04E-01
chromatin organization	2	-	2.04E-01
cellular protein modification process	15	+	2.05E-01
muscle organ development	6	+	2.28E-01
	11	-	2.41E-01

pantherdb.org/workspace/

LOGIN REGISTER CONTACT US

Home | About | PANTHER Data | PANTHER Tools | Workspace | Downloads | Help/Tutorial

PANTHER 9.0 released Click to view details

Results

Analysis details:

Mapped IDs: 204

Unmapped IDs: 38

Graph selected categories | Export results

GO Molecular Function	#	+/-	P value
structural constituent of ribosome	2	+	7.97E-02
neurotrophin receptor binding	1	+	8.63E-02
racemase and epimerase activity	1	+	1.03E-01
anion channel activity	1	+	1.03E-01
structural constituent of myelin sheath	1	-	1.03E-01
nuclease activity	1	+	1.22E-01
G-protein coupled receptor activity	4	-	1.27E-01
lipase activity	1	+	1.30E-01
phospholipase activity	1	+	1.30E-01
ubiquitin-protein ligase activity	3	-	1.34E-01
deacetylase activity	1	-	1.42E-01
neuropeptide hormone activity	1	+	1.44E-01
guanyl-nucleotide exchange factor activity	1	-	1.90E-01
non-membrane spanning protein tyrosine kinase activity	1	-	2.02E-01
DNA helicase activity	1	+	2.14E-01
serine-type peptidase activity	6	+	2.21E-01
GTPase activity	1	-	2.27E-01
pyrophosphatase activity	2	+	2.33E-01
single-stranded DNA binding	2	-	2.33E-01
DNA replication origin binding	2	-	2.33E-01
ion channel activity	8	+	2.35E-01

LOGIN REGISTER CONTACT US

Home | About | PANTHER Data | PANTHER Tools | Workspace | Downloads | Help/Tutorial

PANTHER 9.0 released Click to view details

Results

Analysis details:

Mapped IDs: 204

Unmapped IDs: 38

Graph selected categories | Export results

GO Cellular Component	#	+/-	Δ P value
cytosol	1	+	1.30E-01
vesicle coat	1	-	2.68E-01
intermediate filament cytoskeleton	2	+	2.94E-01
cytoskeleton	14	+	3.17E-01
macromolecular complex	8	-	3.21E-01
cell part	24	+	3.43E-01
intracellular	22	+	3.44E-01
integral to membrane	1	-	3.48E-01
protein complex	5	-	3.51E-01
cell junction	1	-	3.75E-01
organelle	15	+	3.80E-01
MHC protein complex	1	-	4.83E-01
membrane	4	-	5.77E-01
plasma membrane	4	-	5.77E-01
cell projection	1	-	6.36E-01
ribonucleoprotein complex	3	-	6.66E-01
extracellular region	13	-	7.19E-01
nucleus	1	-	7.29E-01
microtubule	3	-	8.65E-01
cytoplasm	5	+	8.75E-01
extracellular matrix	11	+	9.05E-01

LOGIN REGISTER CONTACT US

Home | About | PANTHER Data | PANTHER Tools | Workspace | Downloads | Help/Tutorial

PANTHER 9.0 released Click to view details

Results

Analysis details:

Mapped IDs: 204

Unmapped IDs: 38

Graph selected categories | Export results

PANTHER Protein Class	#	+/-	Δ P value
ribosomal protein	2	+	7.97E-02
KRAB box transcription factor	2	-	8.18E-02
neurotrophic factor	1	+	8.63E-02
membrane-bound signaling molecule	1	-	1.03E-01
anion channel	1	+	1.03E-01
epimerase/racemase	1	+	1.03E-01
myelin protein	1	-	1.03E-01
immunoglobulin receptor superfamily	2	-	1.10E-01
nuclease	1	+	1.22E-01
hydrolase	18	+	1.24E-01
lipase	1	+	1.30E-01
phospholipase	1	+	1.30E-01
ubiquitin-protein ligase	3	-	1.34E-01
dehydrogenase	2	+	1.36E-01
deacetylase	1	-	1.42E-01
neuropeptide	1	+	1.44E-01
zinc finger transcription factor	5	-	1.46E-01
Hsp70 family chaperone	1	+	1.66E-01
actin and actin related protein	3	-	1.79E-01
guanyl-nucleotide exchange factor	1	-	1.90E-01
non-receptor tyrosine protein kinase	1	-	2.02E-01